DEVELOPING AN INTEGRATIVE APPROACH TO INVESTIGAE AND ENHANCE THE EFFICACY OF MSCs

by

PRIYANKA PRIYADARSHANI

(Under the Direction of Luke Mortensen)

ABSTRACT

Mesenchymal stem/stromal cells (MSCs) have acquired considerable attention in regenerative medicine and cell-based therapies due to their remarkable regenerative and immunomodulatory properties. Understanding the molecular mechanisms underpinning MSC function is essential for harnessing their therapeutic potential effectively. This study uses the multifaceted approach to comprehensively characterize the MSC functional activity. First, we employed high resolution mass spec technique to interpret the alteration of lipids during MSC aging and established connections between alterations in cellular lipid composition and overall functionality to determine the number of passages MSCs can go for biomanufacturing processes. Next, we employed label free imaging techniques to establish a direct correlation between single-cell MSC lipidomic profiles and their morphological characteristics to uncovered novel insights into the heterogeneity within MSC populations and its implications for cell therapy outcomes. Finally, we explored the high content imaging technique to perform live imaging of MSC donors seeded in microfluidic device that can closely mimic the *in vivo* culture conditions. Our finding helped in assessing the high potency donor based on migration and locomotion behavior. Overall, this study provides a comprehensive understanding of morphological features, lipid metabolic

networks, functional behavior of MSCs and offers insights into optimizing MSCs efficacy to enhance clinical therapeutics.

INDEX WORDS: MSC, Label-free imaging, high content live imaging, mass spectrometry, MALDI-MSI, MALDI-FTICR, morphological features, lipidomics, microfluidic device, migration.

# DEVELOPING AN INTEGRATIVE APPROACH TO INVESTIGAE AND ENHANCE THE EFFICACY OF MSCs

by

PRIYANKA PRIYADARSHANI

B.Tech., Kathmandu University, Nepal, 2011

M.S., Wichita State University, 2015

A Dissertation Submitted to the Graduate Faculty of The University of Georgia in Partial Fulfillment of the Requirements for the Degree

DOCTOR OF PHILOSOPHY

ATHENS, GEORGIA

2023

# DEVELOPING AN INTEGRATIVE APPROACH TO INVESTIGAE AND ENHANCE THE EFFICACY OF MSCs

by

PRIYANKA PRIYADARSHANI

| | |
|---|---|
| Major Professor: | Luke J. Mortensen |
| Committee: | Steven L. Stice |
| | Leidong Mao |
| | Ross Marklein |
| | Edward A. Botchwey |

Electronic Version Approved:

Ron Walcott
Vice Provost for Graduate Education and Dean of the Graduate School
The University of Georgia
December 2023

*For my family. Thanks for always being there for me.*

—♥—

*My heartfelt gratitude to my husband, Rahil Taujale.*

*For your enduring love, unwavering support, and guidance throughout my Ph.D. journey.*

—♥—

*In memory of my paternal grandma, Ratan Sheela Devi.*

*For your unconditional love and support*

# ACKNOWLEDGEMENTS

I am grateful to my wonderful advisor, Dr. Luke J. Mortensen, for his continued guidance and support during my Ph.D. study, without which this dissertation would not have been possible. I would also like to express my deepest appreciation to my committee members Dr. Steven L. Stice, Dr. Leidong Mao, Dr. Ross Marklein, and Dr. Edward A. Botchwey, who have provided invaluable advice and guidance throughout my research. I would also like to thank all past and present members of Mortensen lab who I've had the pleasure of working with. I also thank to CMaT and NSF for the funding.

# TABLE OF CONTENTS

Page

# LIST OF TABLES

Page

# LIST OF FIGURES

Page

# CHAPTER 1

# INTRODUCTION AND LITERATURE REVIEW

## 1.1 Motivation

Mesenchymal stem/stromal cells (MSCs) are a fascinating and versatile population of adult stem cells that hold great promise in the field of regenerative medicine and tissue engineering. These cells have attracted considerable attention from researchers and clinicians due to their unique properties, including self-renewal capacity, multilineage differentiation potential, and immunomodulatory functions[1-5]. The number of clinical trials investigating MSCs for clinical use has increased from 142 to 1,420 worldwide (https://clinicaltrials.gov) in the last decade however, due to the inconsistencies within outcomes of manufactured MSCs, there are no approved MSC based treatments in the US. A few notable instances of clinical trial setbacks in recent years include Mesoblast's BLA submission (BLA 125 706, August 2020), the use of MSCs for multiple sclerosis treatment, as reported in "Multiple Sclerosis News Today, 2021. These inconsistencies and failure in the clinical outcomes of MSC therapy can be attributed to several factors, including but not limited to passage number i.e the number of passages they go through can affect their characteristics and functionality, the poor-quality control and inconsistent characteristics of MSCs in terms of immunocompatibility, stability, heterogeneity, differentiation, and migratory capacity[5-7]. These factors can impact their therapeutic potential and contribute to variations in clinical

outcomes. While standardizing the expansion and differentiation protocols for MSCs are in efforts for consistent clinical therapy, it has remained challenging to identify a distinct characteristic and establish defined Critical Quality Attributes (CQAs) that enables robust identification and isolation of the multipotent MSCs. Many clinical trials assessing the use of culture expanded MSC therapies have been carried out and mixed clinical response rates are frequently reported[8]. Ongoing studies on CQAs encompass an array of approaches, such as morphometric measurements, evaluation of soluble factors, transcriptional factors, metabolic profiling, and the application of assays to assess functional immunomodulatory potential[8,9].

The ability to generate clinically significant quantities of multipotent MSCs through *in vitro* cultivation is a standard requirement for stem cell-based treatments. New innovative approaches for characterizing and distinguishing heterogeneous cell populations of MSCs will contribute significantly to basic biological understanding and can potentially improve efficacy of MSCs based therapies. So, in this study we use multifaceted analysis of bone marrow derived MSCs by applying imaging techniques, lipidomic analysis, and the study of cell migration to shed new light on cellular character and functional behavior. First, we extracted the morphological features and lipidomic profile of culture expanded MSCs and established correlation between lipid and morphology to determine number of passages MSCs can undergo for biomanufacturing. Next, we examined single cell changes in lipid metabolites after functionally activating the cells with IFN-γ and correlate with the morphological changes of MSCs at a single-cell level which will address the heterogeneous behavior of MSCs and identify the nature of functional subpopulation. Finally, we employed 3D culture device to study the migratory behavior of MSCs that characterize the cells' function and physiology in cell culture system that mimic the *in vivo* environment.

# 1.2 Background

## 1.2.1 History

Mesenchymal stem cells are multipotent stromal cells that can differentiate into various cell types, making them a valuable resource for regenerative medicine and therapeutic applications[10,11]. The concept of stem cells was first proposed by German biologist Ernst Haeckel in the late 19th century[12]. However, it wasn't until the 1960s that the potential of MSCs started gaining attention[13]. In 1966, the first evidence of MSCs was reported when Alexander Friedenstein and colleagues identified a population of cells in bone marrow that had the ability to form colonies of fibroblast-like cells, which they termed "colony-forming units-fibroblastic" (CFU-F). This marked the initial step in understanding the regenerative potential of these cells[14,15].

Throughout the 1970s and 1980s, researchers continued to explore the properties of MSCs. They were found in various tissues, such as adipose tissue, synovial fluid, dental pulp, and umbilical cord. Scientists observed that MSCs could differentiate into multiple lineages, including bone, cartilage, and fat cells. However, due to the lack of specific markers and standardized protocols for isolation, the characterization and understanding of MSCs were somewhat limited during this time. The 1990s brought significant advancements in stem cell research, including MSCs. In 1991, researchers discovered that MSCs had immunomodulatory properties, paving the way for their potential use in treating various immune-related disorders. In 1999, Arnold Caplan introduced the term "mesenchymal stem cell," highlighting their tissue origin and multipotent properties. He also proposed that MSCs had the ability to support hematopoiesis, the process of blood cell formation[6,14,16]. As the field continued to grow, scientists developed more sophisticated techniques for isolating and culturing MSCs. The identification of specific surface markers, such

as CD105, CD73, and CD90, helped to standardize MSC characterization and distinguish them from other cell types[16,17]. These markers became crucial for identifying and isolating MSCs from various tissues, including bone marrow, adipose tissue, and umbilical cord.

In the early 2000s, clinical trials exploring the therapeutic potential of MSCs began to emerge. The immunomodulatory properties of MSCs were particularly promising in the context of autoimmune diseases and graft-versus-host disease (GVHD) following bone marrow transplantation[18]. MSCs were found to reduce inflammation, promote tissue repair, and suppress the immune system's harmful responses[19,20]. In recent years, ongoing research has led to further advancements in the field of MSCs. Scientists have explored novel sources of MSCs, such as menstrual blood, amniotic fluid, and dental tissues, expanding the possibilities for regenerative medicine.

### 1.2.2 Introduction to MSC

MSCs are multipotent cell (Figure 1.1) that can differentiate a subset of non-hematopoietic adult stem cells originating from the mesodermal lineage[21,22] and have self-renewal ability making them capable to divide and generate more MSCs, maintaining a pool of these cells for potential therapeutic use[7]. This versatility makes them valuable for repairing and regenerating damaged or injured tissues. Mesenchymal stem cells (MSCs) exhibit the ability to undergo differentiation, giving rise to various cell lineages derived from mesoderm, including adipocytes, osteocytes, and chondrocytes. These cells can be harvested from different tissues in the body, with bone marrow and adipose tissue being the most common sources[15,23-25]. Other sources include umbilical cord tissue[26], dental pulp[27], and placental tissue[28]. Each source may have slightly different properties and potential applications.

Along with the regenerative properties, MSCs have immunomodulatory capabilities, which means they can regulate the immune system's response. They can suppress inflammation and modulate immune cell activity, making them potentially useful for treating autoimmune diseases and conditions involving excessive inflammation[1,3,29]. Moreover, MSCs secrete a variety of growth factors, cytokines, and extracellular vesicles that can influence neighboring cells. These paracrine signals play a crucial role in tissue repair and regeneration by promoting cell growth and tissue remodeling[30,31]. Due to its tissue repair ability and immunomodulatory properties, MSCs have been investigated for their therapeutic potential in a wide range of medical conditions, including orthopedic injuries[32], cardiovascular diseases[33], neurodegenerative disorders[34], autoimmune diseases[35], and more. They have shown promise in preclinical and clinical studies and are part of several clinical trials for cell-based therapy.

Unlike embryonic stem cells, MSCs are derived from adult tissues, reducing ethical concerns associated with their use[36]. Therefore, MSCs are considered as effective and safe cell sources for stem cell therapy. Additionally, they are generally considered safe for transplantation due to their low immunogenicity. Despite their therapeutic potential, there are challenges in using MSCs for clinical applications. These include standardizing isolation and expansion methods, ensuring consistent quality control, and understanding their behavior in different tissue environments[37-39].

### 1.2.3 Immunomodulation function of MSCs

While MSCs possess the capability to differentiate, their primary therapeutic mechanism in both pre-clinical and clinical investigations is thought to be their paracrine effects. These paracrine effects encompass the promotion of angiogenesis, the prevention of apoptosis, and the suppression of inflammation[40,41]. One of the ways MSCs improves tissue microenvironments is via modulation

of immune system, including macrophages and neutrophils. When tissues or cells sustain injury, MSCs play a crucial role in the activation or suppression of the immune system, thereby regulating the overall tissue regeneration process[29,42].

One of the primary mechanisms through which MSCs exert their immune modulatory effects is by suppressing the activation and function of immune cells. MSCs inhibit the proliferation of T cells, B cells, and natural killer (NK) cells. This inhibition is achieved through pro-inflammatory factors, such as IFN-γ (interferon gamma), TNF-α (tumour necrosis factor alpha) and IL-1β (interleukin-1 beta)[43-45]. IFN-γ plays an even more pivotal role in enhancing the immunosuppressive function of MSCs since it induces the secretion of soluble factors, including indoleamine 2,3-dioxygenase (IDO), prostaglandin E2 (PGE2), and interleukin-10 (IL-10)[46]. These factors create an immunosuppressive microenvironment that dampens the immune response. Several studies have shown IDO activity of MSCs as widely used standard for assessing immunomodulatory potency. This enzyme promotes the conversion of tryptophan into kynurenine, which acts as an immunosuppressive metabolite, reducing the function of pro-inflammatory immune cells[47]. Moreover, MSCs can directly interact with immune cells through cell-to-cell contact. They express cell surface molecules such as programmed death-ligand 1 (PD-L1) and Fas ligand (FasL), which engage with corresponding receptors on immune cells, inducing apoptosis or anergy in these cells[48,49]. By preventing immune cell activation and promoting their death or inactivation, MSCs effectively modulate the immune response.

In addition to suppressing immune cell activation, MSCs possess potent anti-inflammatory properties. They secrete anti-inflammatory cytokines like interleukin-1 receptor antagonist (IL-1RA) and transforming growth factor-beta (TGF-β), which inhibit the production of pro-inflammatory cytokines such as tumor necrosis factor-alpha (TNF-α) and interleukin-6 (IL-6)[50,51].

This shift towards an anti-inflammatory milieu helps reduce tissue damage in inflammatory diseases. Furthermore, MSCs can polarize macrophages towards an anti-inflammatory M2 phenotype. This shift in macrophage polarization promotes tissue repair and regeneration by reducing inflammation and promoting tissue remodeling[52,53]. These anti-inflammatory properties make MSCs promising candidates for the treatment of inflammatory diseases such as Crohn's disease, rheumatoid arthritis, and multiple sclerosis.

Recent studies have shown the metabolic fitness of MSCs is likewise pertinent to their therapeutic capabilities and could offer prospects for uncovering supplementary CQAs by employing metabolomics and alternative methodologies[9,54]. Lipidomics, as an important branch of metabolomics, have been shown to play pivotal roles in immune modulation function of MSCs. They are main structural components of cellular membranes and energy storage molecules but also, as most recently shown, they involved as functional and regulatory components of intra- and intercellular signaling[55,56]

### 1.2.4 Lipidomics for functional potency of MSC

Metabolomics, a growing discipline that evaluates the multifaceted metabolic reactions of cells and tissues in response to external influences. Metabolic pathways have emerged as an important hub to investigate MSC activity. In addition to providing cells with building blocks and energy sources to power cellular processes, metabolites also play important roles in shaping functional activities. Moreover, metabolites are closely associated with the phenotypic and mechanical traits of the cell. As such, an end-to-end understanding of these pathways could hold answers to associate phenotypic and metabolic changes and use them as markers for the production of highly efficient cells. Advent of high-throughput analytical methods has significantly expedited this field, enabling

the acquisition of extensive and resilient metabolomic datasets[57-59]. Lipidomics, a specialized field within metabolomics, are vital components of the membrane that maintains their stability and integrity by forming an organized bilayer membrane along with lipid carriers such as fatty acid binding proteins. This lipid bilayer is very closely associated with the cell structure and function (Figure 1.2) is involved in the formation and maintenance of the overall structure as well as their release to the extracellular environment. Lipids are shown to constitute approximately one-third of all metabolites, demonstrating their dynamic functions in biochemical signaling that could help in the prevention, diagnosis, and treatment of an extensive array of human diseases[60-62].

Lipids play crucial roles in various cellular processes and understanding their composition and functions in different cell types, including mesenchymal stem cells (MSCs). However, currently the number of studies about the lipidome of MSCs is limited primarily concentrating on alterations in lipid composition throughout MSCs growth and differentiation[63-66]. Thus, a deep understanding of the biological and functional mechanisms of MSC lipidomic is still needed. In a recent study, researchers examined the profiles of glycerophospholipids (GPLs) in human bone marrow-derived mesenchymal stem cells (BMSCs) obtained from both young and old donors. They also analyzed these profiles across different passages during *in vitro* culture[64,67]. Moreover, a study by Compos et al. demonstrated the change in Phospholipid (PL) and Phosphatidylcholines (PC) lipid profile of MSCs when induced by proinflammatory cytokines TNFα and IFNγ[68]. These bioactive lipids respond to stimuli, allowing them to control the downstream targets of interest. Lipidomics has demonstrated its effectiveness in the identification of viable and functional cell cultures, offering the potential to ensure the efficient and safe application of MSCs. While data on MSC lipidomics remains somewhat scarce, the diverse biological effects exhibited by various lipid families suggest their promising role in future therapeutic approaches. This highlights the

importance of exploring lipid metabolism to help develop a clear understanding of their complex functions, not just within clinical contexts but also in the field of cell manufacturing.

### 1.2.5 Migration and homing potency of MSC

Cell motility can significantly contribute to the diversity of stem cell functions by influencing their ability to migrate to damaged or tumor-affected tissues. Subpopulations of highly migratory stem cells play a pivotal role in cell-based therapies by enhancing the homing of stem cells to the injury site. This, in turn, can significantly improve and potentially stabilize the therapeutic effectiveness of the transplanted cells [69]. MSCs have gained significant attention in regenerative medicine and cell-based therapies due to their unique migration properties. They have been demonstrated to mobilize into the bloodstream and travel to different tissues when triggered by injuries and various medical conditions, including acute burns, skeletal muscle damage, chronic hypoxia, inflammation, heart ailments, neurological disorders, rheumatoid arthritis, graft-versus-host disease, and more[70,71]. MSCs can respond to chemical signals or gradients of various signaling molecules, such as cytokines including IL-6, PDGF, PDGFR-α (platelet-derived growth factor receptor α), PDGFR-β, PlGF (placenta growth factor), vascular endothelial growth factor receptor 1 (Flt-1), and IGF-1[72], chemokines specifically chemokine ligand 9 (CXCL-9), and C-C receptors such as CCR1, CCR4, CCR7, CCR9, CCR10, CXCR1, CXCR3, CXCR5, CXCR6, CX3CR1, and CXCR4[7]. They also respond to the growth factors including PDGFR-α (platelet-derived growth factor receptor α), PDGFR-β, PlGF (placenta growth factor), vascular endothelial growth factor receptor 1 (Flt-1) and IGF-1[73,74]. These signaling molecules are often produced at sites of tissue injury or inflammation. MSCs have receptors on their surface that can detect these signals and guide them toward the injured or inflamed tissue.

To reach their target tissues, MSCs must first exit the bloodstream and enter the surrounding tissue. This process is known as extravasation or diapedesis. MSCs can adhere to the endothelial cells lining blood vessels and then migrate through the vessel wall to reach the injured site. They do this by interacting with adhesion molecules, such as selectins and integrins. Due to the natural homing ability of MSCs, when injected systemically, MSCs tend to home to damaged or inflamed tissues rather than healthy ones. This property is essential for their therapeutic potential, as it allows them to target and repair damaged areas.

Not only do MSCs have the ability to migrate to the injury site, but also exert their therapeutic effects indirectly through paracrine signaling. Once they reach their destination, MSCs can release a variety of bioactive molecules, including growth factors, anti-inflammatory cytokines, and extracellular vesicles. These factors can modulate the local environment, promote tissue repair, and reduce inflammation[30,31]. Overall, the migration properties of MSCs make them valuable candidates for cell-based therapies and tissue regeneration. They can actively seek out and home to damaged tissues, where they can exert their reparative and anti-inflammatory effects, making them a promising tool in regenerative medicine. Various molecules have been shown to be involved in the process of MSC migration and homing, yet the precise mechanism behind homing remains unclear. Gaining a better understanding of how MSCs migrate and find their way to specific tissues has the potential to enhance the effectiveness of future therapies based on MSCs.

### 1.2.6 MSCs morphology reflects their functional mechanisms

MSC are a heterogeneous cell population, which demonstrates varying morphological and biological properties. Cell morphology has long served as a vital characteristic for cell assessment, continuing to be a widely adopted method for monitoring cell status in cell manufacturing

worldwide. When combined with cutting-edge image processing techniques, the quantitative analysis of morphological features extracted from cell images has been shown to exhibit a strong correlation with the quality attributes of MSCs[75-79]. In recent years several studies have shown connections between MSC functions and cell morphology by employing advanced high-content microscopy techniques[80]. Utilizing imaging techniques MSC morphology has been correlated with differentiation, proliferation, migration, homing and aging[81-83].

While quality attributes cannot be easily characterized using individual bio-marker measurements, detecting overall anomalies can still be achieved by assessing variations in multiple morphological parameters. Multivariate analysis integrating omics and morphology is shown to be a promising approach to dress the heterogeneous characteristics and functionality of MSCs. The integration of imaging information with metabolomics will i) lay a strong foundation for implementing machine learning algorithms and developing new insights based on artificial intelligence, ii) hold opportunities for non-destructive, label-free analysis of cell phenotype in an environment akin to the cell's natural state, that could be adapted for inline monitoring during biomanufacturing, and iii) yield insights into the relationship between cell metabolites and their phenotypes associated with the cell functional activity. The project has a potential for high impact on cell manufacturing industries by providing analytical tools that are broadly applicable for large-scale production of high potency MSCs. The large amounts of digital quantitative data in the form of omics and cell morphological measurements will be an invaluable resource for the scientific community to understand the nature of MSCs functions. The resulting deep cellular characterization that we will conduct using this data will provide an unprecedented level of information for cell manufacturing. As such, this project will pave the way towards understanding cell regulatory mechanisms and harness the power of MSCs to treat chronic autoimmune diseases.

### 1.2.7 Clinical Applications and key challenges

Over the last decade, stem cell therapy has emerged as a groundbreaking tool in the field of regenerative medicine. The cell therapy sector is set for significant growth in the coming decades. In 2019, the worldwide cell therapy market was assessed at $755.4 million USD, and it is anticipated to reach a staggering $11 billion USD by 2029[84-87]. The anticipation of a rise in cell therapies has led to the expansion of processes and manufacturing strategies to meet the growing clinical demand. MSCs have proven to be a valuable therapeutic option for treating various diseases. They offer substantial advantages in tissue repair strategies, including the ability for autologous transplantation, a safe profile concerning cellular division, and the absence of cell tumor formation[88-90]. Many clinical trials have been conducted to evaluate the dependability and efficacy of MSC based cell therapy in order to treat different diseases: graft-versus-host disease (GvHD), malignant neoplasms, heart diseases, immune system diseases, and neurological disorders. At present there are 103 MSC-based clinical trial going on in the US. Among them 1 in early phase 1, 66 in phase 1, 38 in phase 2, 4 in phase 3, and 1 in phase 4 (http://clinicaltrials.gov). In the past few years, MSCs, primarily sourced from bone marrow, adipose tissue, and umbilical cord, have been employed in hundreds of clinical trials aimed at treating a wide range of diseases. Studies have demonstrated MSC-based immunotherapies in addressing conditions such as diabetes mellitus, cardiovascular diseases, graft-versus-host disease, Crohn's disease, and a range of inflammatory disorders[91-93] (Figure 1.3). Despite some notable achievements, MSC-based therapies have also encountered numerous setbacks. While the quantity of new trials involving MSCs is steadily increasing, comprehensive outcomes are currently accessible for only a limited subset of these trials[94].

Although they hold great promise in the treatment of immune disorders such as GvHD and allergic disorders, there remain many challenges to overcome before their widespread clinical application. The main hurdle on the path to an approved clinical trial is the insufficient understanding of how cellular activities are regulated within these cells leading to inconsistencies in outcomes of manufactured MSCs. Phenotypic and functional heterogeneity and lack of knowledge about functional pathways in MSCs limits the therapeutic efficacy and complicates the use of MSCs in regenerative applications[95,96]. Even within the same donors, there are subtle differences in their physical and biological properties[97]. Thus, there is a critical need to establish a better understanding of the fundamental relationships between internal cellular processes and observable physical characteristics to improve cell function and produce consistent clinical outcomes to treat autoimmune diseases. There is growing evidence that lipids play a vital role in MSC functions and are closely associated with the phenotypic and mechanical traits of the cell[68,98]. However, the number of studies at the moment about the lipidome of MSCs is limited and no strong link has been established to understand the direct relationships between MSC lipidome and its function and morphological phenotype. As such, an end-to-end understanding of [96]as markers to produce highly efficient cells. What is now needed are scalable readouts that can integrate and provide a holistic view of cellular mechanisms.

## 1.3 Key challenges and unresolved questions

Overactivation of immune cells and chronic inflammation leads to the damage and dysfunction of multiple organs[99,100]. The few clinical therapies currently adopted for the treatment of autoimmune diseases are not effective at all and instead have several adverse side effects hampering the patients' quality of life[101]. The exclusive immunomodulatory properties of mesenchymal

stem/stromal cells (MSCs) make them a crucial cell type for the treatment of autoimmune disorders and chronic inflammation[102,103]. Although they hold great promise in the treatment of immune disorders such as GvHD and allergic disorders, there remain many challenges to overcome before their widespread clinical application. The main hurdle on the path to an approved clinical trial is the insufficient understanding of how cellular activities are regulated within these cells leading to inconsistencies in outcomes of manufactured MSCs. Phenotypic and functional heterogeneity and lack of knowledge about functional pathways in MSCs limits the therapeutic efficacy and complicates the use of MSCs in regenerative applications[95,96]. Even within the same donors, there are subtle differences in their physical and biological properties[97]. Thus, there is a critical need to establish a better understanding of the fundamental relationships between internal cellular processes and observable physical characteristics to improve cell function and produce consistent clinical outcomes to treat autoimmune diseases.

Cellular morphology could, in part, be considered an overall readout as it represents a combination of genetic, transcriptomic, and metabolic states of the cell[104,105]. Moreover, scientific literatures and pre-clinical studies have shown that MSCs, much like other cells, are dependent on the metabolic fitness for its prominent therapeutic use[96,106]. Among the various metabolites through which MSC regulate its functional mechanisms, there is growing evidence that lipids play a critical role in MSCs behavior and functions[55] and are closely associated with cellular morphology. Multivariate analysis of lipidome and morphology of MSCs and correlating with their functional outcome will provide a clear understanding of the critical associations between the MSCs' immunomodulatory function regulated by metabolic changes along with their external morphological features.

## 1.4 Major research questions addressed

There is a critical need for developing a better understanding of the regulatory and functional mechanism of MSCs for optimum clinical outcome. With my research we were able to leverage complex lipid metabolites signaling that produces measurable changes in MSCs processing of immunomodulatory activity and resulting morphological changes. During my research endeavor, we applied the following approach: (i) characterized the lipid alteration in culture-expanded MSCs, and associating these changes with potency markers (ii) established the association of morphological features of single-cell MSCs with their lipidomic profile to identify functional subpopulation of MSCs (iii) Predicted MSCs functional potency through live imaging on high-throughput microfluidic device. These steps are essential and collectively get us closer to understanding the mechanisms of MSCs functional activity and could result in establishing transformative approaches to study and enhance cell biomanufacturing for clinical use.

### 1.4.1 Investigate and characterize lipid profiles associated with MSCs over multiple passages

**Rationale**

In recent years lipid has emerged as a crucial field of study for understanding cellular physiology and pathology. Lipids are being developed as biomarker to disease phenotype in translational research[107,108]. As in other cells, MSCs lipid play integral part in cell signaling and immunity. Thus, this study focuses on characterizing the lipidomic profile of culture expanded MSCs from the early passage to late passage demonstrating changes in lipid metabolites with cell aging. The

lipidomic profile of various stages of cell aging will be correlated with the cell functional activity to select high performing cells as well as enhance the quality of cells.

**Research goals**

Our goal is to perform lipid profiling of expanded MSCs culture that will identify the lipid metabolites associated with the aging process leading to the senescence of the cells. Moreover, correlating the lipid metabolites with secretory profile of MSCs gives an insight into the lipid network associated with the functional activity of the cell.

### 1.4.2. Integration of imaging modalities with lipidomic characterization to investigate single-cell MSCs potency metrics

**Rationale**

There is growing evidence that lipids play a vital role in MSC functions and are closely associated with the MSCs morphological phenotype. Although lipid metabolism plays a pivotal role in MSCs physiopathology, the number of studies at the moment about the lipidome of MSCs is limited and no strong link has been established to understand the direct relationships between single-cell MSC lipidome and its phenotype. In this aim we examine single cell changes in lipid metabolites after we functionally activate the cells treating with IFN-γ since IFN-γ is shown to induce the immunosuppressive capability of MSCs. The change in lipid metabolites will be correlated with the morphological changes of MSCs after IFN-γ treatment which will reveal a deeper understanding of MSCs functional regulation outcomes.

**Research goals**

This study aims to link morphology of MSCs with the lipid metabolites at single cell level that would help in identifying sub populations of highly functional cells. Moreover, characterization of lipidomic in association with the phenotypic changes can reveal novel predictive biomarker for cell therapy.

### 1.4.3. MSCs potency prediction through live imaging on high-throughput microfluidic device

**Rationale**

For the effective delivery of cells into the patient body, it the critical to characterize the cells function and physiology in cell culture system that mimic the *in vivo* environment. 3D cell cultures are more physiologically relevant and closely represent the *in vivo* tissue. Among the 3D culture system, tissue on chip 3D microfluidic cell culture is gaining popularity since it can better mimic the physiology of the organ and allow well controlled and precise mechanical stimuli for improved resemblance of *in vivo* environments. In this study we will culture the MSCs in engineered high-throughput 3D microfluidic system and analyze and compare the morphological feature, secretory factors and migratory behavior of MSCs in 3D microfluidic device and 2D culture.

**Research goals**

With this study our aim is to obtain improved physiological hMSC secretory responses, lipidomic response, and cellular activity in microfluidic 3D culture system. This can serve as the biomarker to evaluate MSCs functional metrics and potency for therapeutic purposes. Since microfluidic 3D

culture system can mimic the *in vivo* environment, the parameters established in this study will better reflect the cell's *in vivo* state.

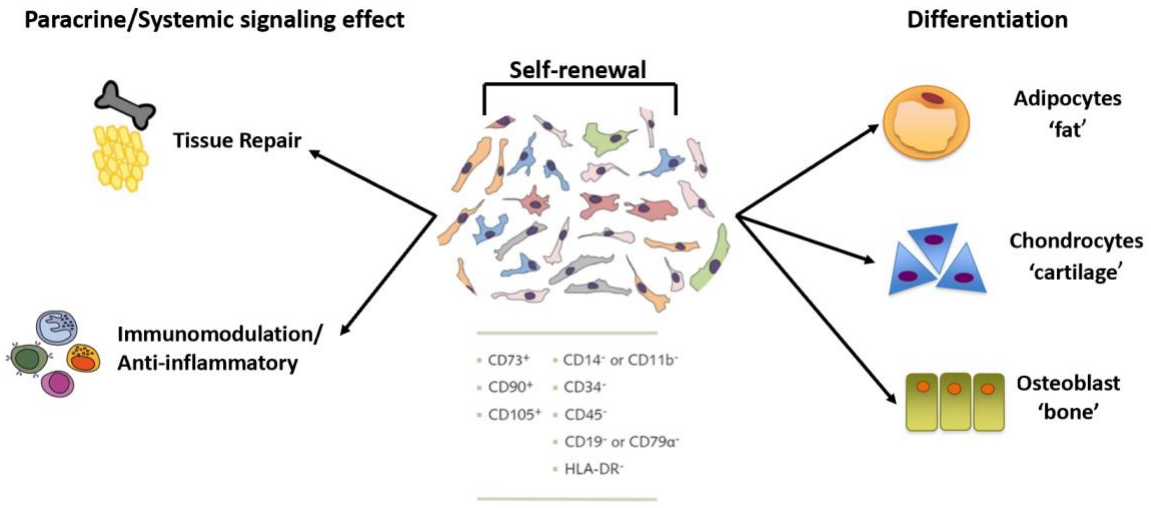


**Figure 1.1: Characteristics of Mesenchymal Stem cells**. Schematic diagram showing the multipotent mesenchymal stem/stromal cells with differentiation and functional characteristics.

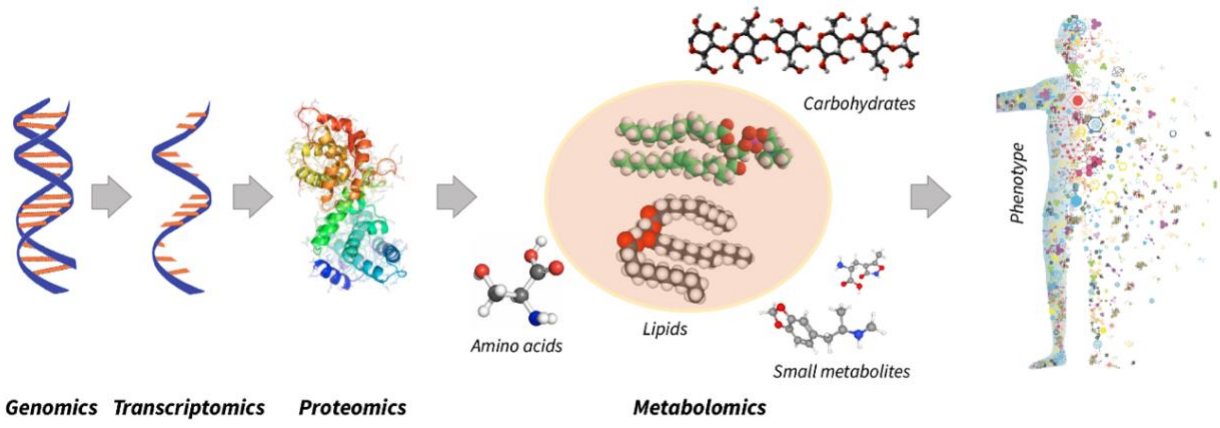


**Figure 1.2: The central dogma of biology**. Schematic diagram emphasizing association of lipid metabolites with the morphological phenotype as the functional readout of the central dogma of biology.

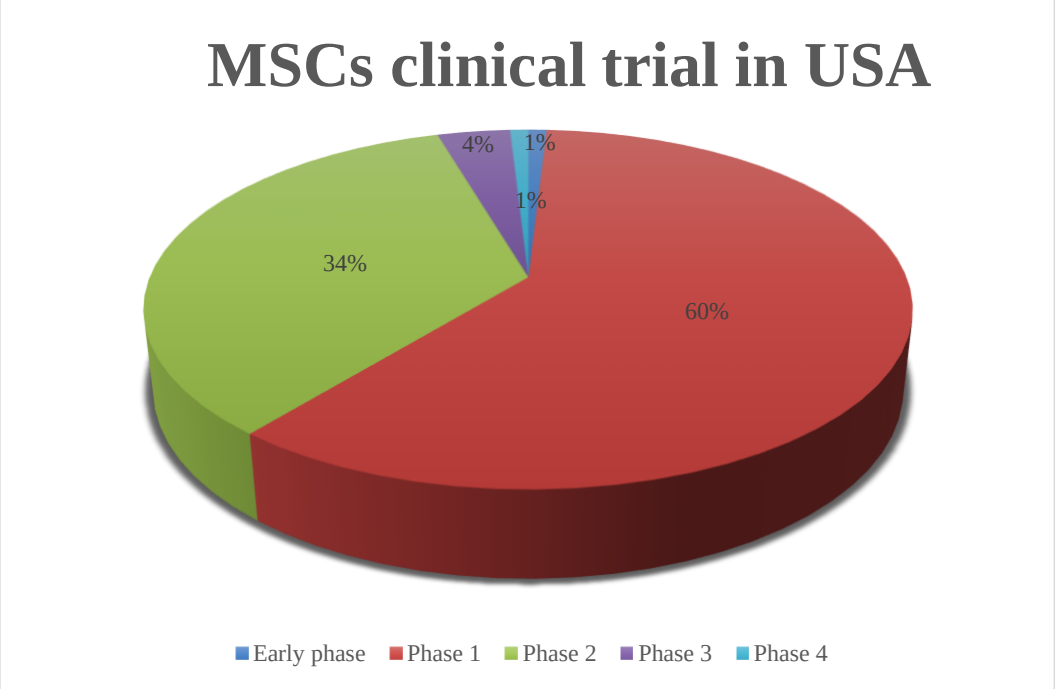


**Figure 1.3: Pie chart showing the percentages of total clinical trials related to MSCs in different phases in the USA**.

## 1.5 Bibilography

1 Castro-Manrreza, M. E. & Montesinos, J. J. Immunoregulation by mesenchymal stem cells: biological aspects and clinical applications. *Journal of immunology research* **2015**, 394917, doi:10.1155/2015/394917 (2015).

2 Li, W. *et al.* Mesenchymal stem cells: a double-edged sword in regulating immune responses. *Cell death and differentiation* **19**, 1505-1513, doi:10.1038/cdd.2012.26 (2012).

3 Gao, F. *et al.* Mesenchymal stem cells and immunomodulation: current status and future prospects. *Cell death & disease* **7**, e2062, doi:10.1038/cddis.2015.327 (2016).

4 Williams, A. R. & Hare, J. M. Mesenchymal stem cells: biology, pathophysiology, translational findings, and therapeutic implications for cardiac disease. *Circulation research* **109**, 923-940, doi:10.1161/circresaha.111.243147 (2011).

5 Zhou, T. *et al.* Challenges and advances in clinical applications of mesenchymal stromal cells. *Journal of hematology & oncology* **14**, 24, doi:10.1186/s13045-021-01037-x (2021).

6 Galipeau, J. & Sensébé, L. Mesenchymal Stromal Cells: Clinical Challenges and Therapeutic Opportunities. *Cell stem cell* **22**, 824-833, doi:10.1016/j.stem.2018.05.004 (2018).

7 Jimenez-Puerta, G. J., Marchal, J. A., López-Ruiz, E. & Gálvez-Martín, P. Role of Mesenchymal Stromal Cells as Therapeutic Agents: Potential Mechanisms of Action and Implications in Their Clinical Use. *Journal of clinical medicine* **9**, doi:10.3390/jcm9020445 (2020).

8 Robb, K. P. *et al.* Failure to launch commercially-approved mesenchymal stromal cell therapies: what's the path forward? Proceedings of the International Society for Cell & Gene Therapy (ISCT) Annual Meeting Roundtable held in May 2023, Palais des Congrès de Paris, Organized by the ISCT MSC Scientific Committee. *Cytotherapy*, doi:10.1016/j.jcyt.2023.09.001 (2023).

9 Maughon, T. S. *et al.* Metabolomics and cytokine profiling of mesenchymal stromal cells identify markers predictive of T-cell suppression. *Cytotherapy* **24**, 137-148, doi:10.1016/j.jcyt.2021.08.002 (2022).

10 Fitzsimmons, R. E. B., Mazurek, M. S., Soos, A. & Simmons, C. A. Mesenchymal Stromal/Stem Cells in Regenerative Medicine and Tissue Engineering. *Stem cells international* **2018**, 8031718, doi:10.1155/2018/8031718 (2018).

11 Han, Y. *et al.* Mesenchymal Stem Cells for Regenerative Medicine. **8**, 886 (2019).

12 Dröscher, A. Images of cell trees, cell lines, and cell fates: the legacy of Ernst Haeckel and August Weismann in stem cell research. *History and Philosophy of the Life Sciences* **36**, 157-186, doi:10.1007/s40656-014-0028-8 (2014).

13 Mizukami, A. & Swiech, K. Mesenchymal Stromal Cells: From Discovery to Manufacturing and Commercialization. *Stem cells international* **2018**, 4083921, doi:10.1155/2018/4083921 (2018).

14 Gothard, D., Dawson, J. I. & Oreffo, R. O. C. Assessing the potential of colony morphology for dissecting the CFU-F population from human bone marrow stromal cells. *Cell and Tissue Research* **352**, 237-247, doi:10.1007/s00441-013-1564-3 (2013).

15 Berebichez-Fridman, R. & Montero-Olvera, P. R. Sources and Clinical Applications of Mesenchymal Stem Cells: State-of-the-art review. *Sultan Qaboos University Medical Journal* **18**, e264-277, doi:10.18295/squmj.2018.18.03.002 (2018).

16 P, M., S, H., R, M., M, G. & W, S. K. Adult mesenchymal stem cells and cell surface characterization - a systematic review of the literature. *The open orthopaedics journal* **5**, 253-260, doi:10.2174/1874325001105010253 (2011).

17 Zhang, L. & Chan, C. Isolation and enrichment of rat mesenchymal stem cells (MSCs) and separation of single-colony derived MSCs. *Journal of visualized experiments : JoVE*, doi:10.3791/1852 (2010).

18 Kikuta, A. & Suzuki, H. Graft-versus-host disease following bone marrow transplantation: clinical feature and diagnosis. *Fukushima journal of medical science* **39**, 95-99 (1993).

19 Shi, M., Liu, Z. W. & Wang, F. S. Immunomodulatory properties and therapeutic application of mesenchymal stem cells. *Clinical and experimental immunology* **164**, 1-8, doi:10.1111/j.1365-2249.2011.04327.x (2011).

20 Wang, M., Yuan, Q. & Xie, L. Mesenchymal Stem Cell-Based Immunomodulation: Properties and Clinical Application. *Stem cells international* **2018**, 3057624, doi:10.1155/2018/3057624 (2018).

21 Guadix, J. A., Zugaza, J. L. & Gálvez-Martín, P. Characteristics, applications and prospects of mesenchymal stem cells in cell therapy. *Medicina clinica* **148**, 408-414, doi:10.1016/j.medcli.2016.11.033 (2017).

22 Viswanathan, S. *et al.* Mesenchymal stem versus stromal cells: International Society for Cell & Gene Therapy (ISCT®) Mesenchymal Stromal Cell committee position statement on nomenclature. *Cytotherapy* **21**, 1019-1024, doi:10.1016/j.jcyt.2019.08.002 (2019).

23 Phinney, D. G. & Prockop, D. J. Concise Review: Mesenchymal Stem/Multipotent Stromal Cells: The State of Transdifferentiation and Modes of Tissue Repair—Current Views. *Stem cells (Dayton, Ohio)* **25**, 2896-2902, doi:10.1634/stemcells.2007-0637 %J Stem Cells (2007).

24 Orbay, H., Tobita, M. & Mizuno, H. Mesenchymal stem cells isolated from adipose and other tissues: basic biological properties and clinical applications. *Stem cells international* **2012**, 461718, doi:10.1155/2012/461718 (2012).

25 Andrzejewska, A., Lukomska, B. & Janowski, M. Concise Review: Mesenchymal Stem Cells: From Roots to Boost. *Stem cells (Dayton, Ohio)* **37**, 855-864, doi:10.1002/stem.3016 (2019).

26 Nagamura-Inoue, T. & He, H. Umbilical cord-derived mesenchymal stem cells: Their advantages and potential clinical utility. *World journal of stem cells* **6**, 195-202, doi:10.4252/wjsc.v6.i2.195 (2014).

27 Huang, G. T., Gronthos, S. & Shi, S. Mesenchymal stem cells derived from dental tissues vs. those from other sources: their biology and role in regenerative medicine. *Journal of dental research* **88**, 792-806, doi:10.1177/0022034509340867 (2009).

28 Vellasamy, S., Sandrasaigaran, P., Vidyadaran, S., George, E. & Ramasamy, R. Isolation and characterisation of mesenchymal stem cells derived from human placenta tissue. *World journal of stem cells* **4**, 53-61, doi:10.4252/wjsc.v4.i6.53 (2012).

29 Jiang, W. & Xu, J. Immune modulation by mesenchymal stem cells. *Cell proliferation* **53**, e12712, doi:10.1111/cpr.12712 (2020).

30 Zhou, Y., Yamamoto, Y., Xiao, Z. & Ochiya, T. The Immunomodulatory Functions of Mesenchymal Stromal/Stem Cells Mediated via Paracrine Activity. *Journal of clinical medicine* **8**, doi:10.3390/jcm8071025 (2019).

31 Doorn, J., Moll, G., Le Blanc, K., van Blitterswijk, C. & de Boer, J. Therapeutic applications of mesenchymal stromal cells: paracrine effects and potential improvements. *Tissue engineering. Part B, Reviews* **18**, 101-115, doi:10.1089/ten.TEB.2011.0488 (2012).

32 Jiazhao, Y. *et al.* in *Stromal Cells* (ed T. Valarmathi Mani) Ch. 9 (IntechOpen, 2018).

33 Guo, Y., Yu, Y., Hu, S., Chen, Y. & Shen, Z. The therapeutic potential of mesenchymal stem cells for cardiovascular diseases. *Cell death & disease* **11**, 349, doi:10.1038/s41419-020-2542-9 (2020).

34 Joyce, N. *et al.* Mesenchymal stem cells for the treatment of neurodegenerative disease. *Regenerative medicine* **5**, 933-946, doi:10.2217/rme.10.72 (2010).

35 Figueroa, F. E., Carrión, F., Villanueva, S. & Khoury, M. Mesenchymal stem cell treatment for autoimmune diseases: a critical review. *Biological research* **45**, 269-277, doi:10.4067/s0716-97602012000300008 (2012).

36 Wang, Y., Chen, X., Cao, W. & Shi, Y. Plasticity of mesenchymal stem cells in immunomodulation: pathological and therapeutic implications. *Nature immunology* **15**, 1009-1016, doi:10.1038/ni.3002 (2014).

37 Bieback, K., Schallmoser, K., Klüter, H. & Strunk, D. Clinical Protocols for the Isolation and Expansion of Mesenchymal Stromal Cells. *Transfusion medicine and hemotherapy : offizielles Organ der Deutschen Gesellschaft fur Transfusionsmedizin und Immunhamatologie* **35**, 286-294, doi:10.1159/000141567 (2008).

38 Naji, A. *et al.* Biological functions of mesenchymal stem cells and clinical implications. *Cellular and molecular life sciences : CMLS* **76**, 3323-3348, doi:10.1007/s00018-019-03125-1 (2019).

39 Sensebé, L., Krampera, M., Schrezenmeier, H., Bourin, P. & Giordano, R. Mesenchymal stem cells for clinical application. **98**, 93-107, doi:https://doi.org/10.1111/j.1423-0410.2009.01227.x (2010).

40 Khubutiya, M. S., Vagabov, A. V., Temnov, A. A. & Sklifas, A. N. Paracrine mechanisms of proliferative, anti-apoptotic and anti-inflammatory effects of mesenchymal stromal

cells in models of acute organ injury. *Cytotherapy* **16**, 579-585, doi:10.1016/j.jcyt.2013.07.017 (2014).

41 Doorn, J., Moll, G., Le Blanc, K., van Blitterswijk, C. & de Boer, J. Therapeutic Applications of Mesenchymal Stromal Cells: Paracrine Effects and Potential Improvements. *Tissue Engineering Part B: Reviews* **18**, 101-115, doi:10.1089/ten.teb.2011.0488 (2011).

42 Salami, F., Tavassoli, A., Mehrzad, J. & Parham, A. Immunomodulatory effects of mesenchymal stem cells on leukocytes with emphasis on neutrophils. *Immunobiology* **223**, 786-791, doi:10.1016/j.imbio.2018.08.002 (2018).

43 Uccelli, A., Moretta, L. & Pistoia, V. Mesenchymal stem cells in health and disease. *Nature reviews. Immunology* **8**, 726-736, doi:10.1038/nri2395 (2008).

44 Bernardo, M. E. & Fibbe, W. E. Mesenchymal stromal cells: sensors and switchers of inflammation. *Cell stem cell* **13**, 392-402, doi:10.1016/j.stem.2013.09.006 (2013).

45 Keating, A. Mesenchymal stromal cells: new directions. *Cell stem cell* **10**, 709-716, doi:10.1016/j.stem.2012.05.015 (2012).

46 Dunn, C. M. *et al.* Interferon-Gamma Primed Human Clonal Mesenchymal Stromal Cell Sheets Exhibit Enhanced Immunosuppressive Function. *Cells* **11**, doi:10.3390/cells11233738 (2022).

47 Mándi, Y. & Vécsei, L. The kynurenine system and immunoregulation. *Journal of Neural Transmission* **119**, 197-209, doi:10.1007/s00702-011-0681-y (2012).

48 Vacaru, A. M. *et al.* Enhanced Suppression of Immune Cells In Vitro by MSC Overexpressing FasL. *International journal of molecular sciences* **22**, doi:10.3390/ijms22010348 (2020).

49 Davies, L. C., Heldring, N., Kadri, N. & Le Blanc, K. Mesenchymal Stromal Cell Secretion of Programmed Death-1 Ligands Regulates T Cell Mediated Immunosuppression. *Stem cells (Dayton, Ohio)* **35**, 766-776, doi:10.1002/stem.2509 (2017).

50 Ortiz, L. A. *et al.* Interleukin 1 receptor antagonist mediates the antiinflammatory and antifibrotic effect of mesenchymal stem cells during lung injury. *Proceedings of the National Academy of Sciences of the United States of America* **104**, 11002-11007, doi:10.1073/pnas.0704421104 (2007).

51 Niu, J., Yue, W., Le-Le, Z., Bin, L. & Hu, X. Mesenchymal stem cells inhibit T cell activation by releasing TGF-β1 from TGF-β1/GARP complex. *Oncotarget* **8**, 99784-99800, doi:10.18632/oncotarget.21549 (2017).

52 Zhang, Q. Z. *et al.* Human gingiva-derived mesenchymal stem cells elicit polarization of m2 macrophages and enhance cutaneous wound healing. *Stem cells (Dayton, Ohio)* **28**, 1856-1868, doi:10.1002/stem.503 (2010).

53 Zanier, E. R. *et al.* Bone marrow mesenchymal stromal cells drive protective M2 microglia polarization after brain trauma. *Neurotherapeutics : the journal of the American Society for Experimental NeuroTherapeutics* **11**, 679-695, doi:10.1007/s13311-014-0277-y (2014).

54 Li, X. *et al.* Dysfunction of metabolic activity of bone marrow mesenchymal stem cells in aged mice. *Cell proliferation* **55**, e13191, doi:10.1111/cpr.13191 (2022).

55 Casati, S. *et al.* Bioactive Lipids in MSCs Biology: State of the Art and Role in Inflammation. *International journal of molecular sciences* **22**, doi:10.3390/ijms22031481 (2021).

56 Das, U. N. Bioactive Lipids as Mediators of the Beneficial Action(s) of Mesenchymal Stem Cells in COVID-19. *Aging and disease* **11**, 746-755, doi:10.14336/ad.2020.0521 (2020).

57 McCartney, A. *et al.* Metabolomics in breast cancer: A decade in review. *Cancer Treatment Reviews* **67**, 88-96, doi:https://doi.org/10.1016/j.ctrv.2018.04.012 (2018).

58 Ren, J.-L., Zhang, A.-H., Kong, L. & Wang, X.-J. Advances in mass spectrometry-based metabolomics for investigation of metabolites. *RSC Advances* **8**, 22335-22350, doi:10.1039/C8RA01574K (2018).

59 Gowda, G. A. N. & Djukovic, D. in *Mass Spectrometry in Metabolomics: Methods and Protocols* (ed Daniel Raftery) 3-12 (Springer New York, 2014).

60 O'Donnell, V. B., Ekroos, K., Liebisch, G. & Wakelam, M. Lipidomics: Current state of the art in a fast moving field. *Wiley interdisciplinary reviews. Systems biology and medicine* **12**, e1466, doi:10.1002/wsbm.1466 (2020).

61 Sethi, S. & Brietzke, E. Recent advances in lipidomics: Analytical and clinical perspectives. *Prostaglandins & other lipid mediators* **128-129**, 8-16, doi:10.1016/j.prostaglandins.2016.12.002 (2017).

62 Fahy, E., Cotter, D., Sud, M. & Subramaniam, S. Lipid classification, structures and tools. *Biochimica et Biophysica Acta (BBA) - Molecular and Cell Biology of Lipids* **1811**, 637-647, doi:https://doi.org/10.1016/j.bbalip.2011.06.009 (2011).

63 Lu, X. *et al.* Integrated Lipidomics and Transcriptomics Characterization upon Aging-Related Changes of Lipid Species and Pathways in Human Bone Marrow Mesenchymal Stem Cells. *Journal of Proteome Research* **18**, 2065-2077, doi:10.1021/acs.jproteome.8b00936 (2019).

64 Kilpinen, L. *et al.* Aging bone marrow mesenchymal stromal cells have altered membrane glycerophospholipid composition and functionality. *Journal of lipid research* **54**, 622-635, doi:10.1194/jlr.M030650 (2013).

65 Gharibi, B. & Hughes, F. J. Effects of medium supplements on proliferation, differentiation potential, and in vitro expansion of mesenchymal stem cells. *Stem cells translational medicine* **1**, 771-782, doi:10.5966/sctm.2010-0031 (2012).

66 Chatgilialoglu, A. *et al.* Restored in vivo-like membrane lipidomics positively influence in vitro features of cultured mesenchymal stromal/stem cells derived from human placenta. *Stem cell research & therapy* **8**, 31, doi:10.1186/s13287-017-0487-4 (2017).

67 Chatgilialoglu, A. *et al.* Restored in vivo-like membrane lipidomics positively influence in vitro features of cultured mesenchymal stromal/stem cells derived from human placenta. *Stem cell research & therapy* **8**, 31, doi:10.1186/s13287-017-0487-4 (2017).

68 Campos, A. M. *et al.* Lipidomics of Mesenchymal Stromal Cells: Understanding the Adaptation of Phospholipid Profile in Response to Pro-Inflammatory Cytokines. *Journal of cellular physiology* **231**, 1024-1032, doi:10.1002/jcp.25191 (2016).

69 Danielyan, L. *et al.* Cell motility and migration as determinants of stem cell efficacy. *EBioMedicine* **60**, 102989, doi:10.1016/j.ebiom.2020.102989 (2020).

70 Si, Y. L., Zhao, Y. L., Hao, H. J., Fu, X. B. & Han, W. D. MSCs: Biological characteristics, clinical applications and their outstanding concerns. *Ageing research reviews* **10**, 93-103, doi:10.1016/j.arr.2010.08.005 (2011).

71 Choi, J. R., Yong, K. W. & Wan Safwani, W. K. Z. Effect of hypoxia on human adipose-derived mesenchymal stem cells and its potential clinical applications. *Cellular and molecular life sciences : CMLS* **74**, 2587-2600, doi:10.1007/s00018-017-2484-2 (2017).

72 Eseonu, O. I. & De Bari, C. Homing of mesenchymal stem cells: mechanistic or stochastic? Implications for targeted delivery in arthritis. *Rheumatology (Oxford, England)* **54**, 210-218, doi:10.1093/rheumatology/keu377 (2015).

73 Zhang, Q. *et al.* Growth factors contribute to the mediation of angiogenic capacity of glioma-associated mesenchymal stem cells. *Oncology letters* **21**, 215, doi:10.3892/ol.2021.12476 (2021).

74 Li, Y. *et al.* Insulin-like growth factor 1 enhances the migratory capacity of mesenchymal stem cells. *Biochemical and biophysical research communications* **356**, 780-784, doi:10.1016/j.bbrc.2007.03.049 (2007).

75 Marklein, R. A. *et al.* High Content Imaging of Early Morphological Signatures Predicts Long Term Mineralization Capacity of Human Mesenchymal Stem Cells upon Osteogenic Induction. *Stem cells (Dayton, Ohio)* **34**, 935-947, doi:10.1002/stem.2322 (2016).

76 Matsuoka, F. *et al.* Characterization of time-course morphological features for efficient prediction of osteogenic potential in human mesenchymal stem cells. *Biotechnology and bioengineering* **111**, 1430-1439, doi:10.1002/bit.25189 (2014).

77 Sasaki, K. *et al.* Non-invasive quality evaluation of confluent cells by image-based orientation heterogeneity analysis. *Journal of bioscience and bioengineering* **121**, 227-234, doi:10.1016/j.jbiosc.2015.06.012 (2016).

78 Sasaki, H. *et al.* Label-free morphology-based prediction of multiple differentiation potentials of human mesenchymal stem cells for early evaluation of intact cells. *PloS one* **9**, e93952, doi:10.1371/journal.pone.0093952 (2014).

79 Oja, S., Komulainen, P., Penttilä, A., Nystedt, J. & Korhonen, M. Automated image analysis detects aging in clinical-grade mesenchymal stromal cell cultures. *Stem cell research & therapy* **9**, 6, doi:10.1186/s13287-017-0740-x (2018).

80 Singh, S., Carpenter, A. E. & Genovesio, A. Increasing the Content of High-Content Screening: An Overview. *Journal of biomolecular screening* **19**, 640-650, doi:10.1177/1087057114528537 (2014).

81 Bertolo, A. *et al.* In vitro cell motility as a potential mesenchymal stem cell marker for multipotency. *Stem cells translational medicine* **4**, 84-90, doi:10.5966/sctm.2014-0156 (2015).

82 Kim, G. *et al.* High throughput screening of mesenchymal stem cell lines using deep learning. *Scientific reports* **12**, 17507, doi:10.1038/s41598-022-21653-y (2022).

83 Lee, W. C. *et al.* Multivariate biophysical markers predictive of mesenchymal stromal cell multipotency. *Proceedings of the National Academy of Sciences of the United States of America* **111**, E4409-4418, doi:10.1073/pnas.1402306111 (2014).

84 Mason, C., Brindley, D. A., Culme-Seymour, E. J. & Davie, N. L. Cell therapy industry: billion dollar global business with unlimited potential. *Regenerative medicine* **6**, 265-272, doi:10.2217/rme.11.28 (2011).

85 Fischbach, M. A., Bluestone, J. A. & Lim, W. A. Cell-based therapeutics: the next pillar of medicine. *Science translational medicine* **5**, 179ps177, doi:10.1126/scitranslmed.3005568 (2013).

86 Rao, M., Mason, C. & Solomon, S. Cell therapy worldwide: an incipient revolution. *Regenerative medicine* **10**, 181-191, doi:10.2217/rme.14.80 (2015).

87 Pereira Chilima, T. D., Moncaubeig, F. & Farid, S. S. Impact of allogeneic stem cell manufacturing decisions on cost of goods, process robustness and reimbursement. *Biochemical Engineering Journal* **137**, 132-151, doi:https://doi.org/10.1016/j.bej.2018.04.017 (2018).

88 Phelps, J., Sanati-Nezhad, A., Ungrin, M., Duncan, N. A. & Sen, A. Bioprocessing of Mesenchymal Stem Cells and Their Derivatives: Toward Cell-Free Therapeutics. *Stem cells international* **2018**, 9415367, doi:10.1155/2018/9415367 (2018).

89 Kusuma, G. D., Carthew, J., Lim, R. & Frith, J. E. Effect of the Microenvironment on Mesenchymal Stem Cell Paracrine Signaling: Opportunities to Engineer the Therapeutic Effect. *Stem cells and development* **26**, 617-631, doi:10.1089/scd.2016.0349 (2017).

90 Teixeira, F. G. & Salgado, A. J. Mesenchymal stem cells secretome: current trends and future challenges. *Neural regeneration research* **15**, 75-77, doi:10.4103/1673-5374.264455 (2020).

91 Galipeau, J. Mesenchymal Stromal Cells for Graft-versus-Host Disease: A Trilogy. *Biology of Blood and Marrow Transplantation* **26**, e89-e91, doi:https://doi.org/10.1016/j.bbmt.2020.02.023 (2020).

92 Bagno, L., Hatzistergos, K. E., Balkan, W. & Hare, J. M. Mesenchymal Stem Cell-Based Therapy for Cardiovascular Disease: Progress and Challenges. *Molecular Therapy* **26**, 1610-1623, doi:https://doi.org/10.1016/j.ymthe.2018.05.009 (2018).

93 Adak, S., Mukherjee, S., Sen, D. J. C. S. C. R. & Therapy. Mesenchymal stem cell as a potential therapeutic for inflammatory bowel disease-myth or reality? **12**, 644-657 (2017).

94 Galderisi, U., Peluso, G. & Di Bernardo, G. Clinical Trials Based on Mesenchymal Stromal Cells are Exponentially Increasing: Where are We in Recent Years? *Stem cell reviews and reports* **18**, 23-36, doi:10.1007/s12015-021-10231-w (2022).

95 Costa, L. A. *et al.* Functional heterogeneity of mesenchymal stem cells from natural niches to culture conditions: implications for further clinical uses. *Cellular and molecular life sciences : CMLS* **78**, 447-467, doi:10.1007/s00018-020-03600-0 (2021).

96 Planat-Benard, V., Varin, A. & Casteilla, L. MSCs and Inflammatory Cells Crosstalk in Regenerative Medicine: Concerted Actions for Optimized Resolution Driven by Energy Metabolism. *Frontiers in immunology* **12**, 626755, doi:10.3389/fimmu.2021.626755 (2021).

97 McLeod, C. M. & Mauck, R. L. On the origin and impact of mesenchymal stem cell heterogeneity: new insights and emerging tools for single cell analysis. *European cells & materials* **34**, 217-231, doi:10.22203/eCM.v034a14 (2017).

98 Burk, J. *et al.* Phospholipid Profiles for Phenotypic Characterization of Adipose-Derived Multipotent Mesenchymal Stromal Cells. *Frontiers in cell and developmental biology* **9**, 784405, doi:10.3389/fcell.2021.784405 (2021).

99 Bennett, J. M., Reeves, G., Billman, G. E. & Sturmberg, J. P. Inflammation-Nature's Way to Efficiently Respond to All Types of Challenges: Implications for Understanding and Managing "the Epidemic" of Chronic Diseases. *Frontiers in medicine* **5**, 316, doi:10.3389/fmed.2018.00316 (2018).

100 Raphael, I., Joern, R. R. & Forsthuber, T. G. Memory CD4(+) T Cells in Immunity and Autoimmune Diseases. *Cells* **9**, doi:10.3390/cells9030531 (2020).

101 Bagchi, S., Yuan, R. & Engleman, E. G. Immune Checkpoint Inhibitors for the Treatment of Cancer: Clinical Impact and Mechanisms of Response and Resistance. *Annual review of pathology* **16**, 223-249, doi:10.1146/annurev-pathol-042020-042741 (2021).

102 Chen, Y., Yu, Q., Hu, Y. & Shi, Y. Current Research and Use of Mesenchymal Stem Cells in the Therapy of Autoimmune Diseases. *Current stem cell research & therapy* **14**, 579-582, doi:10.2174/1574888x14666190429141421 (2019).

103 Tyndall, A. & Houssiau, F. A. Mesenchymal stem cells in the treatment of autoimmune diseases. *Annals of the rheumatic diseases* **69**, 1413-1414, doi:10.1136/ard.2010.132639 (2010).

104 Nassiri, I. & McCall, M. N. Systematic exploration of cell morphological phenotypes associated with a transcriptomic query. *Nucleic acids research* **46**, e116, doi:10.1093/nar/gky626 (2018).

105 Mattiazzi Usaj, M. *et al.* Systematic genetics and single-cell imaging reveal widespread morphological pleiotropy and cell-to-cell variability. *Molecular systems biology* **16**, e9243, doi:10.15252/msb.20199243 (2020).

106 Galipeau, J. *et al.* Mesenchymal stromal cell variables influencing clinical potency: the impact of viability, fitness, route of administration and host predisposition. *Cytotherapy* **23**, 368-372, doi:10.1016/j.jcyt.2020.11.007 (2021).

107 Fernandis, A. Z. & Wenk, M. R. Lipid-based biomarkers for cancer. *Journal of chromatography. B, Analytical technologies in the biomedical and life sciences* **877**, 2830-2835, doi:10.1016/j.jchromb.2009.06.015 (2009).

108 Hinterwirth, H., Stegemann, C. & Mayr, M. Lipidomics: quest for molecular lipid biomarkers in cardiovascular disease. *Circulation. Cardiovascular genetics* **7**, 941-954, doi:10.1161/circgenetics.114.000550 (2014).

# CHAPTER 2

# INTEGRATED LIPIDOMIC, MORPHOLOGICAL PHENOTYPIC AND SECRETED ANALYTES CHARACTERIZATION UPON AGING-RELATED CHANGES OF LIPID SPECIES IN HUMAN BONE MARROW MESENCHYMAL STEM CELLS

---

Priyanka Priyadarshani, Rebecca S. Schneider, Andrés J. García, and Luke J. Mortensen.
*To be submitted to Scientific Reports.*

# Abstract

Human mesenchymal stem/stromal cells (hMSCs) are versatile cell in various clinical applications, notably immune regulation, hematopoietic stem cell engraftment, and tissue repair. Despite their immunomodulatory potential, the long-term expansion of hMSCs can compromise their functionality. Lipids have recently gained significance, but systematic investigations into their role and changes during expansion are lacking. This study investigates the evolving lipidomic profile of culture-expanded hMSCs from early to late passages, revealing changes in lipid metabolites with cell aging. The research establishes connections between alterations in cellular lipid composition and overall functionality, correlating these changes with cell morphology and cytokine secretion. Such insights are crucial as the role of lipids in stem cell physiology and the consequences of extended cell expansion remain relatively less explored. This research contributes to a deeper understanding of hMSC behavior and their potential for clinical use.

## 2.1 Introduction

Human mesenchymal stem/stromal cells (hMSCs) are currently under study in various clinical contexts. These include enhancing the engraftment of hematopoietic stem cell transplants, facilitating myocardial repair, and regulating immunological reactions in conditions such as graft versus host diseases, autoimmune disorders, and organ transplants[1-3].

In addition to holding immunological privilege, these cells can regulate both innate and adaptive immune responses both *in vitro* and within living organisms *in vivo*. hMSCs have demonstrated their capacity to restrain the proliferation of T-cells, impede the maturation of dendritic cells, attract regulatory T-cells, and influence the activities of B-cells. Several studies have demonstrated that direct cell-to-cell interactions and the release of soluble factors is essential for the immune regulation of MSCs[4,5]. Various substances such as cytokines[6], growth factors[7], enzymes[8], and lipid mediators[9] have been identified as pivotal participants in the immunomodulation process. However, the extended period of cell expansion can lead to loss of soluble factors and has been associated with potential negative impacts on the multiplication, differentiation potential, and other functional attributes of precursor cells[10,11].

In recent years lipid has emerged as a crucial field of study for understanding cellular physiology and pathology[12]. A central query within MSC therapy pertains to determining the extent of cell divisions these cells can undergo before the prospects of cellular dysfunction or even malignant transformation emerge. As of now, only a limited number of studies have explored into the lipids present in stem cell membranes, with systematic investigations into alterations in lipid composition during the expansion process remaining lacking.

Lipids are being developed as biomarker to disease phenotype in translational research [13,14]. As in other cells, MSCs lipid play integral part in cell signaling and immunity. New approaches

are emerging to examine alterations in the complex lipid profiles of stem cells using advanced mass spectrometry and imaging methods. These strategies can establish the connections between these compositional changes and altered potency and quality of the cells.

Thus, this research focuses on characterizing the lipidomic profile of culture expanded MSCs from the early passage to late passage demonstrating changes in lipid metabolites with cell aging. The lipidomic profile of various stages of cell aging is correlated with cell morphology and cytokine secretion, aiming to enhance comprehension of potential connections between alterations in cellular lipid composition and overall functionality.

## 2.2 Results

### 2.2.1 MSCs morphology and potency changes over multiple passages

As cells undergo successive passages, their morphological features, including size and shape, can undergo notable alterations. To investigate these changes in mesenchymal stem cells (MSCs) throughout multiple passages, we designed an experimental setup. We cultured these cells on specialized slides coated with indium titanium oxide (ITO) equipped with an attached gasket well system. The cells were systematically subjected to passaging every 2 to 3 days, and at each passage, we captured images, that extended up to passage 7 (Figure 2.1A). These acquired images were then analyzed through a segmentation process utilizing the CellProfiler pipeline (reference), enabling us to extract morphological features for each passage. The resulting data was visually represented through a principal component analysis (PCA) plot, revealing a conspicuous shift in the morphological characteristics of the MSCs with each successive passage (Figure 2.1B). This observation demonstrates that as cells age through successive passages, there is a substantial

variance in their morphological attributes, which can have significant implications for their biological functions.

Further we sought to assess the impact of cellular aging on the functional properties of MSCs. In particular, we focused on the activity of indoleamine 2,3-dioxygenase (IDO), a key enzyme known to play a critical role in immune modulation and tissue repair. Previous research has indicated that MSCs exhibiting higher IDO activity tend to possess greater functional potential. Our experimental findings unveiled a trend: the IDO activity in MSCs increased steadily in early passages and subsequently displayed a declining trend around late passages (Figure 2.1C). This observation underscores the dynamic nature of MSCs during their lifespan in culture and highlights the importance of understanding these changes to harness their therapeutic potential effectively.

### 2.2.2 Lipid and cytokine secretion of MSCs changes with the passage

We successfully identified a comprehensive total of 89 lipids for each passage through the application of FTICR. To gain deeper insights into the dynamic shifts in lipid composition as MSCs pass through different passages, we employed a Uniform Manifold Approximation and Projection (UMAP) model, utilizing the entire set of identified lipids. The resulting UMAP plot unveiled distinct patterns: passages 3 and 4 and 5, representing early stages, clustered closely together, while late passages 7,9, and 12 exhibited a similar proximity (Figure 2.2A).

To provide a more precise characterization of the differential trends and significance of lipid species between early, and late passage MSCs, we employed volcano plots with a cutoff of a 2-fold change. These plots highlighted the most distinctive lipid species differentiating between early passage and late passage. It's noteworthy that in the transitions between early and late passage many of the identified lipids were prevalent in early passage, indicating a potential enrichment of

lipid species during the early stage and decline in specific lipid species as MSCs progressed from early to late passages. The majority of the lipid species including LPC, PC, CerP, PG, SM, and PI were upregulated in early passage while lipid species mostly including PE were where upregulated in late passage (Figure 2.2B). Mostly PC with higher fatty chain were differentially higher in early passage and PC with shorter fatty acid chain were higher in late passage. Mostly PE species were shown to be expressed higher in late passage.

These findings provide valuable insights into the evolving lipid profiles and functional dynamics of MSCs during their different passages, shedding light on their potential applications in regenerative medicine and other fields. Along with changes in lipids and morphological features in aging MSCs we also detected changes alterations in secretion of inflammatory cytokines in culture expanded MSCs. We found an increase in pro-inflammatory cytokines like CCL2, VEGF, and IL12, with a reduction in immune-modulatory cytokines like IFN-ɣ, TIMP-1, and HGF (Figure 2.2C).

### 2.2.3 Lipid metabolite showed correlation with morphology and analyte secretion.

After observing significant alterations in the morphological characteristics and cytokine secretion of aging MSCs, our subsequent investigation delved into the exploration of correlation patterns within the lipidomic profiles of these MSCs in relation to their morphological features and cytokine secretions. We conducted an analysis employing Pearson's correlation coefficients to assess the relationships between the lipidomic profile and the morphological features of the MSCs. We then extended this analysis to explore correlations between the lipidomic profile and cytokine secretion. The results of these correlations revealed several intriguing insights. Notably, a positive

correlation emerged between various morphological features, including area, compactness, diameter, length, and perimeter, and the levels of bioactive lipids belonging to the LPC, PC, SM, PI, PS, and PG lipid families. Conversely, we observed a negative correlation between certain morphological characteristics such as extent, eccentricity, form factor, radius, and solidity and the abundance of these bioactive lipids (Figure 2.3A). Moreover, Pearson's correlation demonstrates the positive and negative correlation between bioactive lipids and cytokine secretions (Figure 2.3B). These findings illuminate the intricate interplay between the lipidomic profile, morphological attributes, and cytokine secretions within aging MSCs, shedding light on potential mechanisms underpinning their functional changes during the aging process.

## 2.3 Discussion

Mesenchymal stem cells (MSCs) have been the subject of extensive research due to their remarkable ability to modulate the immune system, making them promising candidates for the treatment of inflammatory disorders[16,17]. However, the function of MSCs decline as the cells age. Several studies have pointed out cell senescence as one of the major causes of loss of cell functionality. The process has been known to be strongly associated with oxidative stress[18] regulation of p53-p21and p16-RB pathways, and mitochondrial dysfunction. Downregulation of immunosuppressive molecule PD-L1 is also shown to have influence on the progressive MSCs cell aging[19]. Recently lipids have been shown to be highly associated with cell function and are integral components of cellular structures and processes[12]. While it is well-established that downstream metabolites, especially different lipid species, can significantly impact the metabolism of MSCs in various biological contexts, there is a very few study examining alterations in lipids as bone marrow derived MSCs (BMSCs) undergo the aging process. Hence, this current

investigation aims to elucidate the comprehensive alterations in lipid profiles and associated metabolic pathways occurring throughout the aging of BMSCs. In this study, our objective is to shed light on the lipidomics alteration that could potentially influence the functional capabilities of BMSCs during aging process and how these changes are associated with the change in their morphological profile and cytokine secretion.

Our study demonstrates that higher level of PC lipid species mostly with longer FAs chains were expressed in early passage along with PC with shorter FAs chain late passage. It was previously shown that MSCs reaching towards senescence have less immunosuppressive capacity, showed the same pattern of deviation regarding PC species with shorter FAs chains[20]. PC accounts for approximately 50% of the total cellular lipid content and serves as a primary component within eukaryotic cells, primarily playing a structural role[21,22]. As a result, it is unlikely that PC molecular variations directly participate in the immunosuppressive mechanisms of MSCs. However, we estimate that these alterations signify structural adaptations that occur in MSCs when exposed to expansion stress and lose their immunosuppressive capacity. These changes in PC which bring structural changes also signify with our result that demonstrates correlation of alteration in lipid species with the changes in morphological features of MSCs. Several studies of shown association morphological features with the immunosuppressive capacity of MSCs[23,24]. We also observed an increased level of LPC and SM in the early passage. Previous study has shown higher level of LPC and SM in more functional MSCs. LPC 18:0 assumes a pivotal role in the immunomodulatory mechanism utilized by MSCs. Sphingolipids represent fundamental constituents of cellular lipid membranes and lipid rafts. Consequently, alterations in sphingolipid metabolism can lead to lipid membranes and lipid rafts exhibiting distinct properties, potentially disrupting receptor clustering[25-27].

Further our study demonstrated the association of change lipid metabolites with the cytokine secretion. Studies have demonstrated the association of lipids and cytokines, particularly certain types of lipids including SM and Ceramide play a role in the regulation of cytokine production and the immune response in the body. Cytokines are small signaling proteins that play a crucial role in cell-to-cell communication in the immune system and are involved in various physiological processes, including inflammation and immune response[28,29].

## 2.4 Conclusion

In this research, we conducted a comprehensive analysis of lipidomics profiling in sequential passages of BMSCs to investigate how the metabolic landscape of different lipid species changes during the aging process. Our multivariate analysis unveiled a dynamic and reversible pattern in BMSCs as they underwent successive passaging. The majority of lipid types, such as PC, LPC, SM, Cer, and PG were up-regulated, while a minority of lipid species in PC and PE, exhibited a decrease in late-passage BMSCs. Along with the lipid species we also observed changes in the morphological features and cytokine secretion of MSCs. Our correlation analysis reveals the association of lipids with morphology and cytokine secretions. Correlating these changes with cell morphology and cytokine secretion provides insights into the interplay between lipid alterations and cellular functionality, addressing critical questions regarding the safety and efficacy of hMSC expansion and therapeutic applications.

## 2.5 Methods

### 2.5.1 Cell culture

Human bone marrow derived MSCs were obtained from commercially available vender RoosterBio and were expanded and seeded in standard serum containing media. (Millipore Sigma). Culture well gasket of well size 6mm diameter and 1mm depth (Grace Bio-labs) was used on top of ITO slide to hold cells and media. The cells were seeded at the density of 3000 cells per well. MSCs were expanded within passage 2-12 (~12-26 population doubling) to evaluate metabolic changes with increasing passages.

### 2.5.2 MALDI FT-ICR to obtain lipidomic profile of the cell

Mass spectrometry experiment was performed on Solarix FT-ICR equipped with an infinity ICR cell and a MALDI ionization using a SmartBeam II UV laser (Bruker Daltonics, Bremen, Germany). Measurements were done in the positive ion mode with raster width 300μm using norharmane matrix. The mass spectral data was preprocessed in SCiLS Lab (SCiLS GmbH, Bremen, Germany) software. Baseline removal was performed during data import using iterative convolution and Root-Mean-Square (RMS) normalization done in SCiLS.

### 2.5.3 DPC imaging

Cell imaging was performed on ITO coated slide culture as described above. The images were sourced using an illumination based DPC microscope system. The illumination source include 32x32 (4mm pitch) RGB LED matrix panel (product ID 607, Adafruit) controlled by an Arduino

Uno (Arduino.cc) with LED set to hex color #1AFF00, sourced with a light of a broad spectrum around the nominal wavelength of 514 nm. A 10x objective lens (Plan Fluor, Nikon) placed in the chassis of an inverted microscope collected the light relaying the image onto an sCMOS camera (Zyla 4.2, Andor) which is conjugated to the sample plane.

### 2.5.4 Secretome analysis

Multiplex ELISA-based Luminex assay to assess the analyte secretion of MSCs expanded culture. Luminex 24-plex panels, customized for our study, were acquired from R&D Biotech. The analytes chosen for this analysis (n=20) are analytes relevant to MSC *in vivo* secretion[30]. After 24hrs of seeding, cell supernatant was collected for Luminex protein analysis. The Luminex assay was performed without dilution and as per the manufacturer's recommendations.

### 2.5.5 Dimensionality reduction using UMAP and correlation analysis

The processed data matrix consisting of the measurements for 89 lipids for each passage (Passage 3, 4, 5, 7, 9, 12) stimulated with IFN-γ was used for dimensionality reduction using UMAP with the following parameters: n_neighbors=5, min_dist=0.6 and metric=euclidean. Correlation analysis was performed using Pearson's correlation coefficients were calculated between lipid and morphological features and lipid and cytokine secretion of the IFN-γ stimulated MSCs.

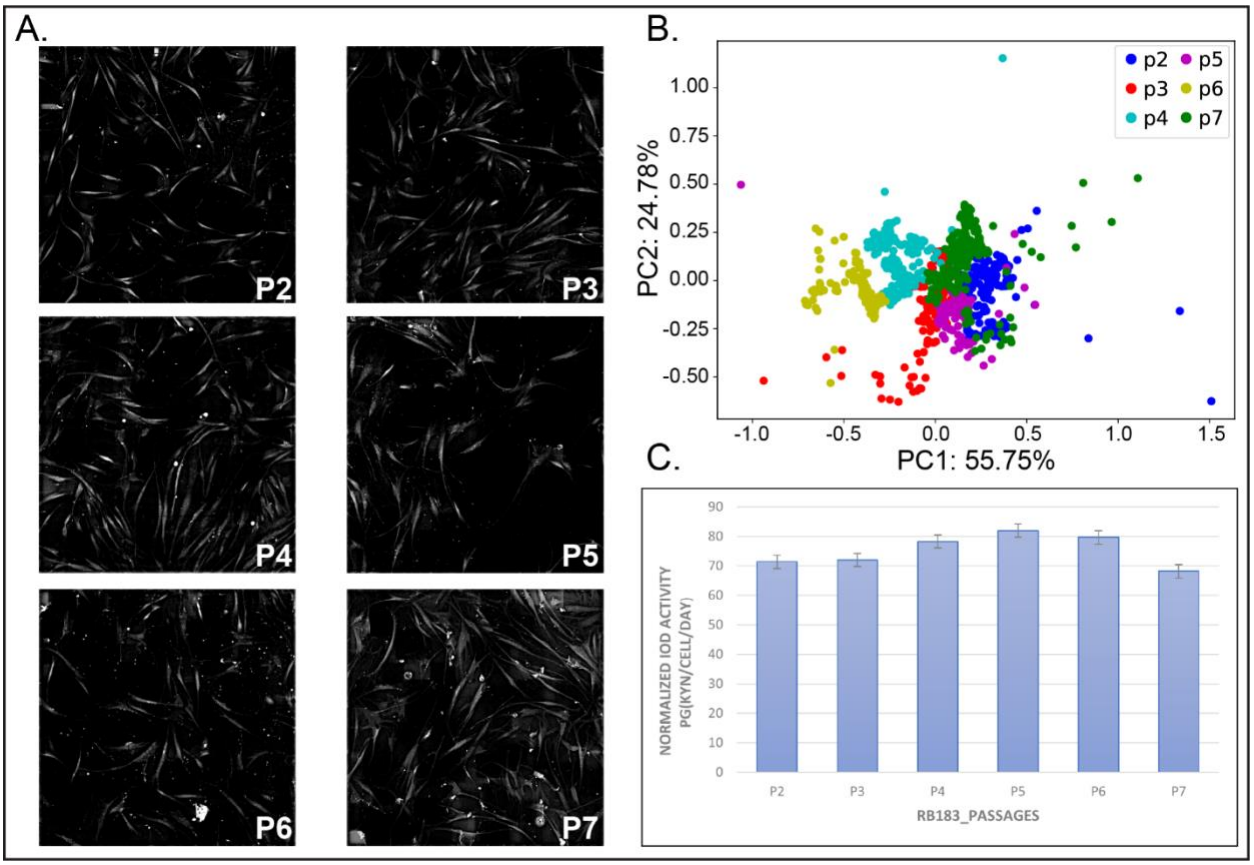


**Figure 2.1: Multiple passages of MSCs show change in morphological featues and IDO activity.** (A) DPC images show MSCs from early pasaage to late passage. (B) PCA plot showing shift in morphological features of MSCs over multiple passages. (C) Bar plot showing changes in IDO activity of MSCs over multiple passages.

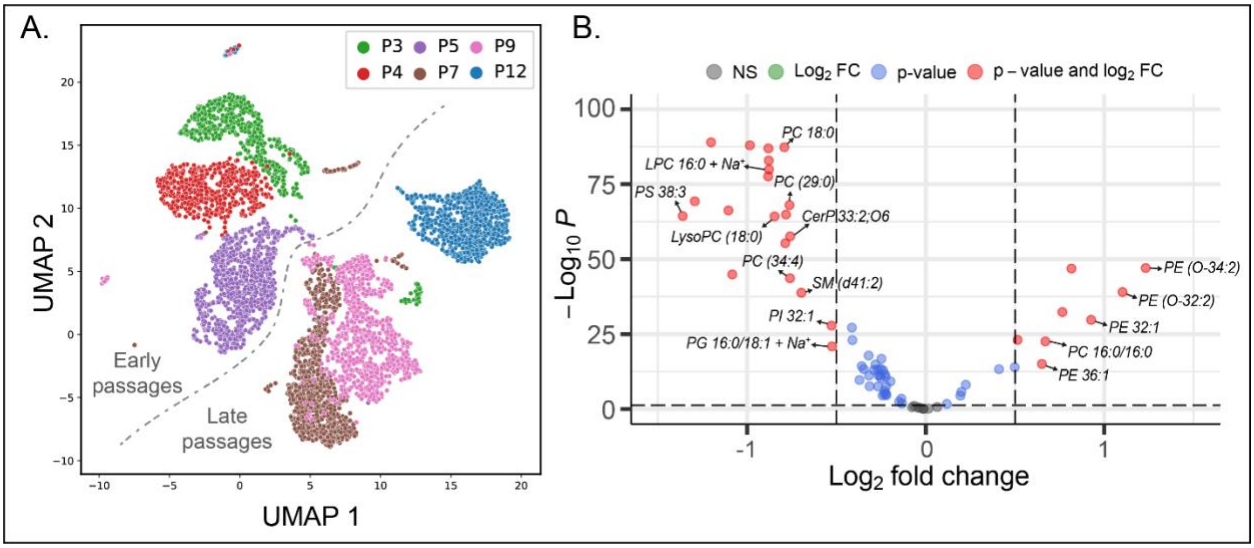


**Figure 2.2: Alteration of lipid profile in aging MSCs**. (A) UMAP shows clustering of MSCs based on the lipid profile. Early passages (Passage 3, 4, and 5) and late passages (passage 7, 9, and 12) show a clear separation indicated by the dotted gray line. (B) Volcano plot showing differentially expressed lipid in early passage (passage 3, left) and late passage (passage 9, right).

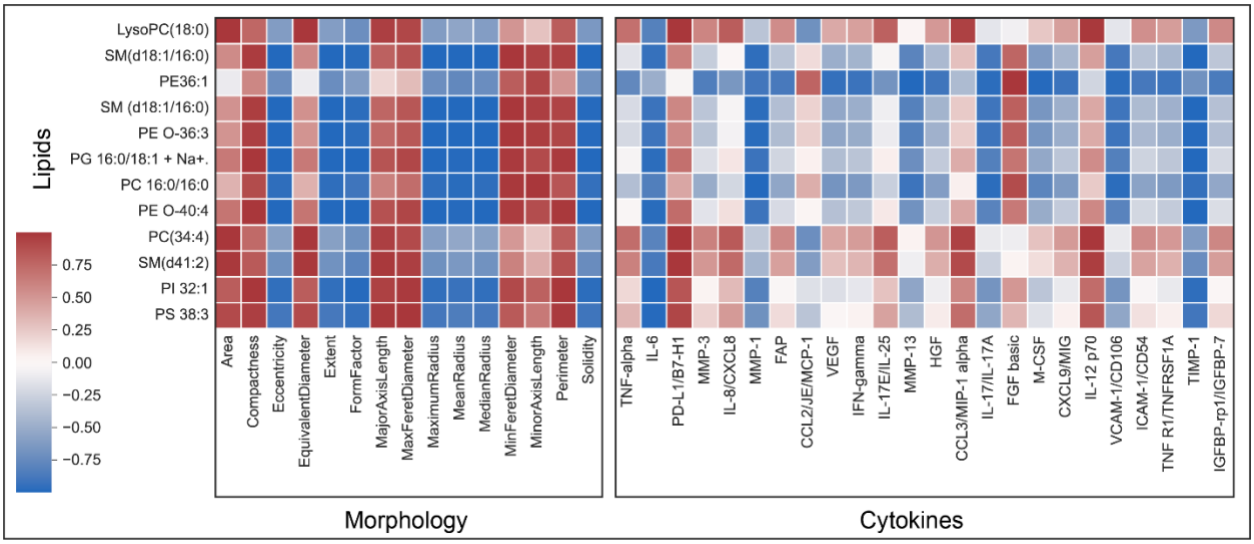


**Figure 2.3: Correlation of lipids with morphology and Cytokines.** Pearson's correlation map showing association of lipidomic profile of MSCs with the morphological features (left) and cytokine secretion (right).

## 2.6 Bibliography


1 Zhao, L., Chen, S., Yang, P., Cao, H. & Li, L. The role of mesenchymal stem cells in hematopoietic stem cell transplantation: prevention and treatment of graft-versus-host disease. *Stem cell research & therapy* **10**, 182, doi:10.1186/s13287-019-1287-9 (2019).

2 Pittenger, M. F. *et al.* Mesenchymal stem cell perspective: cell biology to clinical progress. *NPJ Regenerative medicine* **4**, 22, doi:10.1038/s41536-019-0083-6 (2019).

3 Bagno, L., Hatzistergos, K. E., Balkan, W. & Hare, J. M. Mesenchymal Stem Cell-Based Therapy for Cardiovascular Disease: Progress and Challenges. *Molecular therapy : the journal of the American Society of Gene Therapy* **26**, 1610-1623, doi:10.1016/j.ymthe.2018.05.009 (2018).

4 Müller, L. *et al.* Immunomodulatory Properties of Mesenchymal Stromal Cells: An Update. *Frontiers in cell and developmental biology* **9**, 637725, doi:10.3389/fcell.2021.637725 (2021).

5 Song, N., Scholtemeijer, M. & Shah, K. Mesenchymal Stem Cell Immunomodulation: Mechanisms and Therapeutic Potential. *Trends in pharmacological sciences* **41**, 653-664, doi:10.1016/j.tips.2020.06.009 (2020).

6 Simon, F. *Immunomodulatory cytokines: directing and controlling immune activation*. (Arthritis Res Ther. 2011;13(Suppl 2):O14. doi: 10.1186/ar3418. Epub 2011 Sep 16.).

7 Mindur, J. E. & Swirski, F. K. Growth Factors as Immunotherapeutic Targets in Cardiovascular Disease. *Arteriosclerosis, thrombosis, and vascular biology* **39**, 1275-1287, doi:10.1161/atvbaha.119.311994 (2019).

8 Farhadi, S. A., Bracho-Sanchez, E., Freeman, S. L., Keselowsky, B. G. & Hudalla, G. A. Enzymes as Immunotherapeutics. *Bioconjugate chemistry* **29**, 649-656, doi:10.1021/acs.bioconjchem.7b00719 (2018).

9 Shimizu, T. Lipid mediators in health and disease: enzymes and receptors as therapeutic targets for the regulation of immunity and inflammation. *Annual review of pharmacology and toxicology* **49**, 123-150, doi:10.1146/annurev.pharmtox.011008.145616 (2009).

10 Schultz, M. B. & Sinclair, D. A. When stem cells grow old: phenotypes and mechanisms of stem cell aging. *Development (Cambridge, England)* **143**, 3-14, doi:10.1242/dev.130633 (2016).

11 Liu, J., Ding, Y., Liu, Z. & Liang, X. Senescence in Mesenchymal Stem Cells: Functional Alterations, Molecular Mechanisms, and Rejuvenation Strategies. **8**, doi:10.3389/fcell.2020.00258 (2020).

12 Casati, S. *et al.* Bioactive Lipids in MSCs Biology: State of the Art and Role in Inflammation. *International journal of molecular sciences* **22**, doi:10.3390/ijms22031481 (2021).

13 Fernandis, A. Z. & Wenk, M. R. Lipid-based biomarkers for cancer. *Journal of Chromatography B* **877**, 2830-2835, doi:https://doi.org/10.1016/j.jchromb.2009.06.015 (2009).

14 Hinterwirth, H., Stegemann, C. & Mayr, M. Lipidomics: quest for molecular lipid biomarkers in cardiovascular disease. *Circulation. Cardiovascular genetics* **7**, 941-954, doi:10.1161/circgenetics.114.000550 (2014).

15 Carpenter, A. E. *et al.* CellProfiler: image analysis software for identifying and quantifying cell phenotypes. *Genome biology* **7**, R100, doi:10.1186/gb-2006-7-10-r100 (2006).

16 Jiang, W. & Xu, J. Immune modulation by mesenchymal stem cells. *Cell proliferation* **53**, e12712, doi:10.1111/cpr.12712 (2020).

17 Castro-Manrreza, M. E. & Montesinos, J. J. Immunoregulation by mesenchymal stem cells: biological aspects and clinical applications. *Journal of immunology research* **2015**, 394917, doi:10.1155/2015/394917 (2015).

18 Lee, S. S., Vũ, T. T., Weiss, A. S. & Yeo, G. C. Stress-induced senescence in mesenchymal stem cells: Triggers, hallmarks, and current rejuvenation approaches. *European Journal of Cell Biology* **102**, 151331, doi:https://doi.org/10.1016/j.ejcb.2023.151331 (2023).

19 Gao, Y. *et al.* Multi-omics analysis of human mesenchymal stem cells shows cell aging that alters immunomodulatory activity through the downregulation of PD-L1. *Nature communications* **14**, 4373, doi:10.1038/s41467-023-39958-5 (2023).

20 Kilpinen, L. *et al.* Aging bone marrow mesenchymal stromal cells have altered membrane glycerophospholipid composition and functionality. *Journal of lipid research* **54**, 622-635, doi:10.1194/jlr.M030650 (2013).

21 van Meer, G. Cellular lipidomics. *The EMBO journal* **24**, 3159-3165, doi:10.1038/sj.emboj.7600798 (2005).

22 Cole, L. K., Vance, J. E. & Vance, D. E. Phosphatidylcholine biosynthesis and lipoprotein metabolism. *Biochimica et biophysica acta* **1821**, 754-761, doi:10.1016/j.bbalip.2011.09.009 (2012).

23 Marklein, R. A. *et al.* Morphological profiling using machine learning reveals emergent subpopulations of interferon-γ-stimulated mesenchymal stromal cells that predict immunosuppression. *Cytotherapy* **21**, 17-31, doi:10.1016/j.jcyt.2018.10.008 (2019).

24 Klinker, M. W., Marklein, R. A., Lo Surdo, J. L., Wei, C. H. & Bauer, S. R. Morphological features of IFN-γ-stimulated mesenchymal stromal cells predict overall immunosuppressive capacity. *Proceedings of the National Academy of Sciences of the United States of America* **114**, E2598-e2607, doi:10.1073/pnas.1617933114 (2017).

25 Campos, A. M. *et al.* Lipidomics of Mesenchymal Stromal Cells: Understanding the Adaptation of Phospholipid Profile in Response to Pro-Inflammatory Cytokines. *Journal of cellular physiology* **231**, 1024-1032, doi:10.1002/jcp.25191 (2016).

26 Olivera, A. & Rivera, J. Sphingolipids and the balancing of immune cell function: lessons from the mast cell. *Journal of immunology (Baltimore, Md. : 1950)* **174**, 1153-1158, doi:10.4049/jimmunol.174.3.1153 (2005).

27 Yan, J. J. *et al.* Therapeutic effects of lysophosphatidylcholine in experimental sepsis. *Nature medicine* **10**, 161-167, doi:10.1038/nm989 (2004).

28 Nixon, G. F. Sphingolipids in inflammation: pathological implications and potential therapeutic targets. *British journal of pharmacology* **158**, 982-993, doi:10.1111/j.1476-5381.2009.00281.x (2009).

29 Lee, M., Lee, S. Y. & Bae, Y. S. Functional roles of sphingolipids in immunity and their implication in disease. *Experimental & molecular medicine* **55**, 1110-1130, doi:10.1038/s12276-023-01018-9 (2023).

30 Schneider, R. S. *et al.* High-Throughput On-Chip Human Mesenchymal Stromal Cell Potency Prediction. *Advanced healthcare materials* **11**, e2101995, doi:10.1002/adhm.202101995 (2022).

# CHAPTER 3

# INTEGRATION OF IMAGING MODALITIES WITH LIPIDOMIC CHARACTERIZATION TO INVESTIGATE SINGLE-CELL MSCS POTENCY METRICS

Priyanka Priyadarshani, Alexandria Van Grouw, Adrian Ross Liversage, Kejie Rui, Arina Nikitina, Kayvan Forouhesh Tehrani, Bhavay Aggarwal, Steven L. Stice, Saurabh Sinha, Melissa L. Kemp, Facundo M. Fernández, and Luke J. Mortensen.
*Submitted to Science Advances, November 10, 2023*.

# Abstract

MSC therapies have had limited success so far in clinical trials due in part to heterogeneity in immune-responsive phenotypes. Therefore, techniques to enable evaluation of MSC immune activity and heterogeneity are needed during biomanufacturing. Imaging cell shape, or morphology, has been found to be associated with MSC immune suppressive activity- but a direct relationship between single-cell morphology and function has not been established. We hypothesize that morphological features are closely linked to lipid metabolic profiles and used matrix-assisted laser desorption/ionization mass spectrometry imaging (MALDI-MSI) to evaluate single-cell lipid metabolic response to immune stimulation, with label-free Differential Phase Contrast (DPC) imaging of cell morphology. We found that IFN-γ stimulated MSCs showed a higher expression of lipids from the ceramide phosphate(C1P), phosphatidylcholine (PC), lysophosphatidylcholine (LysoPC), and triglyceride (TAG) families, which are involved in pathways leading to cell survival, proliferation, and differentiation. Furthermore, morphological features correlated with lipid signaling and dynamic cell functions such as migration rate. The predictive relationship between MSC morphological features and functional lipids can be used to select immunocompetent MSCs for potential clinical use.

## 3.1 Introduction

Mesenchymal stem/stromal cells (MSCs) can dampen the body's immune response, providing therapeutic potential for the treatment of autoimmune and inflammatory diseases[1,2]. When stimulated with the pro-inflammatory cytokine interferon-gamma (IFN-γ), MSCs have been shown to effectively inhibit T-cell proliferation and effector function[3]. However, MSCs from different tissue sources, donors, or expansion levels exhibit a varying degree of immunosuppressive response to IFN-γ. This heterogeneous functional response reduces therapeutic efficacy and complicates their use in regenerative applications[4]. To create an effective therapeutic product, evaluation of MSC immune activity is needed during the biomanufacturing process. Some of the most well-accepted methods for quality control and release criteria include cytokine secretion profiles, T-cell proliferation assays, and the activity of the key enzyme indoleamine-2-3-dioxygenase (IDO). However, these assays fail to capture intrapopulation functional heterogeneity and have challenges with reproducibility and specificity, so they have not been widely adopted as markers of cell quality in translational biomanufacturing.

Recently, an alternative approach of imaging cell shape, or morphology, has been also found to be associated with MSC immune suppressive activity and differentiation[5,6].Cell morphology provides a snapshot of underlying cell activities such as migration, cell-cell contact, proliferation, and apoptosis[7]. These processes that involve changes in cell architecture also involve alterations in the lipid plasma cell membrane. More generally, the cell membrane is known to change its lipid content dynamically in response to stimuli like immune activation[8,9]. Recent studies interrogating MSC immune suppressive mechanisms have identified changes in a range of membrane lipid classes including sphingolipids (*e.g.* ceramides), phospholipids (*e.g.* PC, LPC), and glycerolipids (*e.g.* TAG)[10,11] with roles in inflammatory signaling and structural membrane characteristics[12].

Although cell phenotypes like morphology, adhesion, and migration are associated with specific lipid pathways, MSC lipid profiling has so far been limited to bulk cell analyses during activation[8] or differentiation[13] –limiting mechanistic understanding of single-cell phenotypes found within heterogeneous MSC cultures. Therefore, in this work we study single-cell lipid signaling and morphological features with a goal of generating insights into the mechanisms of single-cell variation amongst these cells to understand sources of functional heterogeneity and enhance clinical efficacy.

We developed a study pipeline to simultaneously obtain and link the morphological features and lipidomic profiles of single-cell MSCs using two label-free imaging techniques: DPC microscopy to obtain morphology of MSCs, and MALDI-MSI to obtain a lipidomic profile from the same monolayer MSC culture. Using these methods, we show that the morphological features that change during IFN-γ stimulation are also correlated with the activation of specific classes of lipids. A subset of these morphological features and lipids exhibits single-cell heterogeneity within the culture. Moreover, these phenotypic features are found to be associated with MSC activities such as migration rate via live image analysis. These findings provide evidence for a close association between a subset of structural and signaling lipids and cell morphology that can be used as a marker for functionally active MSC subpopulations and improve their quality for regenerative applications.

## 3.2 Results

### 3.2.1 Coregistration of DPC and MALDI-MS images to link phenotype and lipidome of single-cell MSCs

To explore single-cell correlations between morphology and lipid metabolic profile response to immune stimulus, we created an integrated workflow for sequential imaging and analysis of cell features. Two batches of MSCs were seeded on a MALDI Indium Tin Oxide (ITO) slide fitted with an attached gasket well system. Cells in these wells were either stimulated with IFN-γ or left untreated as a control (Figure 3.1A). We created rapid mosaic images of the MSCs in each whole well at <1um spatial resolution using a home-built quantitative DPC imaging system for rapid label-free non-destructive analysis of morphological cell features and longitudinal live cell imaging. DPC imaging illuminates the sample from four different angles with low light levels and so has minimal impact on cell health or biological function while generating rich cell morphology information. Immediately after imaging, cell culture media was removed from the slides and slides were placed on ice for transport with subsequent matrix deposition and MALDI-MSI analysis (Figure 3.1B). Preliminary experiments found that this procedure preserved cell position and morphology without any additional reagents that might disrupt cell molecular state or lipid content.

We then created a pipeline for linking the microscopically observable single-cell MSC phenotype to its lipidome. We modified a coregistration approach[14] previously developed by Nikitina *et al.* to computationally superimpose whole well DPC and MALDI-MS images of identical wells with iterative optimization of scaling, alignment, and cropping (Figure 3.1C). Once image alignment was completed, each pixel contained phase intensity as well as the full MALDI mass spectrum. The final registered images were then segmented in the phase channel using a

CellProfiler pipeline, yielding single-cell multichannel feature sets with phase morphological features like size, shape, phase intensity, and texture (Table 3.1) along with abundance of the series of detected lipid peaks for both stimulated and unstimulated single-cell MSCs.

### 3.2.2 Label-free imaging shows heterogeneity and a shift in MSC morphology with IFN-γ stimulation

After DPC and MALDI imaging, coregistration, and segmentation protocols, single-cell phase morphology exterior and interior intensity features for both control and IFN-γ stimulated MSCs (Figure 3.2A,B) were scaled using a min-max scaler and variance explored with Principal Component Analysis (PCA). The resulting morphology data in the PCA plot showed a clear separation between IFN-γ stimulated and unstimulated single-cell MSCs (Figure 3.2C). Key morphological features contributing to this inter-group variance are summarized in (Figure 3.2D). Our label-free DPC imaging features yielded similar trends in morphological changes of MSCs upon IFN-γ stimulation as prior work with fluorescently stained cells[5].

Although there was a separation between the two groups along PC1, which explains ~66% of the variance in the data, we observed an overlap of the cell treatment groups in PC space, suggesting that the cell morphologies and the observed response to IFN-γ stimulation is heterogeneous within each culture. Furthermore, we observed a broad, nearly bimodal distribution of some cell morphological phenotypes within the IFN-γ stimulated MSCs (Figure 3.2E), indicating that subpopulations of less immune-responsive MSCs may exist within a given culture.

### 3.2.3 Single-cell lipid analysis obtained from MALDI-MSI show significant differences in abundances between stimulated and unstimulated MSCs

Following analysis of non-invasive DPC imaging, we re-analyzed the same slides using MALDI-MSI for metabolite profiling of lipids at a single-cell level. To enable single-cell MALDI-MSI, parameters were carefully optimized (see methods). A total of 54 specific lipid peaks were extracted from the spectral data, which were used to create corresponding MS images (Figure 3.3A) for each chosen *m/z* value of interest within single MSCs for both IFN-γ stimulated and unstimulated MSCs. Lipid-specific images were false colored based on lipid abundance, which highlighted differences in abundances between groups as well as within each plate. Overall, these MALDI-MSI results suggested a variegated, rather than homogeneous, response of individual cells to IFN-γ stimulation for a number of lipids.

Upon obtaining lipid ion abundances from each MALDI image for each single-cell, we found 23 lipid species that were significantly higher in IFN-γ stimulated cells and 6 that were significantly higher in controls. The remaining 25 MALDI ions were not significantly changed between the two groups (Table 3.2). Further, to identify the most differential lipids in control and IFN-γ stimulated groups, we applied an additional cutoff of 2-fold change as shown in the volcano plot (Figure 3.3B). This yielded 9 lipids defined as differentially detected in IFN-γ stimulated cells and 5 in untreated cells. We also built a logistic regression classifier to identify the top discriminant lipid species (Table 3.3). We found substantial overlap between the top 10 lipids from logistic regression and the lipids identified in the volcano plot. These peaks were consistent in both of our tested experimental batches. To provide further confirmation, we evaluated the abundance of key lipids identified in Figure 3.3B that were expressed higher in IFN-γ stimulated cells in an additional

replicate of donor RB183 and two other bone marrow MSC cell lines from Rooster Bio (RB175 and RB37); finding similar trends for each (Figure 3.4).

We next performed PCA on the matrix of differentially expressed lipid abundances of IFN-γ treated versus untreated cells. Each of the two treatment groups across two separate experimental batches formed a tight group within Hotelling's confidence ellipse, indicating that there is a small but detectable batch-to-batch variance in MALDI-MSI data following normalization. Overall, ~83% variance across treatment groups was explained by the first two PC (Figure 3.3C). While variance within the subpopulation of MSCs was mostly explained by PC1, the separation between stimulated and unstimulated groups occurred mainly along PC2. The lipids contributing to the separation along PC2 are indicated by their PC2 loadings (Figure 3.3D).

We projected PC2 scores back to single-cells in the well using color coding to observe spatial patterning and heterogeneity and found that cells had varying lipid profiles, confirming the heterogeneous activation of cells after treatment with IFN-γ (Figure 3.3E). We then evaluated the spatial patterning of lipid features to look for regions with potentially synergistic lipid profiles in neighboring cells using a SpatialDE[15] approach. Although we did not detect spatial patterning in single-cell PC2 values or in MSC morphological features, we did observe statistically significant spatial patterning of individual lipids with differential expression in untreated and IFN-γ stimulated cells (Table 3.4), which suggests future directions to explore lipid regulation more closely in neighboring cells.

To annotate the differentially-expressed *m/z* peaks detected by ultrahigh resolution MALDI-MSI in control and IFN-γ stimulated cells, we performed UHPLC-MS/MS analysis in a high resolution tribrid mass spectrometer that provide higher confidence in lipid annotations, with additional confirmation from previously published literature[16,17]. Lipids at *m/z* 688.4, 546.3, 758.6,

789.6, 732.6, 780.5, 749.5, 804.6, and 504.3 were the most differentially expressed in IFN-γ stimulated MSCs. These belonged to the C1P, LysoPC, PC, and TAG families. Lipids at *m/z* 542.5, 725.6,703.6, 798.6, and 810.7 were the most differentially expressed in non-stimulated control cells, all belonging to the sphingomyelin (SM), C1P, and PC families.

Having confirmed the identity of differentially expressed *m/*z lipid peaks, we next performed lipid pathway analysis using LIPEA. We combined the resulting enriched pathways from LIPEA with literature reports to describe the resulting lipid classes and their cellular functions (Figure 3.5). Results showed that PC and LPC, major components of the cell membrane, are initiators for a cascade that leads to cell proliferation, differentiation, and protein synthesis[18-20]. The generated arachidonic acid from PLA-2 stimulates sphingomyelinase activity which, in turn, catalyzes the hydrolysis of sphingomyelins to generate ceramides[21]. Further downstream, the phosphorylation of ceramides results in C1P lipids, which are an important class of metabolites with anti-apoptotic properties that are important mediators of cell migration and inflammatory response[22]. The other detected lipid family of TAG molecules are synthesized in the endoplasmic reticulum and hydrolyzed to release glycerol and fatty acids. Both metabolic products of TAG breakdown are vital for cellular function since glycerol is used for energy production and synthesis of cell membrane phospholipids, whereas fatty acids are major factors in immune cell differentiation[23,24].

### 3.2.4 Correlated morphological and lipid phenotypes predict heterogeneity in IFN-γ stimulated MSCs

We next explored correlation patterns in single-cell MSC immune responses between unique morphological and phase intensity features from the DPC dimension and matching lipid abundances from MALDI spectra. Pearson's correlation coefficients were calculated between

morphological features and the IFN-γ stimulation shift in lipid abundances encoded into the MALDI-MSI PC2 values (Figure 3.6A). In IFN-γ stimulated cells, MSC morphological features including compactness, form factor, perimeter, solidity, major axis length, and max feret diameter showed a high correlation with lipid shift PC2 values. Interestingly, the correlation with lipid PC2 values was weaker in unstimulated cells.

Associations between IFN-γ stimulated MSC morphological phenotypes and lipid signaling based on Pearson's correlation analysis highlights trends in immune response of MSCs. Our data and prior literature[4] have suggested the existence of morphological subpopulations within MSC cultures, so we next investigated the existence of cell heterogeneity and lipid prevalence in subpopulations of immune-stimulated MSCs. UMAP dimensionality reduction using morphological measures with agglomerative clustering in the resulting UMAP components revealed a clear separation of the cells into three distinct morphological clusters (Figure 3.6B).

We observed a significant difference in several morphological features across the three clusters. Clusters 1 and 2 included cells with a significantly higher perimeter, compactness, major-axis length, and max-feret diameter; the same features that had a positive correlation with PC2 lipid data. Additionally, cells in these two clusters exhibited lower solidity, extent, and formfactor; morphological features that had a negative correlation with PC2 lipid data. In contrast, cells in cluster 3 showed an opposite trend (Figure 3.6E). The remaining morphological features did not show a similar pattern across the three clusters (Figure 3.7). This is in agreement with our observation that these variables do not show any correlation with PC2 lipid data.

We also traced back the cluster assignments of each cell to their original phase image by color coding to examine the spatial distribution of the single-cell MSCs in the image belonging to each cluster (Figure 3.6D). The color coding based on cluster assignment shows elongated, compact,

and less circular (medium and large sized) MSCs belonging to clusters 1 (orange color) and 2 (green color) and more circular and irregular (smaller in size) MSCs belonging to cluster 3 (magenta color).

To further evaluate if the same morphological features also correlated with the functional activity of the cell, we performed a linear regression of the morphological features of IFN-γ stimulated MSCs with their migration rate obtained via live imaging. It is well established that migration rate reflects cell morphogenesis and cell signaling ability[26]. Regression analysis revealed similar positive and negative trends for the morphological features as those in the PC2 lipid data (Figure 3.8).

Next, we investigated whether the significant differences in morphological phenotypes across these 3 cell clusters also resulted in differences in lipid phenotypes, as suggested by the correlation results. To this end, we mapped lipid abundances to show the spatial distribution of lipids in each cluster for each cell and performed an ANOVA test followed by a post hoc Tukey's HSD test for pairwise comparisons. Figure 3.6C shows representative lipids abundances from each of the PC, LysoPC, TAG, and CerP family that were highly differentiated in IFN-γ stimulated cells for each cluster. Based on this test, we found that lipid abundances from the TAG and PC classes were significantly higher in clusters 1 and 2 compared to cluster 3 (Figure 3.6F, Figure 3.9), suggesting that cell-to-cell heterogeneity in these lipids is closely associated with morphology. This analysis did not reveal a significant difference in C1P lipids in any of the clusters, suggesting that C1P levels were not associated with morphology (Figure 3.6B,E). Based on the relationship between MSC morphology and some of the differential lipids, we hypothesized that label-free non-destructive morphology of IFN-γ stimulated MSCs could be used for prediction of single-cell lipid phenotypes. Using a random forest-based regression model, we found that, indeed, morphology

was predictive of changes in lipids induced by IFN-γ stimulation (Figure 3.6G, Figure 3.10), supporting the potential of phase imaging to provide insight into MSC metabolic signatures.

## 3.3 Discussion

Despite intense interest over the past 10 years in preclinical models and clinical trials[25], MSC-based cell therapies have so far failed to gain approval for human use in the United States. One major challenge has been creating large quantities of culture expanded MSC with uniformly effective immune suppressive behavior. In an attempt to address this situation and enhance cell behavior, a number of so-called "priming" approaches have exposed MSCs to pharmaceuticals[26] or cytokines[27] during the manufacturing process. A cytokine required for the immune function of MSCs is IFN-γ, without which the cells are unable to block immune cell proliferation[27]. Therefore, priming with IFN-γ has become a common method to boost MSC functional behavior[28]. However, MSC functional properties vary between tissue sources, donors, isolation methods, expansion levels, and even within individual cell populations[4,29]. The variability between individual cells in a population is a manufacturing challenge (i.e., all cells are not uniformly functional), but it also provides a unique opportunity to illuminate pathways critical for immune response, since other potentially confounding factors like donor, media formulation, tissue origin, etc. are eliminated. Single-cell analysis techniques increase accuracy when investigating heterogeneous cell populations[30], and in MSCs this has begun to elucidate specific differences within and across different subpopulations of cells. In this work, we probe single-cell lipid metabolic profiles of MSCs responding to an immune stimulus and couple this technique to spatial analysis of cultures together with label-free non-destructive microscopy.

Imaging a snapshot of cell phenotype using morphology readouts has been correlated with key features of bio-manufactured MSC quality such as immune suppressive activity, proliferation rates, and differentiation[31,32]. Here, we leveraged single-cell MALDI lipid imaging to directly correlate individual cell morphological and lipidomic profile differences between IFN-γ stimulated and non-stimulated MSCs. We identified 7 morphological features of IFN-γ modulated MSCs including perimeter, compactness, major axis length, max-feret diameter, solidity, formfactor, and compactness that were correlated with the bioactive lipids identified. These features have been previously shown to be associated with immune function[5] and involved in the migration, proliferation and signaling of MSCs[7]. In our data, we confirmed an association between MSC migration rate and cell morphology, suggesting potential for future studies exploring more extensively the relationship between single-cell functional behaviors, morphology, and lipid network profiles.

Along with morphological features describing cell sizes and shapes, we found key lipids from the PC, LysoPC, C1P, and TAG classes that had a significantly higher expression in IFN-γ stimulated cells. These lipids play a crucial role in immune cell differentiation, proliferation, and signaling. For example, PCs lead to the formation of lipid rafts[33], which have roles in initiating the secretion of immune modulatory cytokines and in receptor-mediated immune responses through Toll-like receptors (TLRs), c-type lectin receptors (CLRs), and B cell antigen receptor (BCR) signaling[34,35]. Similarly, LysoPCs are involved in gene transcription, mitogenesis that regulate cell signaling and membrane remodeling[36],[37]. Another differentially detected lipid class, C1P, is part of sphingolipid metabolism with a key role in immune cell regulation and function[38]. Overall, the higher presence of these lipids in IFN-γ stimulated MSCs is consistent with increased immune regulation.

To further illustrate the utility of morphology-lipid associations in identifying functionally potent cells, we applied UMAP dimensionality reduction followed by agglomerative clustering to identify 3 distinct clusters of IFN-γ stimulated MSC subpopulations. We found that clusters 1 and 2 had a distinct morphological and lipidomic profile associated with enhanced immune activity, characterized by a higher perimeter, compactness, major axis length, and max feret diameter along with high levels of PC, LysoPC, and TAG lipids. In previous literature, PCs and LPCs are some of the most important lipid classes that contribute to membrane organization and cell signaling. PC constitute around 60% of the cell membrane and a reduction in PC abundance causes growth arrest and apoptosis[39]. Since only a small subset of cells undergo these processes at a given time it is not unexpected to observe similarly heterogeneous detected quantities of PCs in cell subpopulations. Interestingly, we did not observe any significant differences in the C1P class of lipids among the three clusters. C1P is involved in a variety of cellular processes, including cell proliferation, differentiation, and apoptosis, but it has dual role as a secondary messenger through transmission of intracellular signals and involved in chemotaxis functions[22,40]. Since it functions as a signaling molecule that is not primarily membrane bound it may be more evenly distributed among cells. Collectively, this indicates that these identified MSC morphological features combined with their correlated lipid profile signatures could distinguish the most immunogenically potent MSC cells from a heterogenous subpopulation, which can be used for the selection and further expansion of functional cells.

## 3.4 Conclusion

In summary, by clustering heterogeneous subpopulations of IFN-γ stimulated MSC cells, we demonstrate correlated simultaneous changes in morphological features and lipid molecules that

can be used to identify and select a more functionally uniform subpopulation of MSCs. This separation method presents a viable strategy for addressing the issue of heterogeneity and the large-scale selection and production of MSCs with uniformly effective immune suppressive behavior for therapeutic and clinical use. Furthermore, phase microscopy can be performed on large sample sizes under different culture conditions, which makes it applicable to solve heterogeneity issues in other cell types that are currently being explored for therapeutic use as well. Our proposed method also holds opportunities for non-destructive, label-free analysis of cell morphology for prediction of metabolites to understand the biological process of the cell. Thus, this approach along with the associated morphological and lipid profiles identified in this study marks a significant stride toward the large-scale production of potent MSCs for clinical applications and therapeutic use.

## 3.5 Methods

### 3.5.1 Cell culture

Human mesenchymal stem cells (hMSCs) (RB183 from RoosterBio) were seeded on an ITO-coated slide (Millipore Sigma) under standard culture conditions. A culture well gasket with 6 mm diameter and 1 mm depth (Grace Bio-labs) was used on top of the ITO slides to hold cells and media in place. Cells were seeded at a density of 1200 cells per well ensuring that each well culture started with an equal number of cells. A total of 4 wells were seeded accounting for two different batches of cells and 2 wells per batch. The cells were grown in MEM alpha medium (Thermo Fisher Scientific) supplemented with 10% fetal bovine serum (FBS), 1% penicillin/streptomycin, and 0.5% of L-glutamine. The cultured cells were incubated with 5% $CO_2$ at 37 $^0$C for 24 hours. After 24 hours of incubation, one well per batch was replaced by a conditioned media having 50

ng/ml IFN-γ (for IFN-γ stimulated cell cultures) while the other well per batch was just replaced with fresh regular culture media (for control cell cultures). Then, the cells were subjected to imaging after being incubated for an additional 24 hours.

### 3.5.2 Cell imaging and whole well DPC image construction and segmentation

Cell imaging was performed on all 4 culture wells described above. The images were sourced using an illumination-based DPC microscope system as described in[41-43]. The illumination source is a 32x32 (4mm pitch) RGB LED matrix panel (product ID 607, Adafruit) controlled by an Arduino Uno (Arduino.cc) with LED set to hex color #1AFF00, which provides light of a broad spectrum around the nominal wavelength of 514 nm (Figure 3.11). A 10x objective lens (Plan Fluor, Nikon) placed in the chassis of an inverted microscope collected the light relaying the image onto an sCMOS camera (Zyla 4.2, Andor) which is conjugated to the sample plane.

To ensure large fields of view of the cells, sub-images of each whole well were captured using a 10X objective lens to focus on the fixed area of the well. Individual DPC images with a field of view of 1.3 $mm^2$ were captured sequentially, as an X-Y stage automatically moved in steps of 1 mm, capturing 49 sub-images (7x7) in total, accounting for the whole circular well with a 6 mm diameter. Once the DPC reconstruction of each sub-image was completed, the central 1 $mm^2$ (where the unused 0.3 mm in both X and Y was discarded) of each sub-image was stitched together, using the built-in “Make Montage” function in Image-J, reconstructing the whole well image. This process was repeated for each well.

Composite whole well DPC images were segmented using an image analysis pipeline in customized CellProfiler pipeline. The whole well DPC image was analyzed as the primary object in cell profiler. A global threshold strategy with a robust background thresholding method was

used to identify the cell outline in the image. Overall, 21 MSCs features including morphology, phase intensity, and texture features were extracted for each stimulated and unstimulated MSC.

### 3.5.3 Statistical analysis of DPC image dataset

The morphological features collected using CellProfiler[44] were scaled using the MinMaxScaler [45] function in sci-kit learn 0.23.2 package in Python 3.9, followed by taking a randomized 15 window rolling mean separately for stimulated and non-stimulated groups. This processed dataset was passed to the PCA function (sklearn.decomposition.PCA) to determine the principal components that separated the stimulated and unstimulated cells. Further, log fold change was calculated for all 21 morphological features to determine the magnitude of their changes. To illustrate heterogeneity within each of the morphological features, the scaled values were plotted as violin plots.

### 3.5.4 MALDI sample preparation

Following DPC imaging, ITO slides with cell monolayers were prepared for MALDI MS imaging. Norharmane matrix was deposited on the ITO slides using a sublimation method. The slide was secured to the bottom of the sublimation apparatus condenser, while solid norharmane was placed at the bottom of the apparatus. Sublimation was performed at 250 $^{0}$C under a vacuum for 6 minutes.

### 3.5.5 MALDI imaging and data collection

MALDI-MSI was performed in positive ion mode on a RapifleX Tissuetyper time-of-flight mass spectrometer (Bruker, Daltonics) equipped with a Smartbeam3D 10 kHz Nd:YAG (355 nm) laser. To control imaging settings, FlexImaging 4.0 software was used. To control pixel size, the smart

beam laser setting (~5 μm in both x and y dimensions) with a laser raster size of 10 μm in both x and y dimensions was selected. Mass calibration was performed prior to data collection with red phosphorus as the calibrant. Preprocessing of the mass spectral data was performed in SCiLS Lab (SCiLS GmbH, Bremen, Germany) software. Baseline removal was performed during data import using iterative convolution and Root-Mean-Square (RMS) normalization done in SCiLS. SCiLS lab was used to isolate the lipid spectra of single-cell using the polygon tool. Only the peaks present within the cells were used to create a peak list. MSI images in SCiLS were exported in imzML and ibd formats for further processing and were imported into Python using a custom script.

An ultrahigh resolution Bruker solariX 12-Tesla Fourier transform ion cyclotron resonance (FTICR) mass spectrometer was used to obtain higher mass resolution MS1 data on the lipids of interest. MS/MS data with sufficient quality for annotation confirmation was not achievable due to spectral overlaps. To provide higher confidence in lipid annotations, UHPLC-MS/MS data was also collected using a tribrid Orbitrap ID-X mass spectrometer (ThermoFisher Scientific). MSC cell pellets from the study were subjected to lipid extraction using isopropanol and cell lysis using glass bead homogenization. Cell lysate lipid extracts were dried and concentrated into 200 μL isopropanol for UHPLC-MS/MS analysis. Reverse phase separation was employed with an Accucore C30 column (2.1 × 150 mm, 2.6 μm particle size) on a Vanquish (ThermoFisher Scientific) liquid chromatograph. Data-dependent acquisition (DDA) was employed to yield fragmentation information for lipids of interest. Collision energies of 15%, 30%, and 45% were employed with HCD and CID 35% to collect MS2 spectra. UHPLC data was preprocessed in Compound Discoverer 3.3 (Thermo Fisher Scientific) with drift correction and blank removal. Not all peaks present in the MALDI imaging dataset were detected in the UHPLC dataset, resulting in

some peaks of interest annotated at a confidence level of 2, while others are annotated with a confidence level of 3.

### 3.5.6 Multimodal image coregistration and segmentation

Datasets obtained from DPC and MALDI imaging experiments were aligned using a coregistration pipeline developed by Nikitina *et. al* in Python[14]. The pixel size of the DPC image (~1 µm) and MALDI ion image (~10 µm) was used as a baseline for scaling, which the script performed together with shift and tilt optimization to minimize error of alignment between the images. After alignment, the images were cropped to the same size by alignment matching the regions. The location and region of each cell were matched in both images.

Following alignment and cropping, all MSC morphological features were obtained from DPC images, and lipid abundances for the same cell were obtained from the MALDI ion images using a customized pipeline in CellProfiler (https://github.com/LukeMortensen/SingleCellMSCpotency). DPC images were analyzed as primary objects and MALDI ion images were analyzed as secondary objects. A global threshold strategy with a robust background thresholding method was used to identify the cell outline in the image.

### 3.5.7 Statistical analysis of the MALDI-MSI dataset

For the MALDI lipid dataset, the abundances at each *m/z* value were first normalized by standard deviation and scaled using a min-max scaler. A Student's t-test (n=66) was performed to determine the highly expressed lipids in IFN-γ stimulated cells. A cutoff of log fold change > 0.2 and P-values <0.05 was used to identify lipids that were differentially expressed between control and

stimulated cells. PCA was performed using these significant lipid abundances across all 4 batches (2 control and 2 stimulated) to determine consistency across batches. The top 4 principal components (PCs) were extracted that explained nearly 91% of the variability in the data. For each of these 4 PCs, a correlation was calculated against all morphological features from control and stimulated cells separately. Since PC2 produced the most separation between control and stimulated cells, the PC2 scores were used to color code the cells using Python scripts.

### 3.5.8 Logistic regression modeling to identify the top 10 discriminant lipids

For logistic regression, scikit-learn (https://scikit-learn.org/stable/about.html) was first used to train the model. Lipidomic features were used to predict whether a cell has been treated with IFN-γ or not, essentially making it a binary classification problem. After training the model, the coefficients of the model were extracted. The coefficients explained how much each input feature contributed to the predicted outcome, and its magnitude reflected the strength of the relationship between the feature and the outcome. Each coefficient corresponds to a lipid feature. The top 10 features with the highest magnitude were extracted.

### 3.5.9 Dimensionality reduction using UMAP and clustering of heterogenous IFN-γ stimulated MSC subpopulation

The processed data matrix consisting of the measurements for 21 morphological features of all 321 IFN-γ stimulated cells was used for dimensionality reduction using UMAP with the following parameters: n_neighbors=8, min_dist=0.3 and metric=euclidean. The first 2 component values of the UMAP projection for each cell were collected and subjected to agglomerative clustering resulting in 3 clusters of heterogenous IFN-γ stimulated MSC subpopulation.

The clustering scores were used to color code the cells using Python scripts (https://github.com/LukeMortensen/SingleCellMSCpotency).

### 3.5.10 Random forest analysis

A nonlinear machine learning model random forest (RF) was used to perform the prediction of each individual lipid abundance feature. A subset of 16 morphological features (texture and intensity features not included) was used as a predictive model. In this network, 80% of cells were randomly picked to establish the training dataset, while the remaining 20% were used for model validation and testing. Test error was determined to estimate the performance of the model. Data processing and machine learning were performed using Python version 3.8.3.

Test error = (1/n) * Σ *(y_true – y_pred)^2, where ‘n’ is the number of samples, ‘y’ is the target intensity values for prediction.

### 3.5.11 SpatialDE analysis

For spatial correlation analysis of lipid and morphology profiles, we used the SpatialDE package[15] with default parameters (https://github.com/Teichlab/SpatialDE).

### 3.5.12 Live cell imaging and cell migration rate calculations

To further verify the morphological features that were found to be correlated with lipid profiles, we performed an additional study comparing these morphological features to the cell migration rate. For this, we first performed live cell imaging using the same batches of cells cultured as described above. A series of images were captured over 24 hours using DPC imaging, automatically capturing the field of view of 2.6 $mm^2$ every 15 minutes. A stage-top incubator was

set at 37 °C with required moisture and a mixture of carbon dioxide and nitrogen for the survival of cells.

Time series images collected over the 24 hours were analyzed through the track object pipeline using the overlap tracking method in the cell profiler[46]. Morphological features along with integrated distance and lifetime for each cell were obtained. Using these features migration rate was calculated as

Migration rate=TrackObjects_IntegratedDistance/TrackObjects_Lifetime

The cell migration rate along with their morphological features was exported to JMP pro-16. Regression analysis was performed using Fit Model in JMP to evaluate associations between individual morphological features and the cell migration rate.

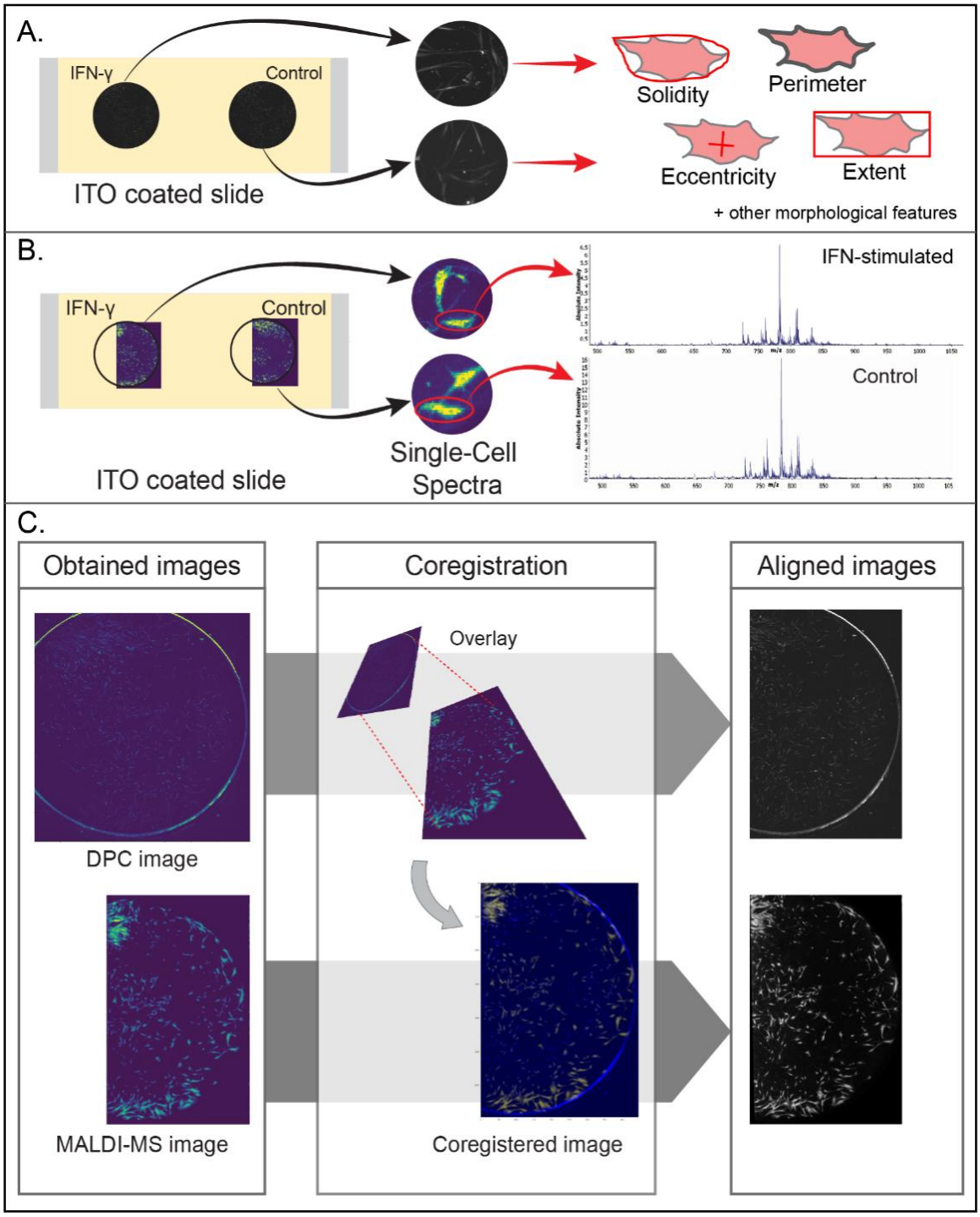


**Figure 3.1: Coregistration of DPC and MALDI-MS images to link phenotype and lipidome of single-cell MSCs.** (A) Schematic of MSCs seeded on ITO-coated slides for MALDI-MSI. Half of the wells were treated with IFN-γ and the other half were untreated control. (B) MALDI imaging workflow showing the detection of lipids in stimulated and unstimulated single MSCs. (C) Schematic showing the coregistration steps to generate single-cell aligned images. Details of the coregistration process can be found in reference 14.

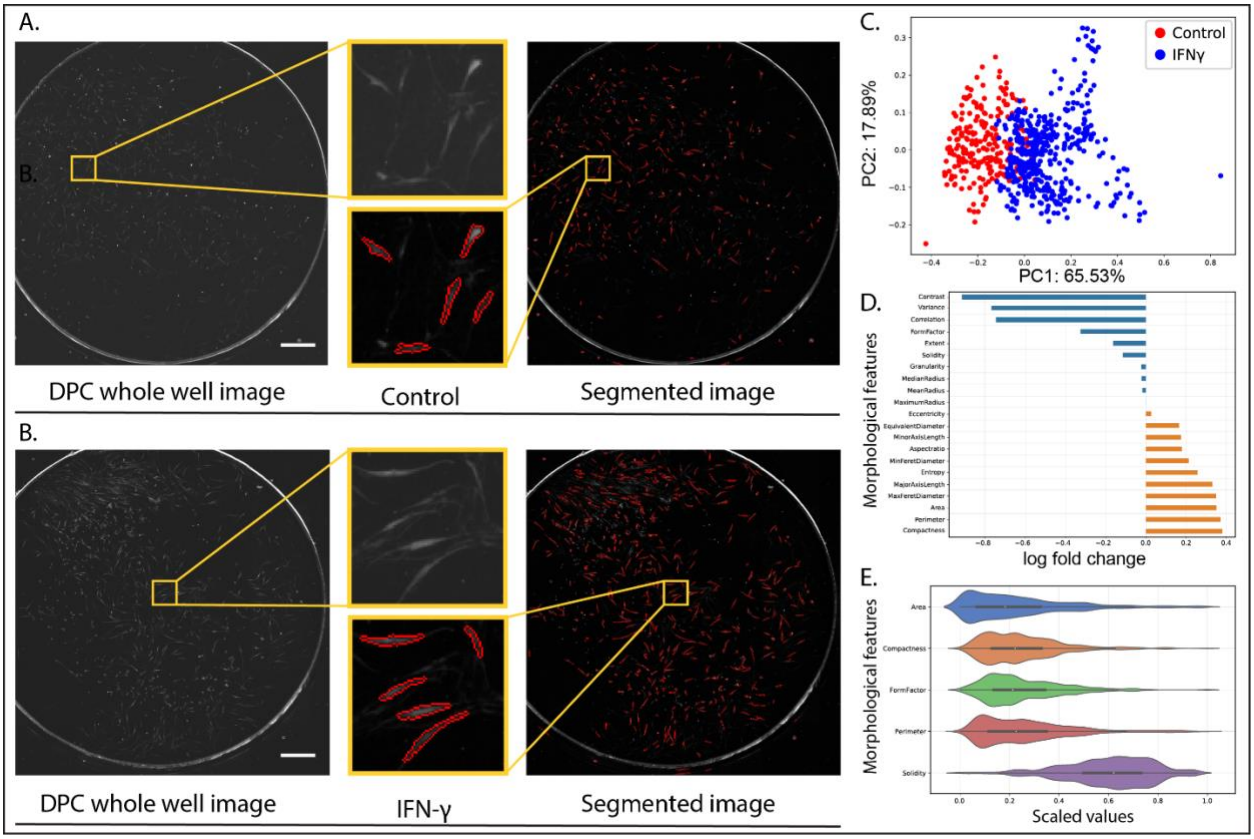


**Figure 3.2: Label-free imaging-based morphology analysis.** (A and B) DPC images (scale bar=500 μm) of MSCs unstimulated (A, left) and stimulated with IFN-γ (B, left). Cell segmentation using cell profiler where the segmented unstimulated cells (A, right) and stimulated cells (B, right) are outlined in red. (C) PCA plot showing the separation between morphological features of stimulated and unstimulated MSCs across the first two components. (D) Log fold change in morphological features after IFN-γ stimulation where a positive log fold change indicates an increased value in IFN-γ stimulated cells. (E) Violin plots showing a bimodal scaled distribution of morphological features within the IFN-γ stimulated subpopulation of MSCs highlighting their heterogeneity.

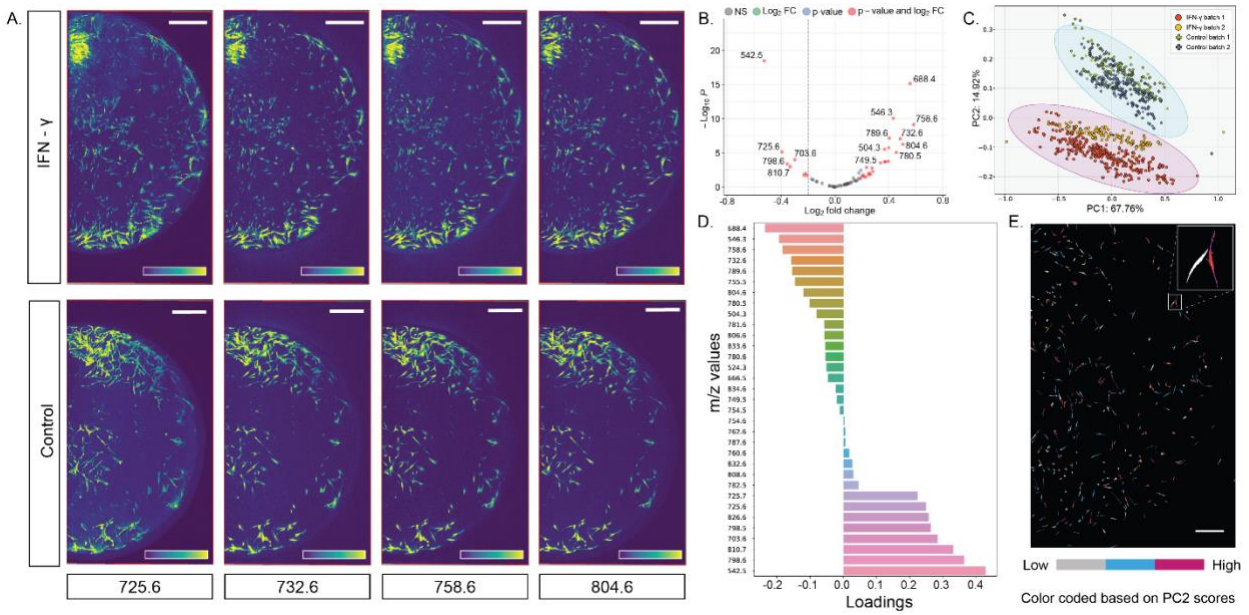


**Figure 3.3: Single-cell lipid detection. (**A) Representative MALDI images for specific lipids, where a bright colored cell indicates a higher relative abundance of that lipid species in that specific cell compared to other cells in the image. (B) Volcano plot highlighting lipid m/z values found to be differentially expressed in stimulated or unstimulated MSCs based on an absolute log2 fold change greater than 0.2 and a p-value lower than 0.05. (C) PCA plot showing separation between stimulated and unstimulated MSCs based on MALDI-MSI data over the first two components. (D) Loadings plot showing the main contributing lipid m/z values along PC2. (E) Color-coded composite image based on PC2 scores obtained from MALDI-MSI data (Scale bar= 100 μm)

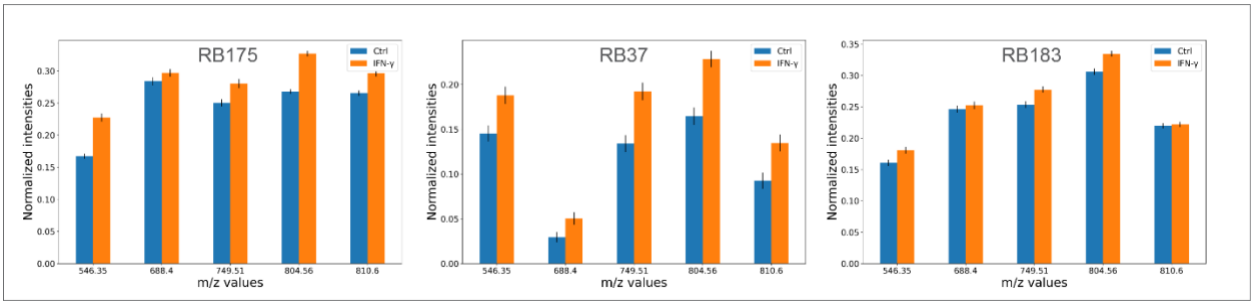


**Figure 3.4: Lipid abundances in MSCs cell lines.** The bar plot showing higher abundances of lipid in IFN-γ stimulated MSCs (orange) compared to the unstimulated control cells (blue).

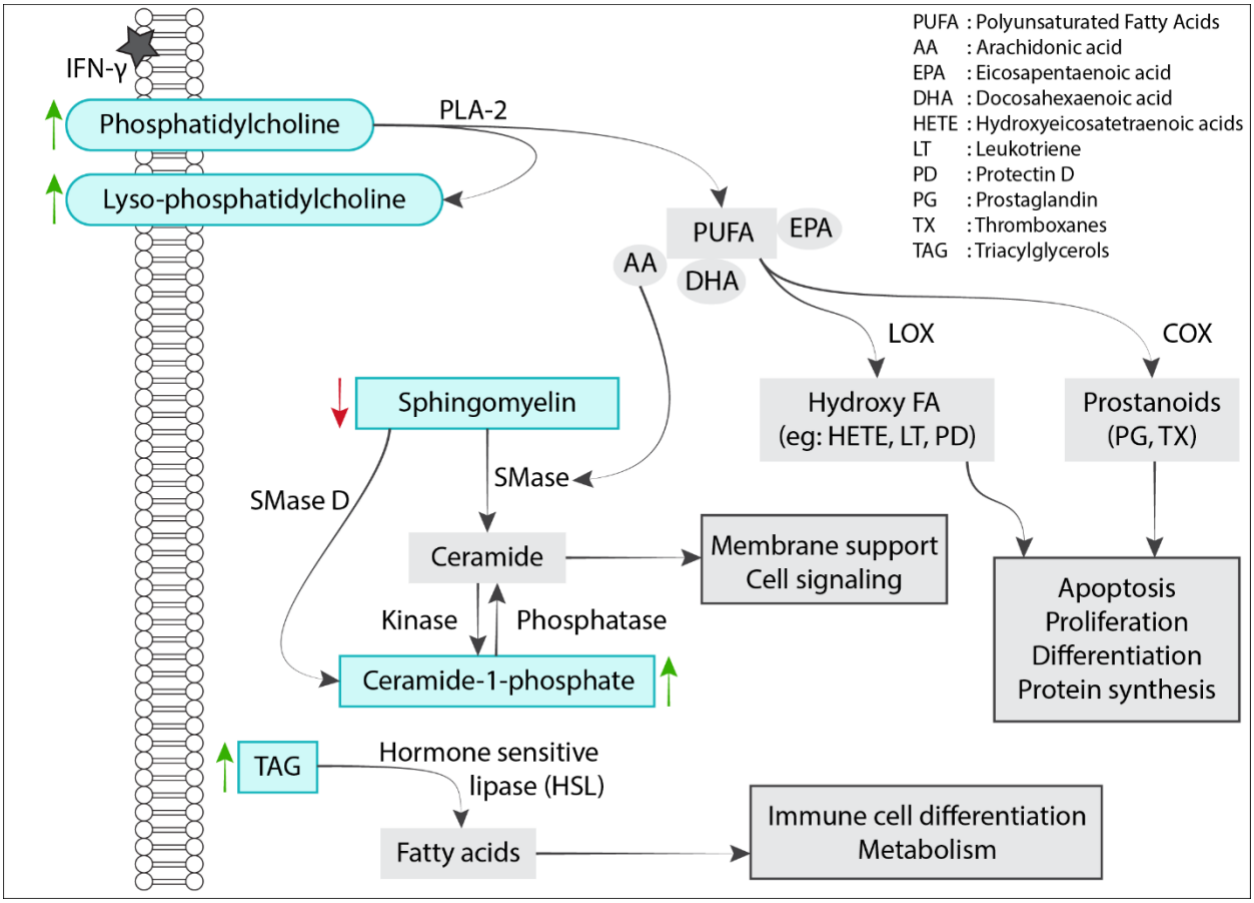


**Figure 3.5: Schematic pathway map highlighting the roles of differential lipid classes in cellular function.** The entities shown in cyan were found to be highly expressed in either IFN-γ stimulated or non-stimulated MSCs. The upward green arrow indicates increases in lipids in IFN-γ stimulated and downward red arrows shows decreases in lipids in IFN-γ stimulated cells. Boxes with dark outlines highlight the end effect of the pathway on cell function.

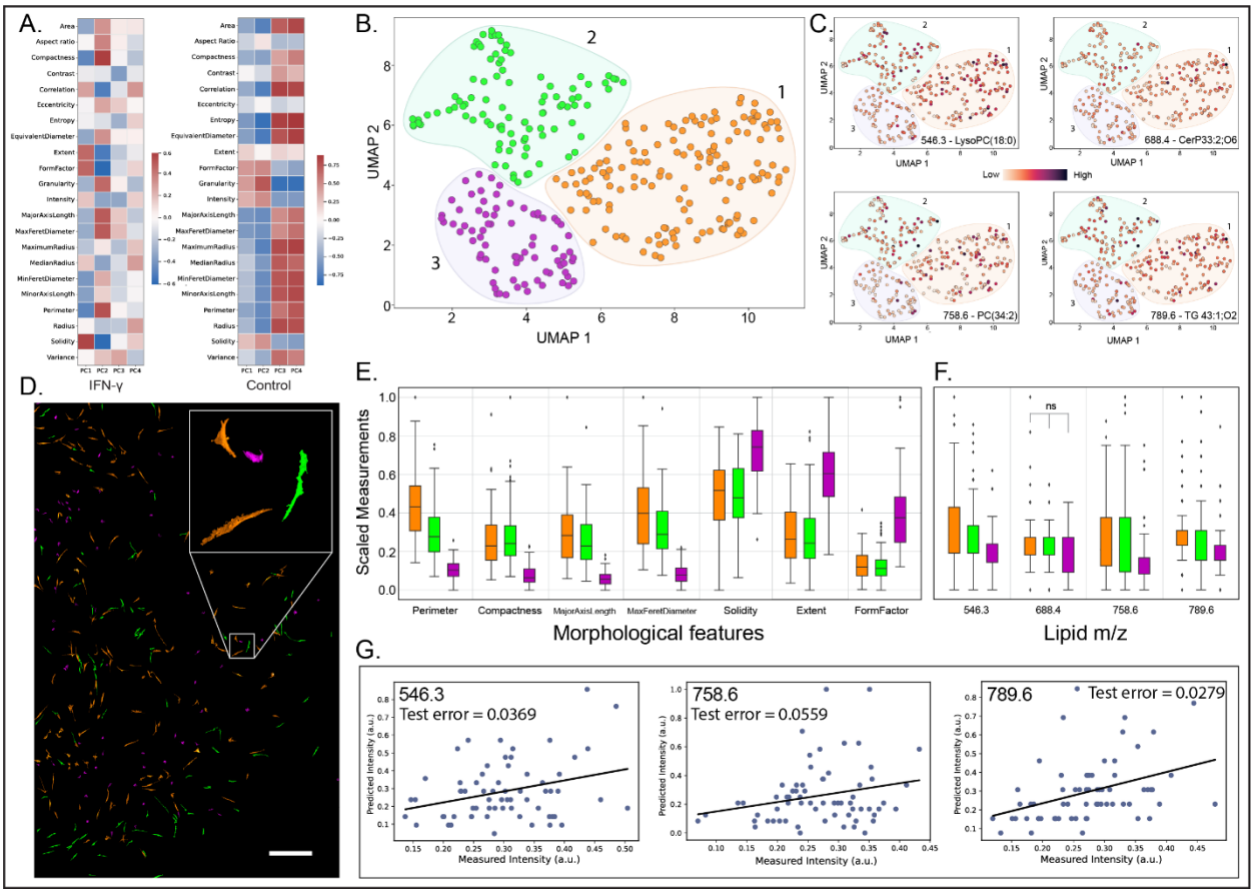


**Figure 3.6: Correlation and UMAP clustering results for MSC subpopulations.** (A) Correlation map showing the association of MSC morphology with PC2 score values obtained from the PCA analysis of the lipid MSI dataset (B) Agglomerative clustering performed on the first 2 components of a UMAP projection resulted in 3 cell clusters. Each point represents a unique cell. (C) The UMAP projections color-coded based on the abundance of a specific lipid m/z value. Bright orange indicates cells with higher abundance of the given lipid m/z value. (D) Color code showing the distribution of MSC based on the clustering group. (Cluster 1-Orange, Cluster 2-Green, Cluster 3-Magenta, Scale bar= 100 μm) (E) Box plots showing scaled measurements of morphological features across the 3 clusters. (F) Box plots showing scaled measurements of lipid abundances across the 3 clusters. (G) Random forest regression prediction of lipid abundance based on morphological features.

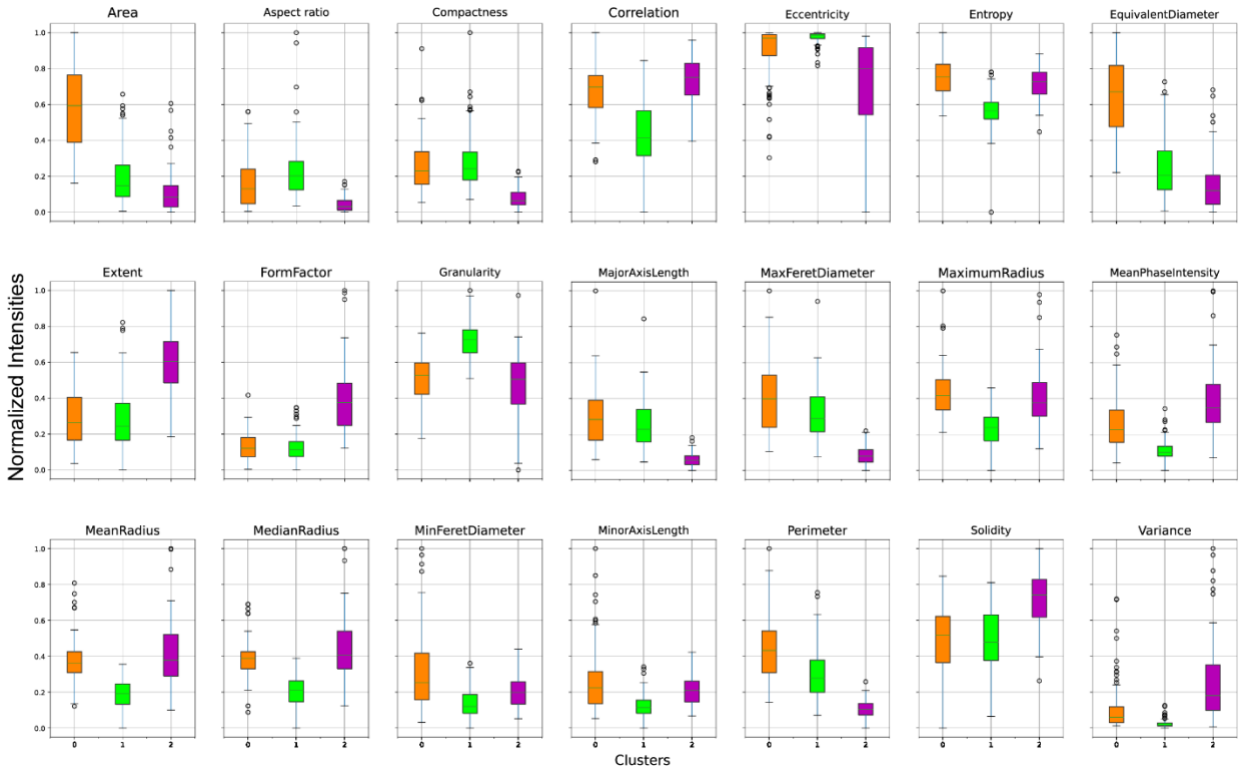


**Figure 3.7: Measurement of morphological features across the three clusters.** Box plot showing measurement of morphological features across the three clusters. Clusters 1 and 2 have higher intensities for perimeter, compactness, major axis length, and max feret diameter and lower intensities for solidity, extent, and form factor (p-val <0.05, t-test, n=321). These morphological features have opposite trends in cluster 3. Apart from these seven morphological features, all other morphological features and texture features did not show any trends.

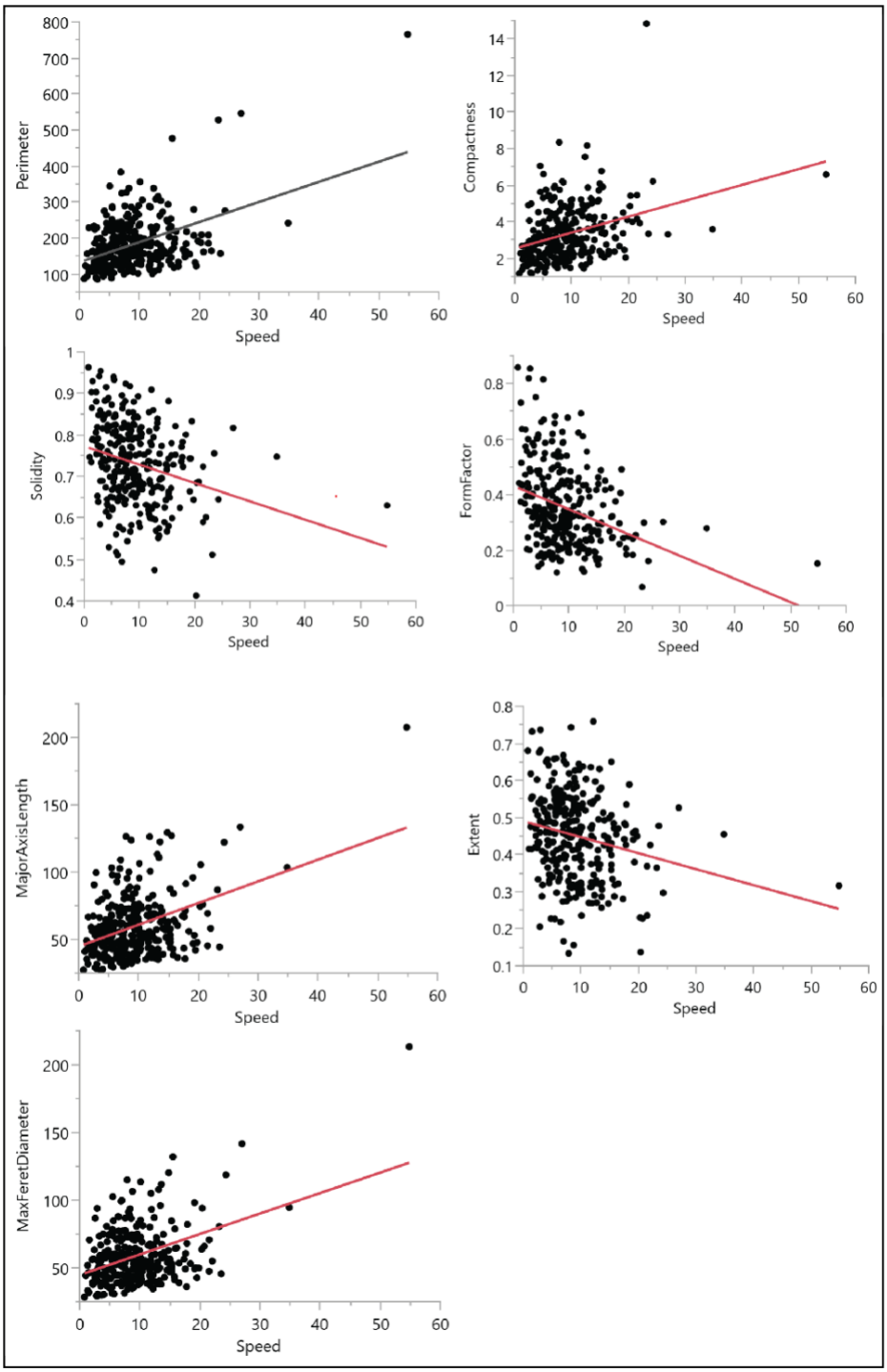


**Figure 3.8: Correlation of IFN-γ stimulated MSCs morphological features to the MSCs speed.** Plot showing regression analysis using Fit Model in JMP between MSC morphological features that were correlated with bioactive lipid and MSCs migration rate. Perimeter, compactness, major axis length, and max feret diameter showed positive correlation with the speed/migration rate of MSCs whereas solidity, form factor, and extent showed negative correlation with MSC's speed/migration rate (pixel units).

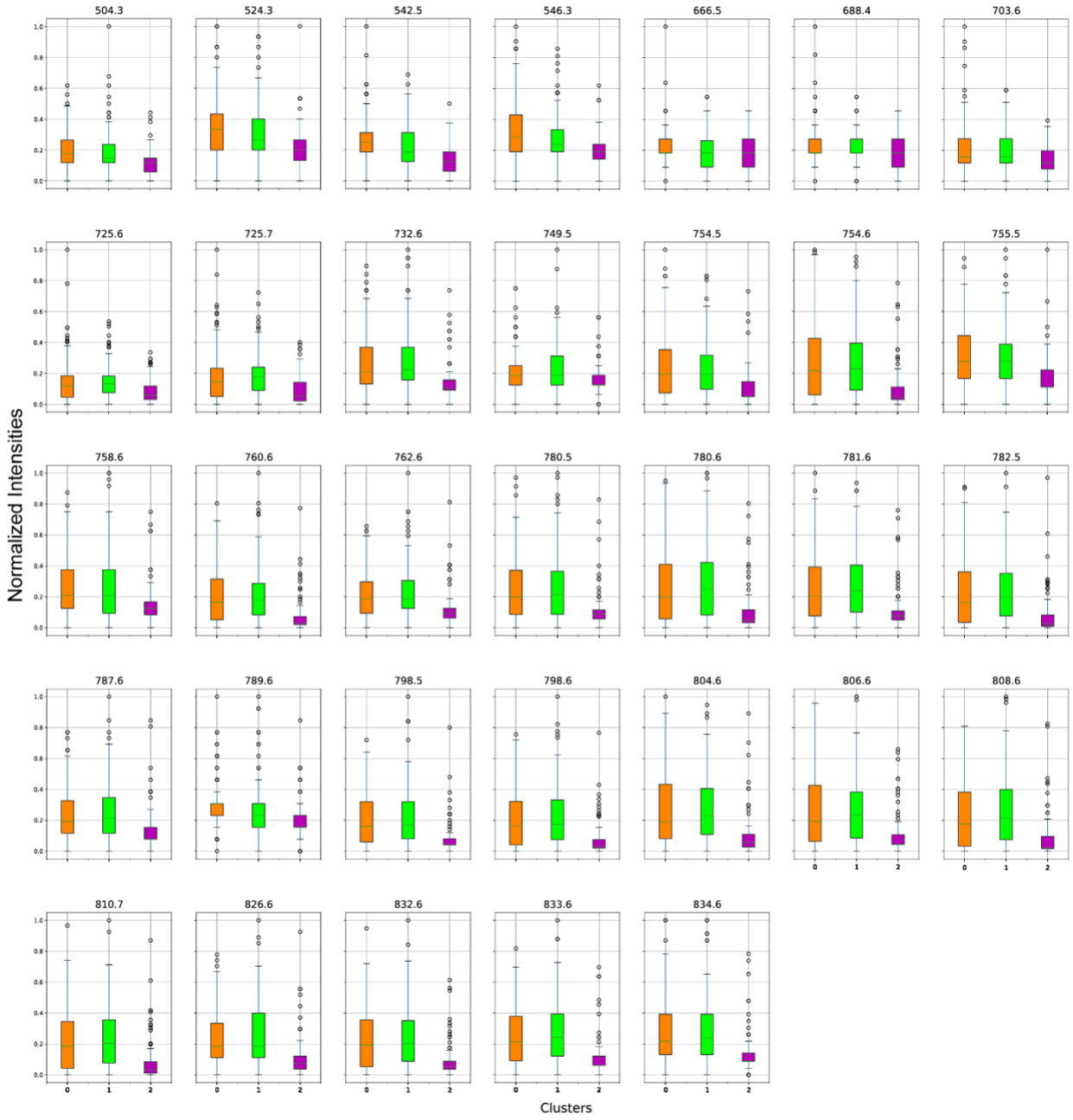


**Figure 3.9: Measurement of lipid intensities across the three clusters.** Box plot showing measurement of lipid intensities across the three clusters. Clusters 1 and 2 have higher lipid abundances whereas cluster 3 has lower lipid abundances (p-val <0.05, t-test, n=321) except in the case of C1P (m/z 666.5 and 688.4), which is uniformly distributed across the three clusters.

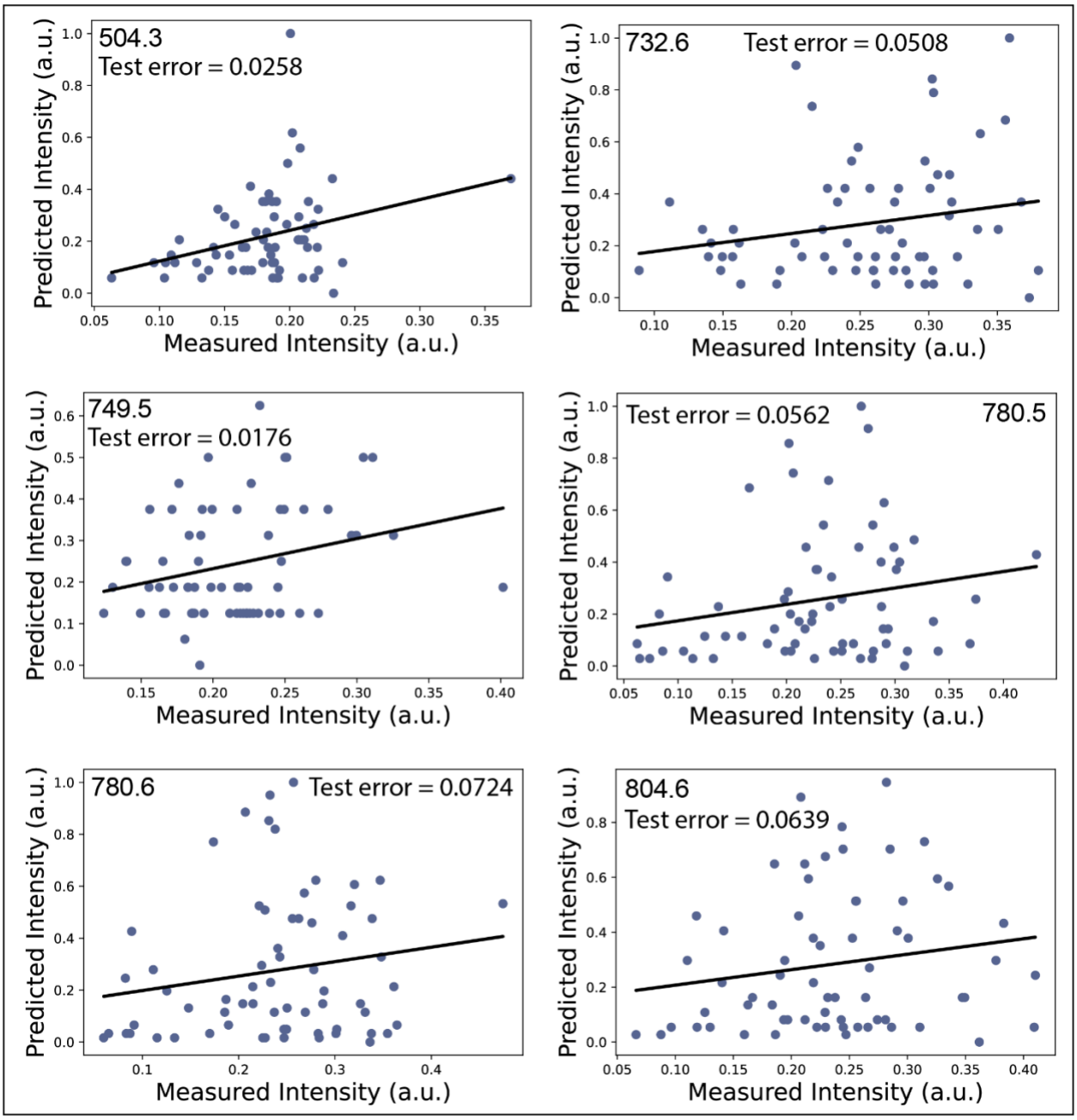


**Figure 3.10: Prediction of lipid signaling using morphological features in IFN-γ stimulated MSCs.**

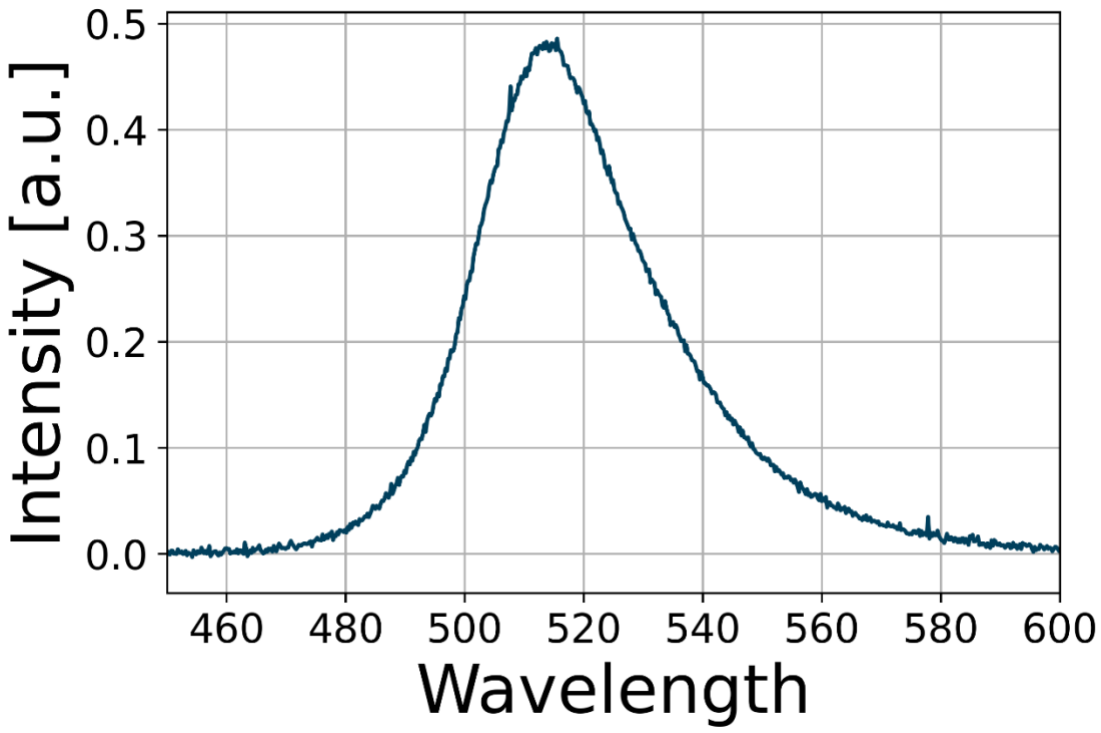


**Figure 3.11: Measured spectrum of the LED array used for illuminating in the DPC microscopy when the software sets the peak to 514nm.**

**Table 3.1: Mesenchymal stem cell features from DPC images extracted using CellProfiler**

| **Mesenchymal Cell morphological features** |
|---|
| Area |
| Aspect ratio |
| Compactness |
| Eccentricity |
| Equivalent Diameter |
| Extent |
| Form Factor |
| Major Axis Length |
| Max Feret Diameter |
| Maximum Radius |
| Mean Radius |
| Median Radius |
| Min Feret Diameter |
| Minor Axis Length |
| Perimeter |
| Solidity |
| |
| **Mesenchymal Cell texture features** |
| Contrast |
| Correlation |
| Entropy |
| Variance |
| |
| **Mesenchymal Cell Intensity** |
| Phase Intensity |

**Table 3.2: Comparison between lipid ions across control and IFN-γ treated samples.** Using Student's t-test (n=54). Lipids with significant differences are highlighted in red (if higher in IFN-γ) and blue (if higher in controls).

| m/z | mean_Ctrl | mean_IFN | P_value | Sig | Higher in |
|---|---|---|---|---|---|
| 496.3 | 0.247 | 0.254 | 0.591 | No | N |
| 504.3 | 0.144 | 0.186 | 0.000 | Yes | IFN |
| 518.3 | 0.248 | 0.272 | 0.051 | No | N |
| 524.3 | 0.254 | 0.287 | 0.009 | Yes | IFN |
| 542.5 | 0.331 | 0.230 | 0.000 | Yes | Control |
| 546.3 | 0.204 | 0.276 | 0.000 | Yes | IFN |
| 622.4 | 0.201 | 0.200 | 0.934 | No | N |
| 666.5 | 0.187 | 0.214 | 0.004 | Yes | IFN |
| 672.4 | 0.245 | 0.241 | 0.763 | No | N |
| 688.4 | 0.147 | 0.217 | 0.000 | Yes | IFN |
| 703.6 | 0.245 | 0.200 | 0.000 | Yes | Control |
| 725.6 | 0.192 | 0.146 | 0.000 | Yes | Control |
| 732.6 | 0.175 | 0.244 | 0.000 | Yes | IFN |
| 734.6 | 0.200 | 0.212 | 0.367 | No | N |
| 735.6 | 0.207 | 0.208 | 0.933 | No | N |
| 749.5 | 0.188 | 0.221 | 0.001 | Yes | IFN |
| 754.5 | 0.174 | 0.208 | 0.010 | Yes | IFN |
| 755.5 | 0.203 | 0.268 | 0.000 | Yes | IFN |
| 756.6 | 0.183 | 0.162 | 0.070 | No | N |
| 757.6 | 0.178 | 0.188 | 0.401 | No | N |
| 758.6 | 0.160 | 0.240 | 0.000 | Yes | IFN |
| 759.6 | 0.177 | 0.195 | 0.119 | No | N |
| 760.6 | 0.157 | 0.186 | 0.017 | Yes | IFN |
| 761.6 | 0.179 | 0.193 | 0.298 | No | N |
| 762.6 | 0.169 | 0.196 | 0.017 | Yes | IFN |
| 780.5 | 0.161 | 0.220 | 0.000 | Yes | IFN |
| 781.6 | 0.188 | 0.242 | 0.000 | Yes | IFN |
| 782.5 | 0.171 | 0.200 | 0.034 | Yes | IFN |
| 783.5 | 0.195 | 0.217 | 0.135 | No | N |
| 784.6 | 0.195 | 0.205 | 0.454 | No | N |
| 784.8 | 0.216 | 0.216 | 0.966 | No | N |
| 785.6 | 0.210 | 0.220 | 0.439 | No | N |
| 786.6 | 0.180 | 0.179 | 0.949 | No | N |
| 786.7 | 0.189 | 0.184 | 0.661 | No | N |
| 787.6 | 0.188 | 0.216 | 0.026 | Yes | IFN |
| 788.6 | 0.170 | 0.185 | 0.185 | No | N |

| | | | | | |
|---|---|---|---|---|---|
| 789.6 | 0.193 | 0.256 | 0.000 | Yes | IFN |
| 798.6 | 0.241 | 0.189 | 0.000 | Yes | Control |
| 799.5 | 0.221 | 0.207 | 0.299 | No | N |
| 804.6 | 0.165 | 0.235 | 0.000 | Yes | IFN |
| 806.6 | 0.176 | 0.228 | 0.000 | Yes | IFN |
| 808.6 | 0.181 | 0.217 | 0.014 | Yes | IFN |
| 809.6 | 0.193 | 0.205 | 0.374 | No | N |
| 810.5 | 0.182 | 0.191 | 0.493 | No | N |
| 810.7 | 0.227 | 0.180 | 0.001 | Yes | Control |
| 811.6 | 0.212 | 0.190 | 0.094 | No | N |
| 812.6 | 0.219 | 0.217 | 0.884 | No | N |
| 824.6 | 0.226 | 0.206 | 0.150 | No | N |
| 826.6 | 0.222 | 0.192 | 0.021 | Yes | Control |
| 830.6 | 0.163 | 0.186 | 0.058 | No | N |
| 831.6 | 0.175 | 0.187 | 0.290 | No | N |
| 832.6 | 0.174 | 0.202 | 0.033 | Yes | IFN |
| 833.6 | 0.177 | 0.224 | 0.000 | Yes | IFN |
| 834.6 | 0.207 | 0.251 | 0.002 | Yes | IFN |

**Table 3.3: Logistic regression classifier to identify the top discriminant lipid species.**

| Lipid m/z | Absolute Coefficient |
|---|---|
| 542.5 | 3.974655 |
| 789.6 | 2.513679 |
| 758.6 | 2.375707 |
| 546.3 | 2.367292 |
| 810.7 | 2.089305 |
| 798.6 | 2.046286 |
| 725.6 | 1.945395 |
| 755.5 | 1.878002 |
| 804.6 | 1.876338 |
| 703.6 | 1.846470 |

**Table 3.4: Spatial distribution of lipids with statistically significant spatial variation as calculated by SpatialDE.** Lipid expression levels and morphological features were measured as a function of spatial coordinates of cells.

| m/z values | P-val | Q-val | Adj. P-val |
|---|---|---|---|
| m/z 749.5 | 0.00015 | 0.00248 | 0.00450 |
| m/z 504.3 | 0.00020 | 0.00248 | 0.00590 |
| m/z 798.5 | 0.00025 | 0.00248 | 0.00751 |
| m/z 703.6 | 0.00032 | 0.00260 | 0.00964 |
| m/z 826.6 | 0.00042 | 0.00286 | 0.01249 |
| m/z 808.6 | 0.00052 | 0.00333 | 0.01571 |
| m/z 783.5 | 0.00063 | 0.00333 | 0.01900 |
| m/z 804.6 | 0.00064 | 0.00333 | 0.01905 |
| m/z 832.6 | 0.00084 | 0.00355 | 0.02531 |
| m/z 833.6 | 0.00099 | 0.00355 | 0.02975 |
| m/z 760.6 | 0.00102 | 0.00355 | 0.03058 |
| m/z 806.6 | 0.00104 | 0.00355 | 0.03112 |
| m/z 782.5 | 0.00111 | 0.00366 | 0.03328 |
| m/z 781.6 | 0.00166 | 0.00400 | 0.04985 |
| m/z 780.5 | 0.00184 | 0.00425 | 0.05514 |
| m/z 787.6 | 0.00186 | 0.00425 | 0.05590 |
| m/z 732.6 | 0.00258 | 0.00535 | 0.07727 |
| m/z 762.6 | 0.00271 | 0.00535 | 0.08117 |
| m/z 725.6 | 0.00301 | 0.00564 | 0.09034 |
| m/z 810.7 | 0.00367 | 0.00667 | 0.11012 |
| m/z 758.6 | 0.00436 | 0.00747 | 0.13085 |
| m/z 755.5 | 0.00909 | 0.01371 | 0.27268 |
| m/z 754.5 | 0.01028 | 0.01525 | 0.30840 |
| m/z 789.6 | 0.01279 | 0.01866 | 0.38365 |
| m/z 542.5 | 0.01696 | 0.02358 | 0.50869 |
| m/z 666.5 | 0.02185 | 0.02992 | 0.65565 |
| m/z 834.6 | 0.02397 | 0.03184 | 0.71897 |
| m/z 688.4 | 0.03714 | 0.04791 | 1.11423 |
| m/z 524.3 | 0.05163 | 0.06564 | 1.54891 |
| m/z 546.3 | 0.16562 | 0.19919 | 4.96847 |

## 3.6 Bibliography


1 Jones, B. J. & McTaggart, S. J. Immunosuppression by mesenchymal stromal cells: from culture to clinic. *Experimental hematology* **36**, 733-741, doi:10.1016/j.exphem.2008.03.006 (2008).

2 Wang, Y., Chen, X., Cao, W. & Shi, Y. Plasticity of mesenchymal stem cells in immunomodulation: pathological and therapeutic implications. *Nature immunology* **15**, 1009-1016, doi:10.1038/ni.3002 (2014).

3 Chinnadurai, R., Copland, I. B., Patel, S. R. & Galipeau, J. IDO-independent suppression of T cell effector function by IFN-γ-licensed human mesenchymal stromal cells. *Journal of immunology (Baltimore, Md. : 1950)* **192**, 1491-1501, doi:10.4049/jimmunol.1301828 (2014).

4 Mabuchi, Y., Okawara, C., Méndez-Ferrer, S. & Akazawa, C. Cellular Heterogeneity of Mesenchymal Stem/Stromal Cells in the Bone Marrow. *Frontiers in cell and developmental biology* **9**, 689366, doi:10.3389/fcell.2021.689366 (2021).

5 Klinker, M. W., Marklein, R. A., Lo Surdo, J. L., Wei, C. H. & Bauer, S. R. Morphological features of IFN-γ-stimulated mesenchymal stromal cells predict overall immunosuppressive capacity. *Proceedings of the National Academy of Sciences of the United States of America* **114**, E2598-e2607, doi:10.1073/pnas.1617933114 (2017).

6 Marklein, R. A. *et al.* Morphological profiling using machine learning reveals emergent subpopulations of interferon-γ-stimulated mesenchymal stromal cells that predict immunosuppression. *Cytotherapy* **21**, 17-31, doi:10.1016/j.jcyt.2018.10.008 (2019).

7 Vasilevich, A. S. *et al.* On the correlation between material-induced cell shape and phenotypical response of human mesenchymal stem cells. *Scientific reports* **10**, 18988, doi:10.1038/s41598-020-76019-z (2020).

8 Campos, A. M. *et al.* Lipidomics of Mesenchymal Stromal Cells: Understanding the Adaptation of Phospholipid Profile in Response to Pro-Inflammatory Cytokines. *Journal of cellular physiology* **231**, 1024-1032, doi:10.1002/jcp.25191 (2016).

9 Chen, Y., Yu, C. Y. & Deng, W. M. The role of pro-inflammatory cytokines in lipid metabolism of metabolic diseases. *International reviews of immunology* **38**, 249-266, doi:10.1080/08830185.2019.1645138 (2019).

10 Casati, S. *et al.* Bioactive Lipids in MSCs Biology: State of the Art and Role in Inflammation. *International journal of molecular sciences* **22**, doi:10.3390/ijms22031481 (2021).

11 Lanekoff, I., Sharma, V. V. & Marques, C. Single-cell metabolomics: where are we and where are we going? *Current opinion in biotechnology* **75**, 102693, doi:10.1016/j.copbio.2022.102693 (2022).

12 Horn, A. & Jaiswal, J. K. Structural and signaling role of lipids in plasma membrane repair. *Current topics in membranes* **84**, 67-98, doi:10.1016/bs.ctm.2019.07.001 (2019).

13 Silva, C. G. D. *et al.* Lipidomics of mesenchymal stem cell differentiation. *Chemistry and physics of lipids* **232**, 104964, doi:10.1016/j.chemphyslip.2020.104964 (2020).

14 Nikitina, A. *et al.* A Co-registration Pipeline for Multimodal MALDI and Confocal Imaging Analysis of Stem Cell Colonies. *Journal of the American Society for Mass Spectrometry* **31**, 986-989, doi:10.1021/jasms.9b00094 (2020).

15 Svensson, V., Teichmann, S. A. & Stegle, O. SpatialDE: identification of spatially variable genes. *Nature Methods* **15**, 343-346, doi:10.1038/nmeth.4636 (2018).

16 Fuchs, B. *et al.* Analysis of stem cell lipids by offline HPTLC-MALDI-TOF MS. *Analytical and bioanalytical chemistry* **392**, 849-860, doi:10.1007/s00216-008-2301-8 (2008).

17 Rocha, B. *et al.* Characterization of lipidic markers of chondrogenic differentiation using mass spectrometry imaging. *Proteomics* **15**, 702-713, doi:10.1002/pmic.201400260 (2015).

18 Li, H., Dai, H. & Li, J. Immunomodulatory properties of mesenchymal stromal/stem cells: The link with metabolism. *Journal of advanced research* **45**, 15-29, doi:10.1016/j.jare.2022.05.012 (2023).

19 Duan, R.-D. Phospholipid signals and intestinal carcinogenesis. *Scandinavian Journal of Food and Nutrition* **50**, 45-53, doi:10.1080/17482970601075703 (2006).

20 Kendall, A. C. *et al.* Distribution of bioactive lipid mediators in human skin. *The Journal of investigative dermatology* **135**, 1510-1520, doi:10.1038/jid.2015.41 (2015).

21 Jayadev, S., Linardic, C. M. & Hannun, Y. A. Identification of arachidonic acid as a mediator of sphingomyelin hydrolysis in response to tumor necrosis factor alpha. *The Journal of biological chemistry* **269**, 5757-5763 (1994).

22 Gómez-Muñoz, A., Gangoiti, P., Granado, M. H., Arana, L. & Ouro, A. Ceramide-1-phosphate in cell survival and inflammatory signaling. *Advances in experimental medicine and biology* **688**, 118-130, doi:10.1007/978-1-4419-6741-1_8 (2010).

23 Li-Beisson, Y. *et al.* Acyl-lipid metabolism. *The arabidopsis book* **8**, e0133, doi:10.1199/tab.0133 (2010).

24 Yaqoob, P. & Calder, P. C. Fatty acids and immune function: new insights into mechanisms. *The British journal of nutrition* **98 Suppl 1**, S41-45, doi:10.1017/s0007114507832995 (2007).

25 Galderisi, U., Peluso, G. & Di Bernardo, G. Clinical Trials Based on Mesenchymal Stromal Cells are Exponentially Increasing: Where are We in Recent Years? *Stem cell reviews and reports* **18**, 23-36, doi:10.1007/s12015-021-10231-w (2022).

26 Wu, H. H., Zhou, Y., Tabata, Y. & Gao, J. Q. Mesenchymal stem cell-based drug delivery strategy: from cells to biomimetic. *Journal of controlled release : official journal of the Controlled Release Society* **294**, 102-113, doi:10.1016/j.jconrel.2018.12.019 (2019).

27 Kyurkchiev, D. *et al.* Secretion of immunoregulatory cytokines by mesenchymal stem cells. *World journal of stem cells* **6**, 552-570, doi:10.4252/wjsc.v6.i5.552 (2014).

28 Noronha, N. C. *et al.* Priming approaches to improve the efficacy of mesenchymal stromal cell-based therapies. *Stem cell research & therapy* **10**, 131, doi:10.1186/s13287-019-1224-y (2019).

29 Yin, J. Q., Zhu, J. & Ankrum, J. A. Manufacturing of primed mesenchymal stromal cells for therapy. *Nature biomedical engineering* **3**, 90-104, doi:10.1038/s41551-018-0325-8 (2019).

30 Griffiths, J. A., Scialdone, A. & Marioni, J. C. Using single-cell genomics to understand developmental processes and cell fate decisions. *Molecular systems biology* **14**, e8046, doi:10.15252/msb.20178046 (2018).

31 Wang, W. *et al.* Live-cell imaging and analysis reveal cell phenotypic transition dynamics inherently missing in snapshot data. *Science advances* **6**, doi:10.1126/sciadv.aba9319 (2020).

32 Daga, K. R. *et al.* Shape up before you ship out: morphology as a potential critical quality attribute for cellular therapies. *Current Opinion in Biomedical Engineering* **20**, 100352, doi:https://doi.org/10.1016/j.cobme.2021.100352 (2021).

33 Lagace, T. A. Phosphatidylcholine: Greasing the Cholesterol Transport Machinery. *Lipid insights* **8**, 65-73, doi:10.4137/lpi.S31746 (2015).

34 Varshney, P., Yadav, V. & Saini, N. Lipid rafts in immune signalling: current progress and future perspective. *Immunology* **149**, 13-24, doi:10.1111/imm.12617 (2016).

35 Cherukuri, A., Dykstra, M. & Pierce, S. K. Floating the raft hypothesis: lipid rafts play a role in immune cell activation. *Immunity* **14**, 657-660, doi:10.1016/s1074-7613(01)00156-x (2001).

36 Corrêa, R. *et al.* Lysophosphatidylcholine Induces NLRP3 Inflammasome-Mediated Foam Cell Formation and Pyroptosis in Human Monocytes and Endothelial Cells. *Frontiers in immunology* **10**, 2927, doi:10.3389/fimmu.2019.02927 (2019).

37 Yuan, Y., Schoenwaelder, S. M., Salem, H. H. & Jackson, S. P. The bioactive phospholipid, lysophosphatidylcholine, induces cellular effects via G-protein-dependent activation of adenylyl cyclase. *The Journal of biological chemistry* **271**, 27090-27098, doi:10.1074/jbc.271.43.27090 (1996).

38 Maceyka, M. & Spiegel, S. Sphingolipid metabolites in inflammatory disease. *Nature* **510**, 58-67, doi:10.1038/nature13475 (2014).

39 Papangelis, A. & Ulven, T. Synthesis of Lysophosphatidylcholine and Mixed Phosphatidylcholine. *The Journal of organic chemistry* **87**, 8194-8197, doi:10.1021/acs.joc.2c00335 (2022).

40 Presa, N., Gomez-Larrauri, A., Dominguez-Herrera, A., Trueba, M. & Gomez-Muñoz, A. Novel signaling aspects of ceramide 1-phosphate. *Biochimica et biophysica acta. Molecular and cell biology of lipids* **1865**, 158630, doi:10.1016/j.bbalip.2020.158630 (2020).

41 Tian, L. & Waller, L. Quantitative differential phase contrast imaging in an LED array microscope. *Optics express* **23**, 11394-11403, doi:10.1364/oe.23.011394 (2015).

42 Phillips, Z. F., Chen, M. & Waller, L. Single-shot quantitative phase microscopy with color-multiplexed differential phase contrast (cDPC). *PloS one* **12**, e0171228, doi:10.1371/journal.pone.0171228 (2017).

43 Chen, M., Phillips, Z. F. & Waller, L. Quantitative differential phase contrast (DPC) microscopy with computational aberration correction. *Optics express* **26**, 32888-32899, doi:10.1364/oe.26.032888 (2018).

44 Carpenter, A. E. *et al.* CellProfiler: image analysis software for identifying and quantifying cell phenotypes. *Genome biology* **7**, R100, doi:10.1186/gb-2006-7-10-r100 (2006).

45 Bisong, E. in Building Machine Learning and Deep Learning Models on Google Cloud Platform: A Comprehensive Guide for Beginners (ed Ekaba Bisong) 215-229 (Apress, 2019).

46 McQuin, C. *et al.* CellProfiler 3.0: Next-generation image processing for biology. *PLoS biology* **16**, e2005970, doi:10.1371/journal.pbio.2005970 (2018).

# CHAPTER 4

# MESENCHYMAL STEM/STROMAL CELL POTENCY PREDICTION THROUGH LIVE IMAGING ON HIGH-THROUGHPUT 3D MICROFLUIDIC DEVICE

---

Priyanka Priyadarshani, Rebecca S. Schneider, Andrés J. García, and Luke J. Mortensen.
*To be submitted to Cell Reports.*

# Abstract

Mesenchymal stem cells (MSCs) hold great promise in regenerative medicine and cell-based therapies due to their multipotent nature and immunomodulatory properties. However, a significant challenge in harnessing their therapeutic capabilities lies in accurately assessing their potency and predicting their behavior in clinic use. Traditional methods of characterizing MSCs potency often rely on endpoint assays, which are time-consuming, labor-intensive, and may not capture the dynamic behavior of these cells in real-time. The morphology of a cell and its ability to migrate are intimately linked to its function and play pivotal roles in development, tissue repair, pathological processes, and immune responses. Understanding these aspects of MSC biology to predict its functional potency in the culture conditions akin to their *in vivo* is crucial for advancing our knowledge of physiology, and potential therapeutic interventions. However, MSCs morphological features and migration ability in their natural growing conditions have not been explored well as a marker for potency prediction.

In this research, we introduce an innovative approach to gain deeper insights into the behavior of MSCs derived from five different donors. Our method involves the utilization of a cutting-edge microfluidic device, which simulates an *in vivo* culture environment for these cells. Through this setup, we comprehensively assessed the morphological characteristics and migration patterns of MSCs in a real-time manner using high content live imaging and compared them to already established potency prediction methods. The combination of microfluidics and live imaging not only enhanced our understanding of MSCs but also paves the way for more accurate and reliable assessments of their potential in clinical and research settings.

## 4.1 Introduction

MSCs, a subpopulation of adult stem cells, have emerged as a significant resource for tissue engineering, regenerative medicine, and immunotherapy. Their ability to differentiate into various cell lineages including osteocytes, chondrocytes, adipocytes, and myocytes makes them an attractive candidate for repairing damaged tissues and promoting healing processes. In addition, MSCs hold immunomodulatory properties that promote tissue regeneration by suppressing inflammation and modulating the immune response[1-4]. However, the clinical efficacy of MSC-based therapies strongly depends on the potency and functionality of the administered cells. Traditionally, MSC potency has been evaluated through the combination of phenotypic markers, differentiation assays, and profiling of relevant secreted factors[5,6]. These approaches often involve endpoint measurements that provide limited insights into the dynamic behavior of MSCs over time. Furthermore, these methods require extensive sample processing which makes them time-consuming, labor-intensive, and prone to batch-to-batch variability. To address these limitations, we propose a cutting-edge strategy for predicting MSC potency by leveraging live imaging on a 3D microfluidic device.

Three-dimensional culture systems (3D) represent one of the rapidly growing experimental approaches in the field of life sciences. Cells grown in 3D culture models demonstrate characteristics that closely mimic the environment of *in vivo* conditions. These 3D culture models have proven to be more realistic in translating research findings into practical applications within living organisms[7] Microfluidic technology offers a powerful 3D platform for manipulating and analyzing cells in a controlled environment[8,9]. Incorporating live imaging in microfluidic device allows real-time monitoring in natural culture conditions of cellular processes and dynamic

characterization of cell morphology and behavior, enabling a comprehensive assessment of MSC functional capacity.

We used an on-chip microfluidic device developed by Rebecca et.al[10] capable of providing an optimal microenvironment for 3D MSC culture and imaging. The device includes controlled and precise mechanical stimuli to recapitulate *in vivo* environments. Live imaging techniques was incorporated alongside a microfluidic device to extract dynamic quantitative parameters associated with the cellular morphology, migration, and locomotory behavior of MSC. These parameters are related to the essential biological function including immunological cell activities, cell differentiation, and tissue regeneration[11,12]. Out of the five MSCs donors evaluated, two of the donors showed higher functional capacity based on morphological and migratory profile. Acquiring this dynamic behavior of MSCs, our microfluidic imaging-based approach provides valuable insights into the functional characteristics of MSCs, allowing us to predict their potency faster and more accurately.

## 4.2 Results

### 4.2.1 Live imaging platform to characterize MSCs potency on-chip 3D microfluidic device.

The objective of this study is to characterize the potency of MSC donors seeded on-chip 3D microfluidic device via live imaging and compare them with established potency metrics (Figure 4.1). To accomplish this, we seeded MSCs in a microfluidic device to perform real-time monitoring of MSCs in an environment similar to their natural state. The on-chip 3D microfluidic device was engineered as described by Schneider et. al., where MSCs were seeded in a synthetic

4-arm maleimide-functionalized poly(ethylene-glycol) (PEG-4MAL) hydrogel cross-linked with dithiolated protease-degradable VPM (GCRDVPMSMRGGDRCG) and non-degradable dithiothreitol (DTT) with the presentation of the cell-adhesive peptide RGD (GRGDSPC). The MSCs were cultured for 24 hours in the microfluidic device in IFN-$\gamma$-supplemented media (Figure 4.1A).

Zeiss LSM 710 confocal microscope was used to obtain live imaging of MSCs on-chip 3D microfluidic devices with a constant supply of fresh media for 7 hours (Figure 4.1B). The microscope allowed us to obtain thin optical sections of MSCs inside the microfluidic device with high sensitivity and image contrast. We acquired axial stacks of live MSCs in the microfluidic device for 3D visualization from 5 different donors that were stimulated with IFN-$\gamma$. In recent years morphology and migratory pattern of cells are considered one of the critictal marker to predict cell functional potency. So, the obtained live images were segmented, using the track object pipeline in CellProfiler to obtain live cell features, including morphological features, lifetime, migration and locomotion behavior of the MSC donors. The live cell features acquired from multiple MSC donors underwent characterization to assess their functional potential (Figure 4.1C), and these characteristics were subsequently employed to predict the immunosuppressive capabilities of the MSCs (Figure 4.1D).

### 4.2.2 MSCs donors exhibit distinct morphological characters and immnuno suppressive capacity

MSCs obtained from different donors and sources account for variability in their function, which leads to inconsistencies in their clinical outcomes[13,14]. In order to characterize the MSC donors, we evaluated their morphological features and performed T-cell suppression assay. Specifically,

we evaluated human bone marrow derived MSCs from five different donors: RB183, RB177, RB179, RB114, and RB71. We employed the longitudinal imaging analysis to investigate differences in morphological features between multiple bone marrow MSC donors. Live imaging of the MSC donors cultured in a microfluidic device infused with IFN-$\gamma$ alpha mem media was performed for seven hours with a 15-minute interval. 3D images of the MSC donors were obtained from stacks of live images to evaluate their morphological features (Figure 4.2A). Z-stacks of confocal images were segmented using Track object pipeline in CellProfiler to obtain the morphological features of each MSC donor.

The principal component analysis (PCA) plot shows differences in morphological features among the different donors. Overall ~96% variation is explained by first two components of the PCA. PC1 and PC2 loadings show the morphological features. (Figure 4.2B) PC1 and PC2 loading show the morphological features that contribute to the variation of morphological features among the MSC donors (Figure 4.2C,D). We further wanted to understand the difference in features among these MSC donors. We found that MSC donors RB177, and RB183 have higher compactness and eccentricity and have lower solidity, formfactor, and extent compared to RB179, RB71, and RB114 donors (Figure 4.3). These MSC donors not only differ in their morphological features but also in their functional potency, which we evaluated by performing MSC:PBMC co-culture in a 1:2 ratio to assess CD3+ and CD4+ T-cell suppression as per recommendations of the International Society for Cellular Therapy (ISCT)[15]. In this case, lower proliferation of CD3+ and CD4+ T-cells indicates higher suppression by MSCs. RB177 and RB183 demonstrated higher T-cell suppression, followed by RB179, RB71, and RB114 indicating that the donor RB177 and RB183 are the most potent MSCs.

### 4.2.3 Live imaging shows difference in MSCs locomotion and migratory potential

It is well established that 3D culture provides a more physiologically relevant model for studying *in vivo* migratory behavior[16,17]. The primary objective of this research is to develop an image-based analysis pipeline to predict the potency of MSCs seeded on chip microfluidic device through live imaging. One way to measure the potency of the cell is to assess their migration capacity, since cell migration is an essential biological function involved in cell development, and growth, immunological activities, differentiation, and regeneration. Thus, an essential parameter for the systemic delivery of the cell to the target site[18,19]. To measure and compare the migration of MSCs donors in real time in 3D culture environment, we utilized live imaging on a chip microfluidic device to measure the overall lifetime, speed, and locomotory behavior of the MSCs donor. Sequential 3D image stacks were acquired at 15-minute intervals, and the x, y coordinates of individual MSCs were tracked using CellProfiler. We plotted the total integrated distance traveled by each MSCs donor over time. Our result shows that not all MSCs donors travelled equal distance over the span of 6 hours (Figure 4.4A). To examine the migratory behavior of the MSCs donor within the microfluidic device, we plotted the migration rate of each donor against time. This provides insight into how quickly MSCs are traveling within the microfluidic device within a given time frame. Among the MSCs donors, RB183 and RB177 exhibited the highest migration rate, along with the greatest distance traveled over a span of 6 hours, compared to the other three donors (RB179, RB71, and RB114) (Figure 4.4B). Our findings suggest that during the early hours, three of the donors exhibit a nearly equal migration rate. However, as time progressed, we observed a growing difference in their migration rates. This underscores the significance of conducting real-time assessments of potency as opposed to relying solely on endpoint assays.

Furthermore, we measured the number of cells remaining in the microfluidic device over time to determine cell loss during the cell migration. The number of cells decreased over time for all donors. However, we observed that RB183 and RB177 consistently maintained a higher cell count. Notably, there was a significant decrease in the number of cells for the RB179, RB71, and RB114 donors (Figure 4.4C). To further analyze the locomotion pattern of MSCs on chip microfluidic device, we created trajectory plot that overlaid normalized MSCs tracks for individual cells. These plots helped us measure the dispersion and range of motility of each MSCs donors within the microfluidic device. The tracks from RB183 and RB177 cell lines exhibited more dispersion and greater motility, while RB179, RB71, and RB114 showed less dispersion and lower motility (Figure 4.4D). Overall, our live image analysis outcome for each donor is similar to an already established potency assay shown in Figure 4.2. This indicates that the potency of MSCs can be measured faster in real time and accurately in microfluidic device through live imaging.

### 4.2.4 Migratory behavior of MSCs shows association with specific morphological features and analyte secretion.

Cell morphology and cell migration are intimately connected processes[20,21]. The dynamic changes in cell shape and the organization of the cytoskeleton, driven by various intracellular and extracellular cues, are critical determinants of how cells move within tissues. Understanding these relationships is essential for elucidating the mechanisms underlying various physiological and pathological processes involving cell migration. So, to study the intriguing relationship between morphology and migration we performed linear regression. Our study demonstrates the positive correlation of migration with morphological features like compactness, major axis length, and max feret diameter and negative correlation with morphological features like extent, formfactor (Figure

4.5A). To further determine if morphological features of MSCs are correlated with the potency of MSCs which is measured as CD3+ T-cell proliferation inhibition by MSCs shown in Figure 4.2. i.e lower the proliferation of CD3+ T-cell, higher the potency. Cluster map demonstrate the negative correlation of CD+ proliferation with morphological features like compactness, major axis length, and max feret diameter and positive correlation with extent, formfactor, and solidity (Figure 4.5B). This indicates cell population with higher compactness, major axis length, and max feret diameter and lower extent, formfactor, and solidity have higher potency.

The assessment of the cellular suppressive capacity of MSCs is a critical method for evaluating their functional potency in various research and clinical applications. So we aimed to predict the suppressive capacity of MSCs donors by analyzing their morphological characteristics and migratory patterns. To accomplish this, we employed a sophisticated non-linear machine learning regression method known as gradient boost regression (GBR). The GBR approach demonstrated its effectiveness in predicting the T-cell suppressive capacity of MSCs based on data derived from live imaging, which included key features related to the cells' morphology and migratory behavior. (Figure 4.5C).

### 4.2.5 MSCs showed difference in morphology and limited locomotion in 2D surface compared to the 3D surface

To explore how MSCs morphology and locomotion behavior is influenced by the culture surface, we compared the change in morphological features and locomotive capabilities of MSCs in 3D microfluidic device and 2D culture surface. MSCs demonstrated change in morphological features when seeded in 2D culture surface and microfluidic device (Figure 4.6A). Morphological features like minor axis length, maximum radius, mean and median radius, extent and eccentricity mostly

contributed to difference in MSCs morphology in 2D culture surface and microfluidic device as shown in the PCA loading plot.

While comparing the locomotion behavior of MSCs, MSCs displayed limited cell movement in 2D culture surface. Although some cells showed migratory behavior, their overall locomotion remained restricted, likely due to the planar nature of the culture environment. Conversely, in 3D culture surfaces, MSCs demonstrated markedly enhanced locomotion (Figure 4.6B). The 3D scaffold's porous structure provided spatial freedom and better mimicked the native extracellular matrix, facilitating cell migration and interactions with the surrounding microenvironment. This was evident by the increased number of extended protrusions, indicative of active cell migration, in the 3D environment compared to the predominantly observed in 2D.

## 4.3 Discussion

The microfluidic device helped maintain optimal environmental conditions by providing the correct pH, gas conditions, and a constant supply of fresh medium for optimal growth of the cells that mimic their *in vivo* culture conditions. Live imaging of cells *in vivo* culture conditions is the most straightforward and often the most robust approach to studying the dynamic nature of cell processes[22,23]. In this study, the coupling of the 3D microfluidic device and high-content live imaging modalities provides a versatile platform for studying MSC potency. By obtaining the dynamic features of MSC donors cultured in the microfluidic device via live imaging, we can provide a robust comparison of their potency in a fast and non-invasive way in their natural environments. With this approach, we obtained dynamic features to measure the MSCs potency in different donors which otherwise would have taken multiple experimental time-consuming process.

Imaging based analysis showed differences in morphology of MSCs donors. These differences in morphology can influence MSCs' immunomodulatory properties. Recent research suggests that the shape of MSCs may affect their ability to suppress immune responses[24,25]. RB183 and RB177 MSCs donors have higher shape with higher compactness, eccentricity, major axis length and max feret diameter and smaller solidity, and form factor. Previous studies have shown functional MSCs tend to have increased in compactness, eccentricity, major axis length and max feret diameter and decreased in solidity, and form factor[25]. This suggests that the potency of cells can be predicted based on cellular shape. Therefore, donor-specific morphological characteristics could impact the efficacy of MSC-based immunotherapy.

In addition to variances in the morphological characteristics of MSC donors seeded on chip microfluidic device, we observed differences in their migratory and locomotion tendencies among these donors, with RB183 and RB177 demonstrating notably heightened migratory abilities. Several studies have demonstrated role of cell migration in the immune response by facilitating communication among immune cells[26] and enabling cell interactions[27] to reach and effectively target pathogens, infected cells, or damaged tissue for elimination.

Our results demonstrated the association between the migration of the cell and their morphological features. The positive correlation between specific cell morphology and migration highlights the interconnectedness of cellular attributes such as elongated or spindle-shaped cells with higher compactness, major axis length, and max feret diameter and low form factor, and extend may possess structural advantages that facilitate movement through tissues. By integrating live imaging data and machine learning techniques, we can gain valuable insights into the suppressive capabilities of MSCs from different donors. This predictive model not only enhances our understanding of the biological characteristics of MSCs but also has the potential to inform

more personalized and effective therapeutic strategies in fields such as regenerative medicine and immunotherapy.

To further illustrate if the locomotion behaviour of MSCs is enhanced on 3D surface we compared the locomotory track of MSCs seeded on microfluidic device and 2D tissue culture surface. Our results of this study suggest that the dimensionality of the culture surface significantly impacts the locomotion of MSCs with enhanced locomotion on the microfluidic device compared to the 2D culture surface. While 2D culture systems remain useful for certain experimental purposes, the limited spatial freedom and lack of physiological cues may hinder MSC migration and functionality. On the other hand, 3D cultures surfaces offer a more biologically relevant environment that fosters enhanced locomotion, potentially leading to improved cellular integration, tissue regeneration, and therapeutic outcomes.

## 4.4 Conclusions

We anticipate that this technology will revolutionize the assessment of MSC quality and enhance the development of more effective cell-based therapies. The utilization of microfluidic devices combined with live imaging represents a significant advancement in the field of MSC potency prediction. This innovative approach enables real-time monitoring and analysis of MSC behavior, providing a more comprehensive understanding of their functional properties. By facilitating the selection of high-potency MSC populations, this technology has the potential to greatly improve the success and reliability of cell-based therapies, leading to improved patient outcomes and advancing the field of regenerative medicine.

## 4.5 Methods

### 4.5.1 MSC culture

Five bone marrow derived MSC cell lines were obtained from the Roosterbio Inc. (RB; Frederick, MD). Cells were received frozen at passage P1 or P2. Each cell vial was expanded and cryopreserved prior to experimental use. For each experiment, cells were culture rescued for 48h prior to use and used at PDL<20. MSC culture media used alpha-MEM (ThermoFisher) supplemented with 16.5% MSC-qualified fetal bovine serum (FBS) (ThermoFisher), 2-4mM L-glutamine (ThermoFisher), 100 U/mL Penicillin (ThermoFisher), and 100μg/mL Steptomycin (ThermoFisher).

### 4.5.2 Synthesis and set up of on-chip microfluidic devices

As described in Schneider et al., microfluidic chips of polydimethylsiloxane (PDMS, Sylgard 184 Dow Chemical) were cast in an aluminum macro-mold with steel wire (d = 0.02 in) and bonded with oxygen plasma to glass slides. The steel wires were removed to form the fluidic channel. The chip was sealed with a glass cover slip by oxygen plasma treatment, the cross-linked cell-laden hydrogel was placed in the PDMS device, and the system was sealed by plasma treatment.

The microfluidic chips were connected to syringes secured in PHD Ultra Pumps with attached 6/10 multi-racks (Harvard Apparatus) with PTFE tubing (#30 AWG, Cole Parmer), PE/PVC tubing adaptors (0.024 × 0.064 in, Instech Labs) and 20-gauge blunt tip needles (Industrial Dispensing Tips).

### 4.5.3 On-chip microfluidic assay

As previously reported in Schneider et al., MSC cells were encapsulated within on-chip hydrogels as outlined here. 20 kDa 4-arm maleimide-functionalized poly(ethylene-glycol) (PEG-4MAL, Laysan Bio) was dissolved in PBS and mixed with 5mM adhesive peptide RGD (G**RGD**SPC, Genscript) at a 2:1 volume ratio. Crosslinkers VPM (GCRDVPMSMRGGDRCG, Genscript) and dithiothreitol (DTT, Sigma-Aldrich) were dissolved at 24.8 mM and mixed 80:20 ratio by vol. Components were sterilized using 0.22 μm pore filter centrifuge tubes (Costar, Spin-X). PEG-4MAL and RGD components were allowed to functionalize at room temperature (RT) for 30 min. Following 48hr culture rescue, each donor cell line was harvested, counted (≥95% viability), and suspended in solution at 5M cells/mL. PEG-4MAL+RGD solution and cell solution were combined just prior to encapsulation at a 3:1 vol ratio. Hydrogel gelation occurred by mixing PEG-4MAL+RGD+cell solution and crosslinking solution at 4:1 vol ratio for a 20 μL hydrogel (pre-swelling, 20 000 cells per gel) onto a sterilized hydrophobic surface.

The system was sealed and pumps were arranged as described prior. MCS culture medium with 50ng/mL IFN-ɣ (Biolegend) were perfused through the devices at 1.0 μL $min^{-1}$ for 24hr, at which time, the on-chip devices with cells were stained for live-cell imaging and the cell effluent was collected for Luminex analysis

### 4.5.4 2D assay

Cells were seeded onto a tissue culture treated 96-well plate (Costar) at 20,000 cells per well. Cells were treated with 200uL MCS culture medium with 50ng/mL IFN-ɣ (Biolegend). After 24hrs, the cells were stained for live-cell imaging and the cell supernatant was collected for Luminex analysis

### 4.5.5 T Cell Suppression Assay

hMSCs of each donor were culture resuced for 48hrs in hMSC media. PBMCs (donor PBMC-052219A, Zen-Bio Inc.) were washed with anti-aggregate (Fisher Scientific) and culture-rescued for 24 hours in RPMI 1640 HEPES media (ThermoFisher) supplemented with 9% MSC-qualified FBS (ThermoFisher), 100 U mL−1 penicillin, and 100 μg mL−1 streptomycin (both from ThermoFisher). Day 1 of the assay PBMC was stained with carboxyfluorescein succcinimidyl ester (CFSE, ThermoFisher) for generational tracking. Approximately 100,000 T cells from %CD3+ T cells provided by the manufacturer were seeded per well in a 96-well plate. The hMSCs were lifted (0.25% trypsin) and seeded at 50,000 MSC per well. Additional wells were set up for activated and non-activated PBMC-only controls, fluorescent minus one (FMO) controls, and unstained controls. Activation was achieved using anti-CD3+/anti-CD28+ Dynabeads (ThermoFisher) at a 1:1 T cell to bead ratio. All groups received 12 U rIL-2 (PeproTech). After 3 days of co-culture, cells were harvested and stained with Zombie UV Fixable Viability Kit, PE-Cy7 anti-human CD3 (UCHT1), PE anti-human CD4 (RPAT4), and APC anti-human CD8 (RPA-T8) (all from Biolegend). The gating scheme was applied to select for the CD3+ T cell population, with FMO controls used to establish population gates. Student's t-test was performed using the scipy.stats package in python.

### 4.5.6 Live Imaging

For live imaging, MSCs were prepared by staining cell bodies with CellTracker Geen CMFDA Dye (Thermo Fisher) and cell nuclei with NucBlue Live Ready Probes Reagent (Hoechst 33342) (Thermo Fisher) as per the manufactures recomendations. The imaging process was conducted using The Zeiss LSM 710 confocal microscope system, which included a Zeiss AXIO Observer

Z1 inverted microscope stand with transmitted (HAL), UV (HBO), and laser illumination sources (Zeiss, Oberkochen, Germany). Live imaging was performed with a 10X objective and numerical aperture of 0.55. To excite Cell Tracker Green, the 488 nm laser was used, and for NucBlue, the 405 nm laser was utilized. The laser power was kept at a minimum to prevent phototoxicity.

For each MSCs donor, Z-stacks of the cells and cell nuclei were acquired. Live imaging was conducted continuously over a 6-hour period for each MSCs donor. The obtained live images were then segmented using the track object pipeline, employing the overlap tracking method in the CellProfiler (Ref). Various morphological features, as well as lifetime, integrated distance, distance traveled, and displacement of each MSCs donor, were extracted and analyzed. Imaris software was used to generate the 3D images of each MSCs donors from Z-stacks. Python Script was used to create PCA plot to visualize the difference in MSCs donors based on morphological features.

### 4.5.7 Integrated distance and migration rate analysis

Using custom Python script, the integrated distance traveled by each MSCs donor throughout their lifetime, as well as the number of cells for each donor after every 15 minutes of travel distance, were plotted. The analysis was limited to donors with a lifetime of up to 24. Any dividing cells were excluded from the analysis. To calculate the migration rate of each MSCs, the integrated distance and lifetime of each donor were utilized:

Migration rate = Tracked Integrated Distance / Tracked Lifetime

The Python script was then used to visualize the calculated migration rate over the specified time period.

### 4.5.8 Rose plot

Centroids of the cell nuclei were computed and tracks of individual cells were generated using Python script. The cells position at lifetime 0 was considered the center. Using the Trajectory_X and Trajectory_Y values at each lifetime for every cell, its displacement from that normalized center was plotted across the entire lifetime of each cell. All the dividing cells were discarded.

### 4.5.9 Linear regression and Cluster analysis

Linear regression analysis was conducted using GraphPad Prism 10 (Graph- Pad Software Inc., La Jolla, CA), as indicated, with R2 and the corresponding P-values displayed. The X values were entered as means, while the Y replicates were considered independent samples. The solid lines in the graphs represent the best-fit lines, accompanied by dotted lines denoting the corresponding 95% confidence intervals. The P-values serve as an indicator of confidence regarding the deviation of the slope from zero under the null hypothesis. A P-value less than 0.05 is considered statistically significant. All data represents as mean ± SEM. The heatmap in Figure 4.5B was generated using the seaborn.clustermap package. Clustering was performed using the "Euclidean" distance and "average" method.

### 4.5.10 Gradient boost regression (GBR)

Non-linear machine learning regression method, GBR, was used for logistic regression modeling. The regression model is as a part of the Scikit-learn 1.3.1 package implemented in Python 3.9. Single-cell migration measurement as well as morphological features were scaled using the StandardScaler function in Scikit-learn 1.3.1 in python 3.9 then used for prediction through GBR.

Proliferation of T-cells co-cultured with MSC was used to represent MSCs' T-cell suppressive capacity as the target value for prediction. (I guess it's the explanation of the predict targets from T cell suppression assay) Average of predicted single-cell T cell suppressive capacity was calculated within each donor to represent the bulk cell T cell suppressive capacity.

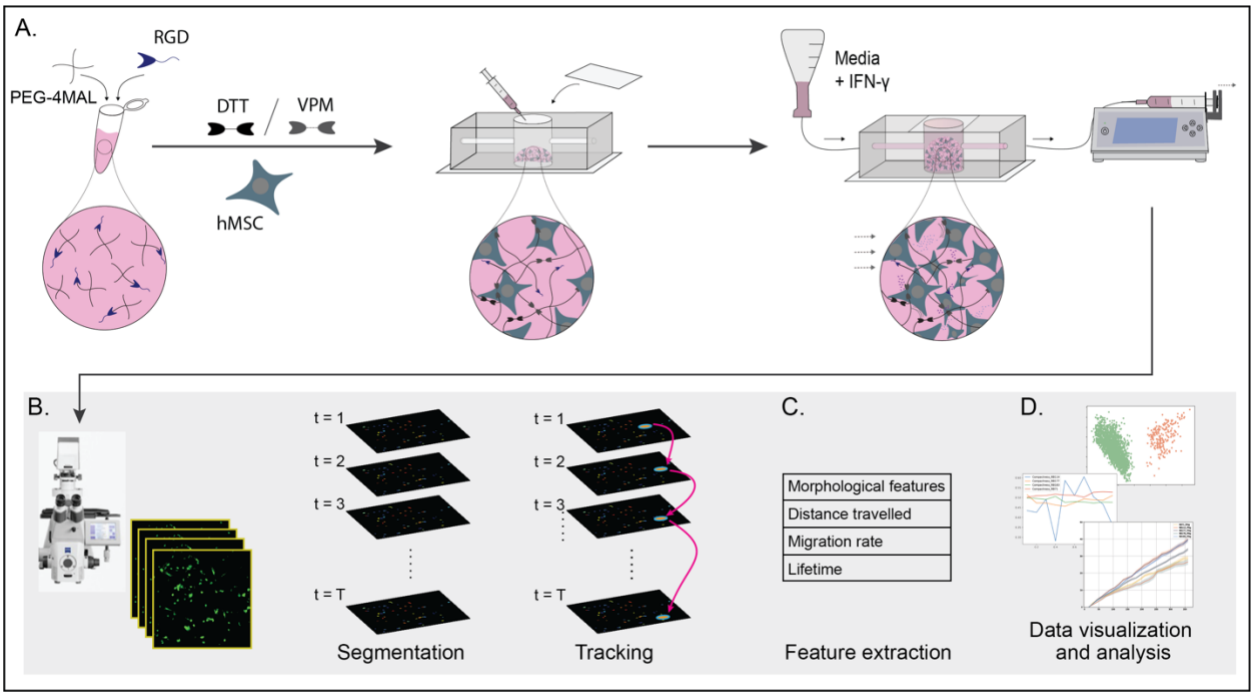


**Figure 4.1: Schematic of the process to integrate a 3D microfluidic device with advanced high-content live imaging techniques for assessing the efficacy of MSC donors**.

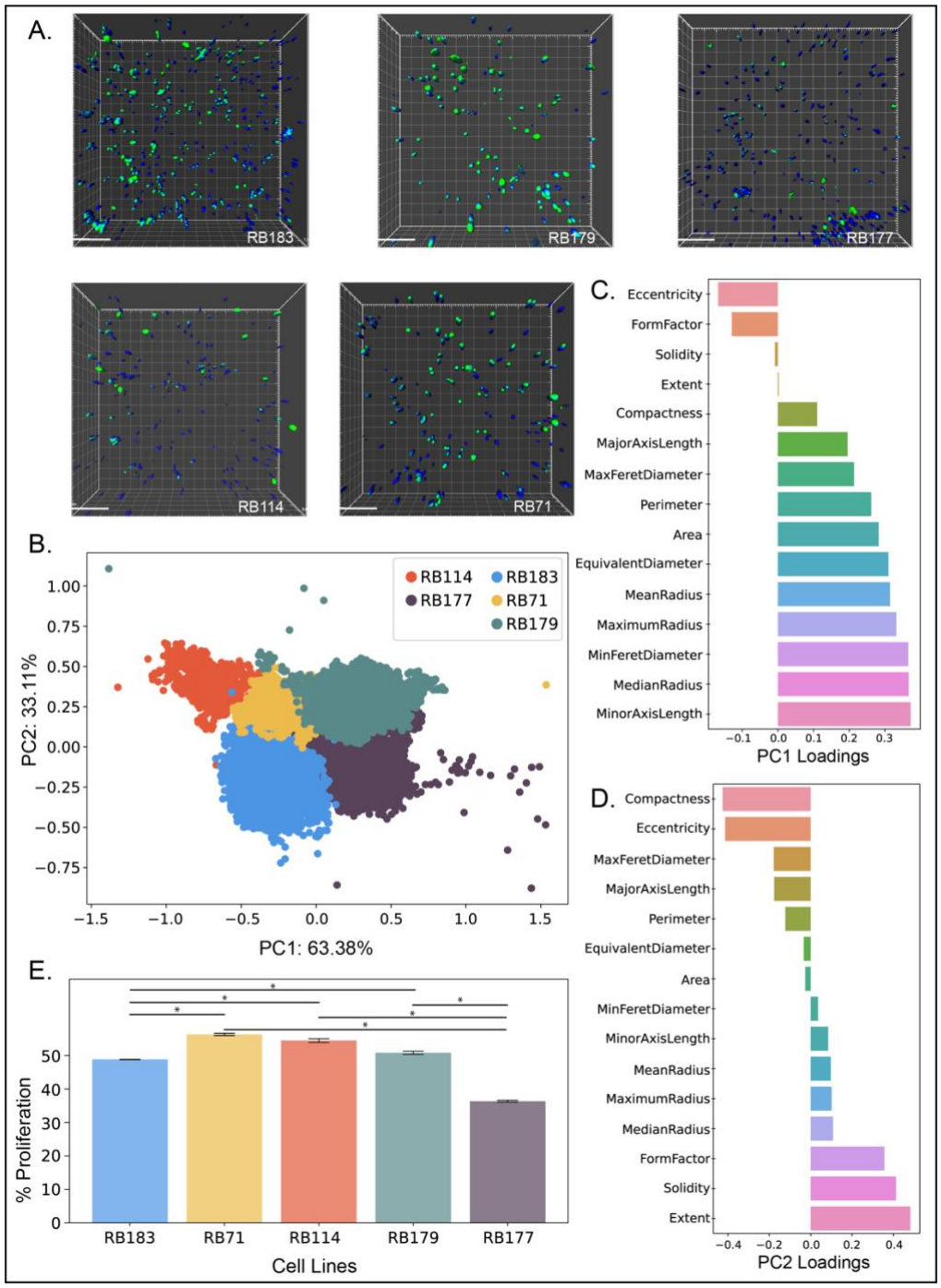


**Figure 4.2: Characterization of MSCs donors MSCs donors exhibit distinct morphological characters and potency.** (A) 3D images of the MSC donors obtained from stacks of live images. Starting from left, RB183, RB179, RB177, RB114, and RB71. Cell body (green) stained with Cell tracker green. Cell nuclei (blue) stained with Hoechst. (Scale bar=150 μm). (B) PCA plot showing the separation between MSCs donors based on the morphological features. (C). PC1 Loading plot showing the contributing features in separation between MSC donors. (D). PC2 Loading plot showing the contributing features in separation between MSC donors. (E). CD3+ T cell suppression for various hMSC donors (* P<0.05).

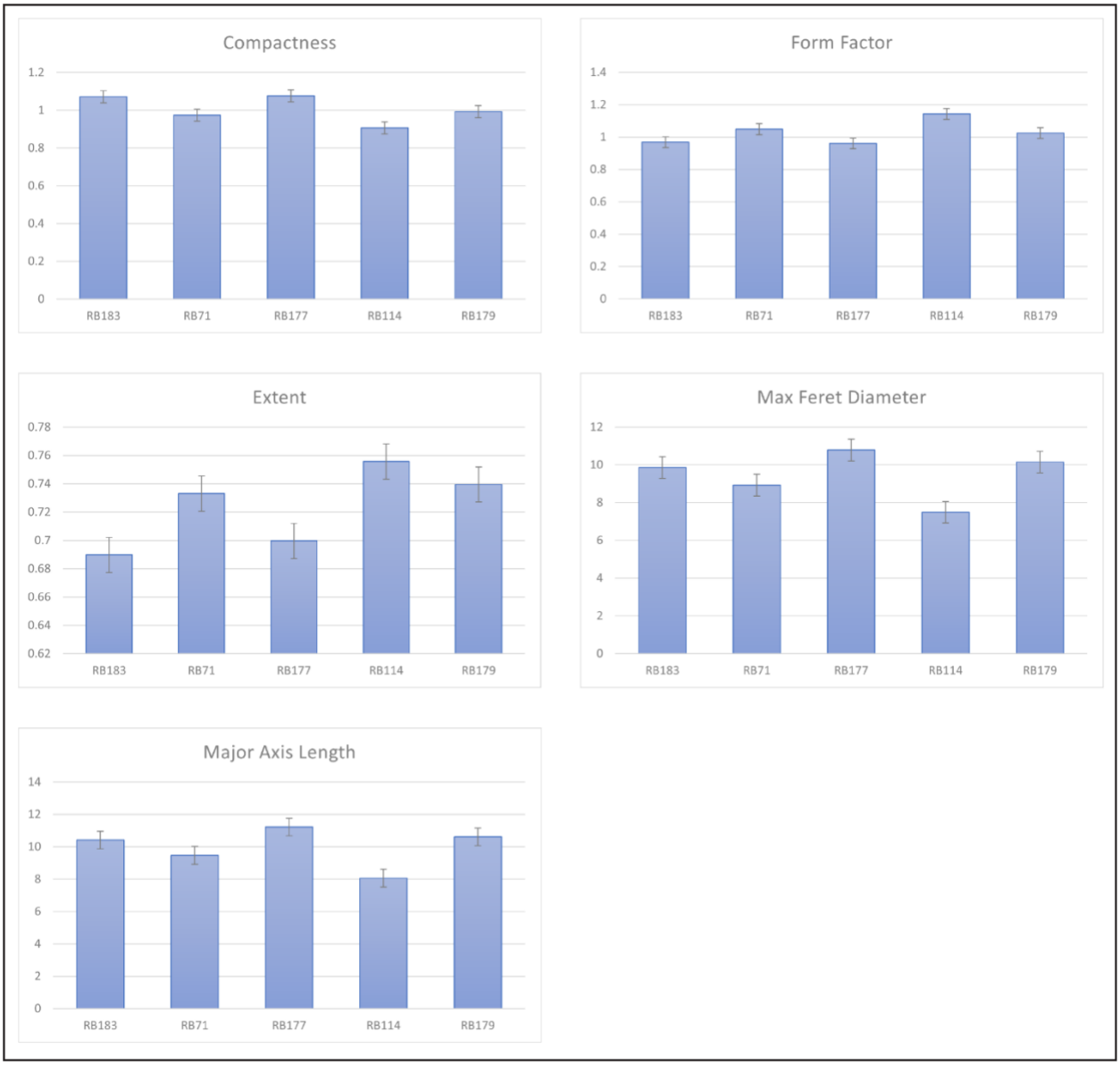


**Figure 4.3: MSCs morphology comparison.** Barplot showing comparison of MSCs morphological features among all donors.

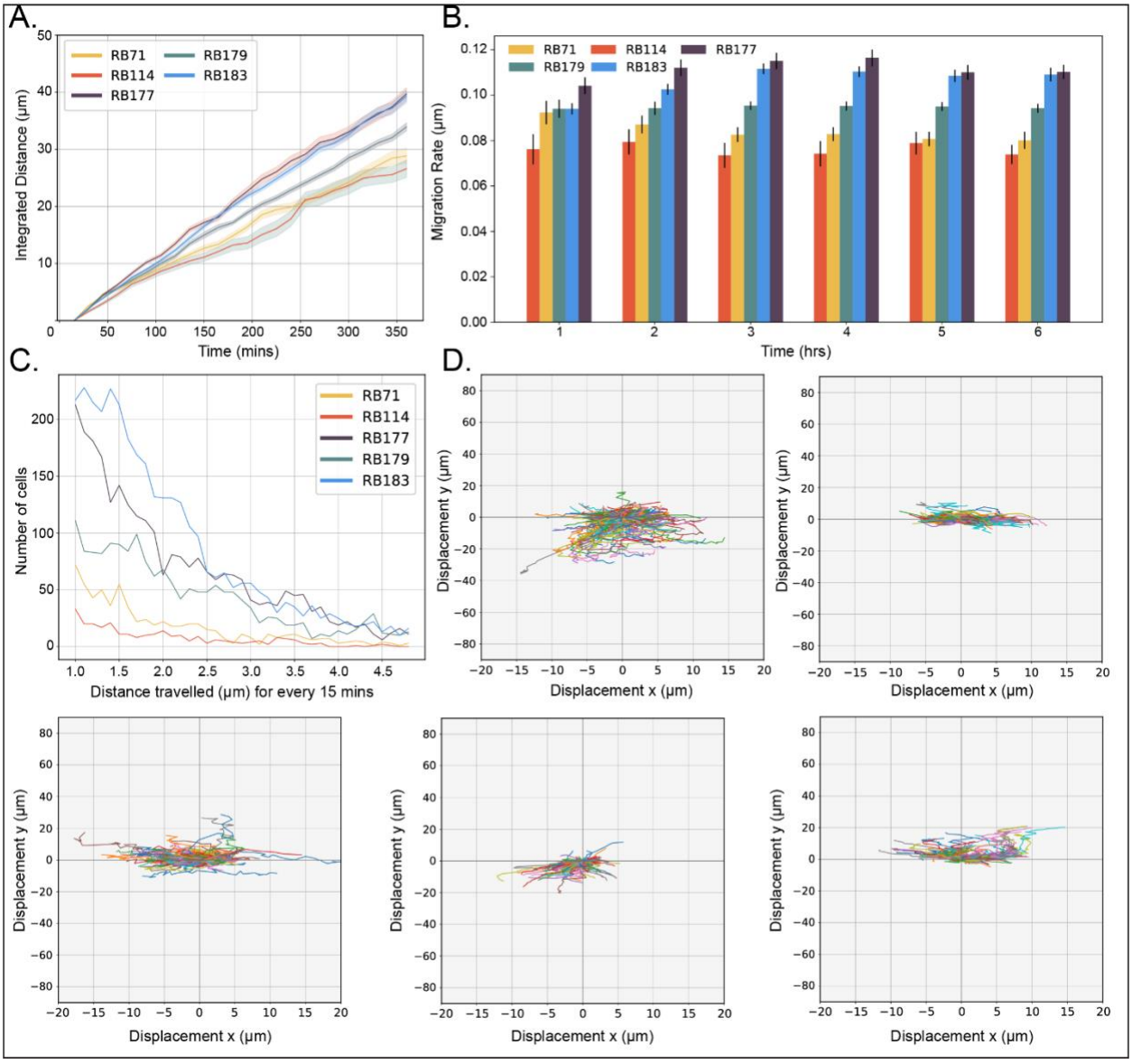


**Figure 4.4: Difference in MSCs locomotion and migratory potential**. (A) Integrated distance travel by MSCs donors over time. Shaded region indicated the standard error of the mean (SEM). (B). Comparison of migration rate of MSC donors during each hour. Bar chart represents ± SEM (C). The number of cells for each donor migrated in the microfluidic device over time. (D) Rose plots show MSCs locomotion behavior in microfluidic device for each donor.

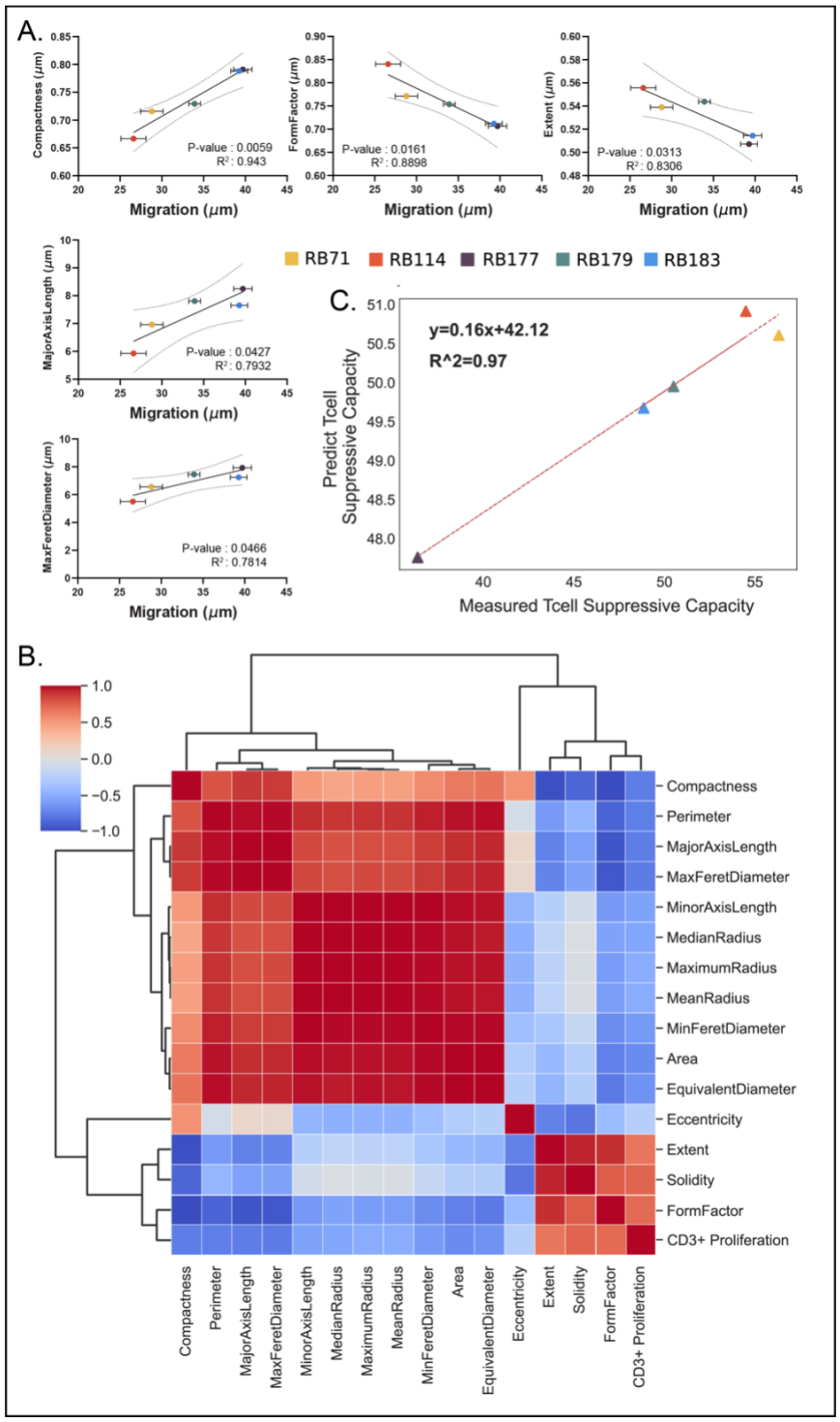


**Figure 4.5: Potency prediction through migration and morphology.** (A) Linear regression showing statistically significant relationships with positive correlation of MSC migration with compactness, major axis length, max feret diameter and negative correlation with form factor, and extent. (B) Heat map and hierarchal clustering of CD+ proliferation as a measure of MSCs potency and morphological features ±SEM. (C) Logistic regression modeling showing prediction of T-cell suppression capacity my MSCs.

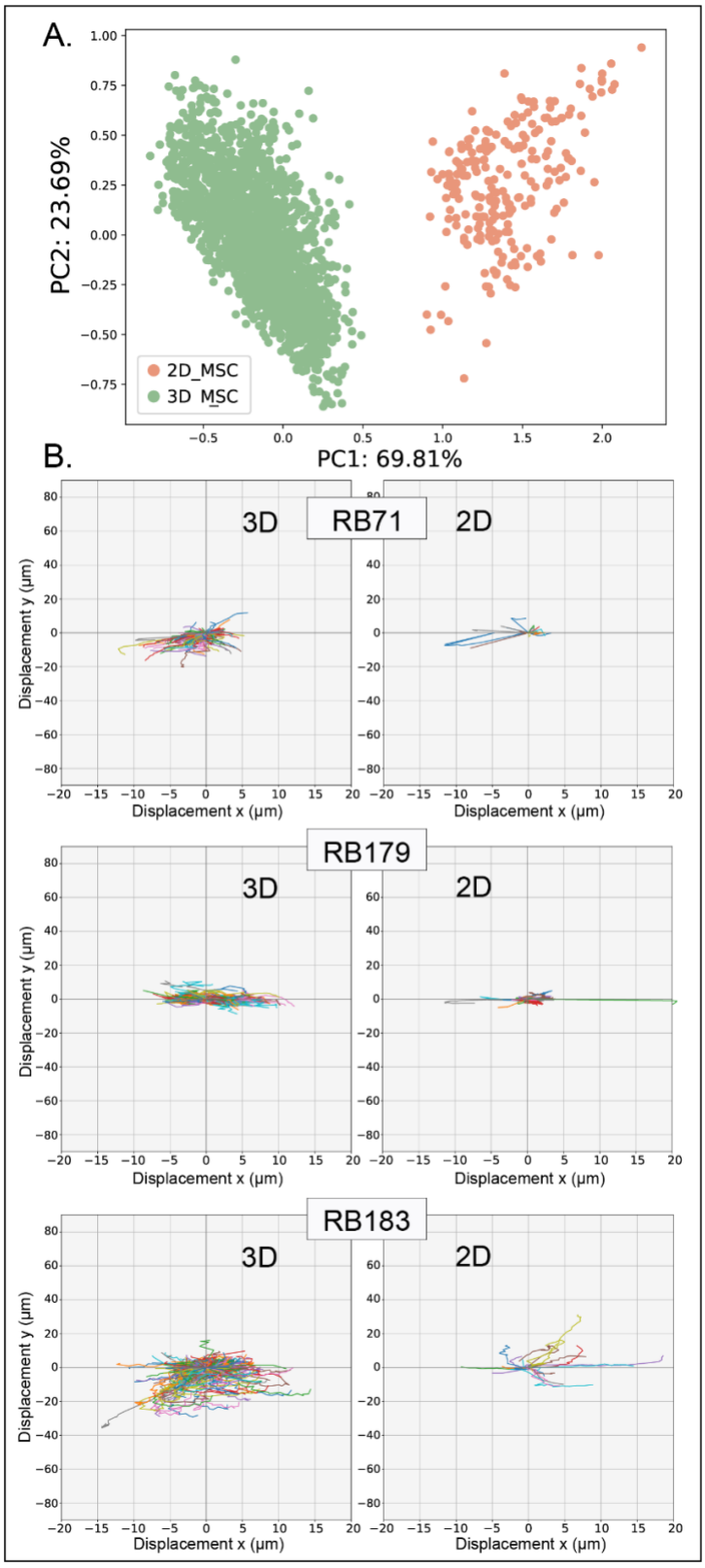


**Figure 4.6: Comparison of MSC morphology features and locomotion behaviour on 3D microfluidic device and 2D tissue culture surface**.

## 4.6 Bibliography


1 Caplan, A. I. Adult mesenchymal stem cells for tissue engineering versus regenerative medicine. *Journal of cellular physiology* **213**, 341-347, doi:10.1002/jcp.21200 (2007).

2 Rodríguez-Fuentes, D. E. *et al.* Mesenchymal Stem Cells Current Clinical Applications: A Systematic Review. *Archives of medical research* **52**, 93-101, doi:10.1016/j.arcmed.2020.08.006 (2021).

3 Jiang, W. & Xu, J. Immune modulation by mesenchymal stem cells. *Cell proliferation* **53**, e12712, doi:10.1111/cpr.12712 (2020).

4 Hwang, N. S., Zhang, C., Hwang, Y. S. & Varghese, S. Mesenchymal stem cell differentiation and roles in regenerative medicine. *Wiley interdisciplinary reviews. Systems biology and medicine* **1**, 97-106, doi:10.1002/wsbm.26 (2009).

5 Rojewski, M. T., Weber, B. M. & Schrezenmeier, H. Phenotypic Characterization of Mesenchymal Stem Cells from Various Tissues. *Transfusion medicine and hemotherapy : offizielles Organ der Deutschen Gesellschaft fur Transfusionsmedizin und Immunhamatologie* **35**, 168-184, doi:10.1159/000129013 (2008).

6 Lipat, A. J. *et al.* Chemokine Assay Matrix Defines the Potency of Human Bone Marrow Mesenchymal Stromal Cells. *Stem cells translational medicine* **11**, 971-986, doi:10.1093/stcltm/szac050 (2022).

7 Ravi, M., Paramesh, V., Kaviya, S. R., Anuradha, E. & Solomon, F. D. 3D cell culture systems: advantages and applications. *Journal of cellular physiology* **230**, 16-26, doi:10.1002/jcp.24683 (2015).

8 Coluccio, M. L. *et al.* Microfluidic platforms for cell cultures and investigations. *Microelectronic Engineering* **208**, 14-28, doi:https://doi.org/10.1016/j.mee.2019.01.004 (2019).

9 Li, R., Lv, X., Zhang, X., Saeed, O. & Deng, Y. Microfluidics for cell-cell interactions: A review. *Frontiers of Chemical Science and Engineering* **10**, 90-98, doi:10.1007/s11705-015-1550-2 (2016).

10 Schneider, R. S. *et al.* High-Throughput On-Chip Human Mesenchymal Stromal Cell Potency Prediction. *Advanced healthcare materials* **11**, e2101995, doi:10.1002/adhm.202101995 (2022).

11 Fu, X. *et al.* Mesenchymal Stem Cell Migration and Tissue Repair. *Cells* **8**, doi:10.3390/cells8080784 (2019).

12 Sun, Y., Yuan, Y., Wu, W., Lei, L. & Zhang, L. The effects of locomotion on bone marrow mesenchymal stem cell fate: insight into mechanical regulation and bone formation. *Cell & bioscience* **11**, 88, doi:10.1186/s13578-021-00601-9 (2021).

13 Wilson, A., Hodgson-Garms, M., Frith, J. E. & Genever, P. Multiplicity of Mesenchymal Stromal Cells: Finding the Right Route to Therapy. *Frontiers in immunology* **10**, 1112, doi:10.3389/fimmu.2019.01112 (2019).

14 Mastrolia, I. *et al.* Challenges in Clinical Development of Mesenchymal Stromal/Stem Cells: Concise Review. *Stem cells translational medicine* **8**, 1135-1148, doi:10.1002/sctm.19-0044 (2019).

15 Galipeau, J. *et al.* International Society for Cellular Therapy perspective on immune functional assays for mesenchymal stromal cells as potency release criterion for advanced phase clinical trials. *Cytotherapy* **18**, 151-159, doi:10.1016/j.jcyt.2015.11.008 (2016).

16 Antoni, D., Burckel, H., Josset, E. & Noel, G. Three-dimensional cell culture: a breakthrough in vivo. *International journal of molecular sciences* **16**, 5517-5527, doi:10.3390/ijms16035517 (2015).

17 Duval, K. *et al.* Modeling Physiological Events in 2D vs. 3D Cell Culture. **32**, 266-277, doi:10.1152/physiol.00036.2016 (2017).

18 Barbash, I. M. *et al.* Systemic Delivery of Bone Marrow–Derived Mesenchymal Stem Cells to the Infarcted Myocardium. **108**, 863-868, doi:doi:10.1161/01.CIR.0000084828.50310.6A (2003).

19 Trepat, X., Chen, Z. & Jacobson, K. Cell migration. *Comprehensive Physiology* **2**, 2369-2392, doi:10.1002/cphy.c110012 (2012).

20 Aman, A. & Piotrowski, T. Cell migration during morphogenesis. *Developmental biology* **341**, 20-33, doi:10.1016/j.ydbio.2009.11.014 (2010).

21 Tang, Q. Y. *et al.* Control of cell migration direction by inducing cell shape asymmetry with patterned topography. *Journal of biomedical materials research. Part A* **103**, 2383-2393, doi:10.1002/jbm.a.35378 (2015).

22 Nketia, T. A., Sailem, H., Rohde, G., Machiraju, R. & Rittscher, J. Analysis of live cell images: Methods, tools and opportunities. *Methods (San Diego, Calif.)* **115**, 65-79, doi:10.1016/j.ymeth.2017.02.007 (2017).

23 Liu, Z., Lavis, L. D. & Betzig, E. Imaging live-cell dynamics and structure at the single-molecule level. *Molecular cell* **58**, 644-659, doi:10.1016/j.molcel.2015.02.033 (2015).

24 Marklein, R. A. *et al.* Morphological profiling using machine learning reveals emergent subpopulations of interferon-γ-stimulated mesenchymal stromal cells that predict immunosuppression. *Cytotherapy* **21**, 17-31, doi:10.1016/j.jcyt.2018.10.008 (2019).

25 Klinker, M. W., Marklein, R. A., Lo Surdo, J. L., Wei, C. H. & Bauer, S. R. Morphological features of IFN-γ-stimulated mesenchymal stromal cells predict overall immunosuppressive capacity. *Proceedings of the National Academy of Sciences of the United States of America* **114**, E2598-e2607, doi:10.1073/pnas.1617933114 (2017).

26 Delgado, M. G. & Lennon-Duménil, A. M. How cell migration helps immune sentinels. *Frontiers in cell and developmental biology* **10**, 932472, doi:10.3389/fcell.2022.932472 (2022).

27 Mishra, A. K., Campanale, J. P., Mondo, J. A. & Montell, D. J. Cell interactions in collective cell migration. *Development (Cambridge, England)* **146**, doi:10.1242/dev.172056 (2019).

28 Ding, Q. *et al.* Potential role of CXCL9 induced by endothelial cells/CD133+ liver cancer cells co-culture system in tumor transendothelial migration. *Genes & cancer* **7**, 254-259, doi:10.18632/genesandcancer.116 (2016).

29 Yu, F. L., Liao, M. H., Lee, J. W. & Shih, W. L. Induction of hepatoma cells migration by phosphoglucose isomerase/autocrine motility factor through the upregulation of matrix metalloproteinase-3. *Biochemical and biophysical research communications* **314**, 76-82, doi:10.1016/j.bbrc.2003.12.056 (2004).

30 Shi, J. *et al.* Membrane-type MMPs enable extracellular matrix permissiveness and mesenchymal cell proliferation during embryogenesis. *Developmental biology* **313**, 196-209, doi:10.1016/j.ydbio.2007.10.017 (2008).

31 Forte, D. *et al.* The tissue inhibitor of metalloproteinases-1 (TIMP-1) promotes survival and migration of acute myeloid leukemia cells through CD63/PI3K/Akt/p21 signaling. *Oncotarget* **8**, 2261-2274, doi:10.18632/oncotarget.13664 (2017).

32 Lee, S. Y. *et al.* TIMP-1 modulates chemotaxis of human neural stem cells through CD63 and integrin signalling. *The Biochemical journal* **459**, 565-576, doi:10.1042/bj20131119 (2014).

33 Morton, P. E. *et al.* TNFR1 membrane reorganization promotes distinct modes of TNFα signaling. *Science signaling* **12**, doi:10.1126/scisignal.aaw2418 (2019).

34 Lo, C. H., Huber, E. C. & Sachs, J. N. Conformational states of TNFR1 as a molecular switch for receptor function. *Protein science : a publication of the Protein Society* **29**, 1401-1415, doi:10.1002/pro.3829 (2020).

# CHAPTER 5

# CONCLUSION AND FUTURE STUDIES

## 5.1 Achievement of goals

This study demonstrates the comprehensive analysis of MSC characteristics by applying integrative approaches to study external phenotype and internal functional mechanisms that would lead to consistent and effective clinical MSC based therapeutics. By the application of high content label-free imaging techniques, live imaging technique and high-resolution mass spectrometry, we obtained morphological features and lipidomic profile of MSCs correlated with the functional activity to obtain in depth analysis of cell functional activity. Analyzing bulk MSCs for associations between lipidomic profiles and functional activity over multiple passages helped to identify cell stages with the best fitness levels and the effectors of such elevated fitness. This is critical in order to provide sufficient cells through expansion for the biomanufacturing processes and for therapeutic uses. To that effect, this study provides an informed decision in terms of the expansion limits of the cell lines and how pathways can be manipulated to get the best cells during biomanufacturing expansion.

Identification and characterization of the lipidomic link with their morphological phenotype at a single cell level allowed for the selection of functionally potent and superior MSC subpopulations based on their physical attributes. In addition, analyzing how cell culture environments influenced

the morphology, and migratory behavior helped in selection of most functional cells. Overall, this research showed the dynamic features of MSCs, both in bulk and at a single-cell level, to predict cell immunosuppressive capacity for successful and consistent clinical use. Identification of key lipidomic markers allowed for their manipulation to adjust the functional activity of cells associated with immune regulation. In addition, key lipidomic and morphological markers identified through this study will allow for a high throughput screening of potent MSC cells, marking a significant stride towards the large-scale production of MSCs with consistent efficacy for clinical applications and therapeutic use.

### 5.1.1 Investigate and characterize lipid profiles associated with MSCs over multiple passages

We explored the lipid alterations in lipid profile during *in vitro* expansion of MSCs. Multivariate analysis of lipids dynamics during MSC aging using MALDI-FTICR provides lipid features that evolved in early and late passage MSCs. The relationship between the lipidomic profile at different stages of cell aging, cell morphology, and cytokine secretion provided better understand potential links between changes in cellular lipid composition and overall cellular functionality.

These strategies can establish the connections between these compositional changes and altered potency and quality of the cells. This work emphasizes the potential of high mass resolution spectrometry revealing metabolic spectral features of aging MSCs to map their changes in biological processes, and offers understanding of lipid metabolism pathways including PC, LysoPC, SM, CerP, PG, PI and PE that are impaired in aged cells that could be adjusted to improve cellular performance.

### 5.1.2 Integration of imaging modalities with lipidomic characterization

By applying coregistration pipeline we simultaneously obtained the link between morphological and features and lipidomic profiles of single-cell MSCs using two label-free imaging techniques: DPC microscopy to obtain morphology of MSCs, and MALDI-MSI. For the first time, this study describes the association of change in MSCs morphological features with the change in lipid metabolites after stimulating with inflammatory cytokines IFN-γ. With this study we found correlation of morphological features such as perimeter, compactness, major axis length, max feret diameter, solidity, form factor, and extent with the functional lipid profile of immune activated MSCs. A study at the single cell level provided a clear understanding of the critical associations between the MSCs immunomodulatory function regulated by metabolic changes with their external morphological features. This separation technique offers a promising approach to tackle the challenge of heterogeneity and the selection and generation of MSCs in large scale that consistently exhibit effective immune-suppressive properties for therapeutic and clinical applications. Our proposed method also holds opportunities for non-destructive, label-free analysis of cell morphology for prediction of metabolites to understand the biological process of the cells that can be applicable for the potency analysis of not only MSCs but also for the other cell lines essential for the clinical therapeutics.

### 5.1.3 MSCs potency prediction through live imaging on high-throughput microfluidic device

Live imaging provides a powerful tool for visualizing and studying the real-time dynamic processes of cells in microfluidic devices. Use of high content live imaging in a microfluidic device can

transform in the evaluation of MSC quality further bolstered the progression of more efficient cell-based therapies. We investigated imaging strategies for monitoring the morphological cell features associated with MSC secretory response to inflammatory stimuli in real-time. While live imaging can monitor cell behavior in real time and 3D microfluidic device can mimic the *in vivo* environment providing natural growth conditions for the cells, the integration of live imaging with 3D microfluidic device allowed for the continuous observation and assessment of MSC behavior in real time mimicking *in vivo* like environment, yielding a more in-depth comprehension of their functional attributes. MSCs real time features such as migration and locomotion differed from donor to donor indicating the difference in their functional potency. MSCs morphological features were also related to their functional potency. These discoveries enabled predictive monitoring of MSC culture potency. By streamlining the identification of high-potency MSC groups, this technology holds the promise of significantly enhancing the effectiveness and dependability of cell-based treatments, ultimately resulting in better patient outcomes and pushing forward the frontiers of regenerative medicine.

## 5.2 Future directions

The observations and findings shared in this study offer a comprehensive dataset and valuable resources for comprehending the changes in MSCs' functionality as they age. This encompasses insights into the characteristics of functionally active MSC subpopulations and their functional behavior within 3D microfluidic culture environments. Throughout this endeavor, I acquired expertise in advanced imaging and mass spectrometry techniques, alongside analytical tools. All of my projects involved collaboration, affording me the opportunity to work within diverse teams and gain insights from experts in various fields. The outcomes of these studies hold great promise for

enhancing the effectiveness of MSC-based therapies. Future students can build upon this research to move closer to their objectives. I outlined potential areas for future investigation stemming from the innovative findings presented here.

### 5.2.1 Integration of transcriptomics and proteomic with lipidomic

Our comprehensive study of bulk cell MSCs has shed light on the pivotal role that lipids play in the aging process of these mesenchymal stem cells. It is increasingly evident that lipids, which are fundamental components of cell membranes and regulators of various cellular functions, play a critical role in modulating the aging trajectory of MSCs. To gain a more profound and comprehensive understanding of the complex mechanisms underlying the functional changes that occur as MSCs age or enter senescence, it is critical to integrate the lipidome, encompassing the entire lipid composition and dynamics within these cells, with their transcriptomic profile which details the gene expression patterns and regulatory networks at play[1] and proteomic profile which details the involvement of proteins[2]. Several studies highlight the importance of either integrating lipidome and transcriptome or transcriptome and proteome[3-5]. However, the holistic [6]insights into how lipids, gene expression, and proteins are interconnected and jointly pathway can be mapped to define the aging process in MSCs.

Different approaches have been described to study the joint pathways[3,6] (https://www.creative-proteomics.com/services/integrated-transcriptomic-and-lipidomics-analysis.htm). Such insights can pave the way for targeted interventions and therapies aimed at rejuvenating or optimizing the functionality of aging MSCs for large scale biomanufacturing, holding great promise for regenerative medicine and the treatment of diseases. In essence, the fusion of lipidomic and

transcriptomics represents a powerful approach for unlocking the mechanism behind the aging of MSCs and has the potential to revolutionize our approach to cellular rejuvenation.

### 5.2.2 Enhance MSCs with the lipid treatment and select and filter potent cells based on morphological features.

In our research, we conducted a comprehensive coregistration analysis that examined the morphological characteristics and lipidomic profiles of individual MSCs. This analysis revealed a notable correlation between the unique morphological features and the lipid composition of MSCs that had been activated by immune responses. This groundbreaking finding highlights the complex interplay between cell structure and lipid content, shedding new light on the understanding of MSC behavior at the single-cell level.

Building on this significant discovery, our study is poised to take the next critical step. We intend to subject MSCs to controlled treatments with specific lipid doses, with the goal of enhancing the functional properties of these cells. By precisely manipulating the lipid environment of MSCs, we aim to enhance their therapeutic potential and efficacy in various applications, such as regenerative medicine and immunotherapy.

Furthermore, our research paves the way for the isolation of a subpopulation of particularly potent MSCs. This isolation process will be based on the careful assessment of cell shape and size, allowing label free selection and separation of the MSCs with the most promising attributes. Recently use of microfluidic device as one of the viable option for separating cells based on shape and size has been propsed[7,8]. This subpopulation of MSCs holds immense promise for advancing the field of cell-based therapies and has the potential to revolutionize the way we harness the regenerative capabilities of these cells for the betterment of clinical therapeutics. Overall, our study

represents a significant advancement in our understanding of MSC biology and opens exciting direction for further exploration and application in the field of regenerative medicine.

### 5.2.3 Study of spatial pattern of cells

Our advanced high-content live imaging technique, conducted within a microfluidic device, has provided us with a powerful tool for discerning the most potent source of MSCs from a pool of donors in real time akin to their natural environment. This selection is based on a comprehensive assessment of MSC migration and locomotion behavior. The ability of cells to migrate is linked to their functionality and plays a pivotal role in numerous biological processes, including, tissue regeneration, pathological mechanisms, and immune responses[9,10].

In this study, our analysis focused on bulk cell populations from various MSC donors, offering a valuable initial insight into their potential. However, to gain a deeper understanding and identify the functional subpopulations within these potent donors, a more detailed examination at the single-cell level is required. To achieve this, we intend to employ cutting-edge techniques such as spatial lipidomics and transcriptomics[11,12].

In our single cell-based study (Chapter 3) we used spatial DE method to study the spatial distribution of lipids. By integrating these methodologies, we aim to correlate spatial features within the microenvironment of individual cells with their migration patterns and morphological characteristics. This multi-dimensional approach promises to unravel the intricate details of MSC functionality, facilitating the selection of functional subpopulation for specific therapeutic applications.

### 5.2.4 *In vivo* study using potent MSCs

The determination and selection of a functional subpopulation of MSCs from the heterogeneous population (as described in section 5.2.2) represent a crucial step in advancing our understanding and utilization of these remarkable cells. MSCs, known for their regenerative potential and immunomodulatory properties, exist as a diverse group with variations in their regenerative capabilities and immunosuppressive functions. The identification and isolation of a specific subset with enhanced therapeutic potential can greatly enhance the efficacy of MSC-based therapies.

Once this enhanced and carefully selected functional subpopulation of MSCs can be isolated, it paves the way for exciting *in vivo* studies. These studies involve the transplantation of the selected MSCs into relevant disease animal models. Since this study targeted to enhance the immune functional capacity of MSCs, the animal model with immunocompromised diseases can be studied. These *in vivo* studies can encompass a wide range of investigations. Researchers can explore the optimal dosage and administration method for the selected MSC subpopulation, seeking to determine the precise amount and dosing of MSCs required to achieve the best therapeutic outcomes.

In summary, the determination and isolation of a functional subpopulation of MSCs from the heterogeneous pool offer the promise of more potent and targeted therapeutic interventions. *In vivo* studies involving the transplantation of these selected cells provide a platform for refining treatment strategies, optimizing dosages, and gaining deeper insights into the mechanisms through which MSCs exert their therapeutic effects. Ultimately, these endeavors contribute to the advancement of regenerative medicine and the development of novel therapies for a wide range of medical conditions.

## 5.3 Bibliography


1 Raghavachari, N. & Garcia-Reyero, N. Overview of Gene Expression Analysis: Transcriptomics. *Methods in molecular biology (Clifton, N.J.)* **1783**, 1-6, doi:10.1007/978-1-4939-7834-2_1 (2018).

2 Carneiro, D. G., Clarke, T., Davies, C. C. & Bailey, D. Identifying novel protein interactions: Proteomic methods, optimisation approaches and data analysis pipelines. *Methods (San Diego, Calif.)* **95**, 46-54, doi:10.1016/j.ymeth.2015.08.022 (2016).

3 Lucarelli, G. *et al.* Integration of Lipidomics and Transcriptomics Reveals Reprogramming of the Lipid Metabolism and Composition in Clear Cell Renal Cell Carcinoma. *Metabolites* **10**, doi:10.3390/metabo10120509 (2020).

4 Du, Y. *et al.* Integration of transcriptomic and proteomic data identifies biological functions in cell populations from human infant lung. *American journal of physiology. Lung cellular and molecular physiology* **317**, L347-l360, doi:10.1152/ajplung.00475.2018 (2019).

5 Zhou, J. *et al.* Integrated Transcriptomic and Proteomic Analysis Reveals Up-Regulation of Apoptosis and Small Heat Shock Proteins in Lens of Rats Under Low Temperature. *Frontiers in physiology* **12**, 683056, doi:10.3389/fphys.2021.683056 (2021).

6 Xu, J. *et al.* Integrated lipidomics and proteomics network analysis highlights lipid and immunity pathways associated with Alzheimer's disease. *Translational neurodegeneration* **9**, 36, doi:10.1186/s40035-020-00215-0 (2020).

7 Venugopal, D. *et al.* Clog-free high-throughput microfluidic cell isolation with multifunctional microposts. *Scientific reports* **11**, 16685, doi:10.1038/s41598-021-94123-6 (2021).

8 Zhang, X., Zhu, Z., Xiang, N., Long, F. & Ni, Z. Automated Microfluidic Instrument for Label-Free and High-Throughput Cell Separation. *Analytical chemistry* **90**, 4212-4220, doi:10.1021/acs.analchem.8b00539 (2018).

9 Fu, X. *et al.* Mesenchymal Stem Cell Migration and Tissue Repair. *Cells* **8**, doi:10.3390/cells8080784 (2019).

10 Delgado, M. G. & Lennon-Duménil, A. M. How cell migration helps immune sentinels. *Frontiers in cell and developmental biology* **10**, 932472, doi:10.3389/fcell.2022.932472 (2022).

11 Chen, P. *et al.* Single-Cell and Spatial Transcriptomics Decodes Wharton's Jelly-Derived Mesenchymal Stem Cells Heterogeneity and a Subpopulation with Wound Repair Signatures. *Advanced science (Weinheim, Baden-Wurttemberg, Germany)* **10**, e2204786, doi:10.1002/advs.202204786 (2023).

12 Mutuku, S. M. *et al.* Unravelling Prostate Cancer Heterogeneity Using Spatial Approaches to Lipidomics and Transcriptomics. *Cancers* **14**, doi:10.3390/cancers14071702 (2022).

# APPENDIX A

# EXTENDED RESULTS

In addition to the results presented in the main dissertation, I contributed to multiple collaborative projects during my Ph.D. study that resulted in multiple co-authored journal publications and manuscript submissions. The abstract for these bodies of work are listed below.

# Differential chondrogenic differentiation between iPSC derived from healthy and OA cartilage is associated with changes in epigenetic regulation and metabolic transcriptomic signatures

Nazir M Khan, Martha Elena Diaz-Hernandez, Samir Chihab, Priyanka Priyadarshani, Pallavi Bhattaram, Luke J Mortensen, Rosa M Guzzo, Hicham Drissi

Induced pluripotent stem cells (iPSCs) are potential cell sources for regenerative medicine. The iPSCs exhibit a preference for lineage differentiation to the donor cell type indicating the existence of memory of origin. Although the intrinsic effect of the donor cell type on differentiation of iPSCs is well recognized, whether disease-specific factors of donor cells influence the differentiation capacity of iPSC remains unknown. Using viral based reprogramming, we demonstrated the generation of iPSCs from chondrocytes isolated from healthy (AC-iPSCs) and osteoarthritis cartilage (OA-iPSCs). These reprogrammed cells acquired markers of pluripotency and differentiated into uncommitted mesenchymal-like progenitors. Interestingly, AC-iPSCs exhibited enhanced chondrogenic potential as compared OA-iPSCs and showed increased expression of chondrogenic genes. Pan-transcriptome analysis showed that chondrocytes derived from AC-iPSCs were enriched in molecular pathways related to energy metabolism and epigenetic regulation, together with distinct expression signature that distinguishes them from OA-iPSCs. Our molecular tracing data demonstrated that dysregulation of epigenetic and metabolic factors seen in OA

Nazir M Khan, Martha Elena Diaz-Hernandez, Samir Chihab, Priyanka Priyadarshani, Pallavi Bhattaram, Luke J Mortensen, Rosa M Guzzo, Hicham Drissi. 2023. eLife 12:e83138

chondrocytes relative to healthy chondrocytes persisted following iPSC reprogramming and differentiation toward mesenchymal progenitors. Our results suggest that the epigenetic and metabolic memory of disease may predispose OA-iPSCs for their reduced chondrogenic differentiation and thus regulation at epigenetic and metabolic level may be an effective strategy for controlling the chondrogenic potential of iPSCs.

# Shape up before you ship out: morphology as a potential critical quality attribute for cellular therapies

Kanupriya R Daga, Priyanka Priyadarshani, Andrew M Larey, Kejie Rui, Luke J Mortensen, Ross A Marklein

Cell therapies have been explored for regenerative medicine; however, this immense promise has been met with limited clinical success. While many clinical trials aim to demonstrate product safety and efficacy, a number of issues remain related to product heterogeneity that must be addressed in order to fully realize the potential of cell therapies. A critical unmet need in cell manufacturing is a lack of critical quality attributes (CQAs) that predict the quality of different cell products. To address this need, researchers have begun exploring the potential of morphological profiling, using various imaging approaches and analytical tools, to identify morphological features that could serve as CQAs and enable better quality control of cell manufacturing, and thus improved clinical outcomes. Here, we present recent efforts that successfully use morphology as a CQA, as well as identify other potential uses of morphological profiling to improve cell manufacturing and ultimately accelerate clinical translation.

Kanupriya R Daga, Priyanka Priyadarshani, Andrew M Larey, Kejie Rui, Luke J Mortensen, Ross A Marklein. 2021. Current Opinion in Biomedical Engineering Vol.20, p.100352

# Heparin/Collagen Surface Coatings Modulate the Growth, Secretome and Morphology of Human Mesenchymal Stromal Cell Response to Interferon-Gamma

Said J Cifuentes, Priyanka Priyadarshani, David A Castilla-Casadiego, Luke J Mortensen, Jorge Almodóvar, Maribella Domenech

The therapeutic potential of human mesenchymal stromal cells (h-MSC) is dependent on the viability and secretory capacity of cells both modulated by the culture environment. Our previous studies introduced heparin and collagen I (HEP/COL) alternating stacked layers as a potential substrate to enhance the secretion of immunosuppressive factors of h-MSCs. Herein, we examined the impact of HEP/COL multilayers on the growth, morphology, and secretome of bone marrow and adipose-derived h-MSCs. The physicochemical properties and stability of the HEP/COL coatings were confirmed at 0 and 30 days. Cell growth was examined using cell culture media supplemented with 2 and 10% serum for 5 days. Results showed that HEP/COL multilayers supported h-MSC growth in 2% serum at levels equivalent to 10% serum. COL and HEP as single component coatings had limited impact on cell growth. Senescent studies performed over three sequential passages showed that HEP/COL multilayers did not impair the replicative capacity of h-MSCs. Examination of 27 cytokines showed significant enhancements in eight factors, including

Said J Cifuentes, Priyanka Priyadarshani, David A Castilla-Casadiego, Luke J Mortensen, Jorge Almodóvar, Maribella Domenech. 2020. Journal of Biomedical Materials Research Part A 109(6): pp 951-965

intracellular indoleamine 2, 3-dioxygenase, on HEP/COL multilayers when stimulated with interferon-gamma (IFN-γ). Image-based analysis of cell micrographs showed that serum influences h-MSC morphology; however, HEP-ended multilayers generated distinct morphological changes in response to IFN-γ, suggesting an optical detectable assessment of h-MSCs immunosuppressive potency. This study supports HEP/COL multilayers as a culture substrate for undifferentiated h-MSCs cultured in reduced serum conditions.